

University of Montana

ScholarWorks at University of Montana

Graduate Student Theses, Dissertations, &
Professional Papers

Graduate School

2010

Spatio-temporal optimization of tree removal to efficiently minimize crown fire potential

Marco A. Contreras
The University of Montana

Follow this and additional works at: <https://scholarworks.umt.edu/etd>

Let us know how access to this document benefits you.

Recommended Citation

Contreras, Marco A., "Spatio-temporal optimization of tree removal to efficiently minimize crown fire potential" (2010). *Graduate Student Theses, Dissertations, & Professional Papers*. 908.
<https://scholarworks.umt.edu/etd/908>

This Dissertation is brought to you for free and open access by the Graduate School at ScholarWorks at University of Montana. It has been accepted for inclusion in Graduate Student Theses, Dissertations, & Professional Papers by an authorized administrator of ScholarWorks at University of Montana. For more information, please contact scholarworks@mso.umt.edu.

**SPATIO-TEMPORAL OPTIMIZATION OF TREE REMOVAL TO
EFFICIENTLY MINIMIZE CROWN FIRE POTENTIAL**

Submitted by

Marco Antonio Contreras Salgado

B.S. en Ciencias Forestales, Universidad de Talca, Chile, 2003

Ingeniero Forestal, Universidad de Talca, Chile, 2003

M.S. in Forestry, University of Montana, MT, USA, 2006

Presented in partial fulfillment of the requirements

for the degree of

Doctor of Philosophy

The University of Montana

December 2010

Committee Members:

Dr. Woodam Chung, Department of Forest Management

Dr. Carl Seielstad, Department of Forest Management

Dr. David Affleck, Department of Forest Management

Dr. Mark Kayll, Department of Mathematical Sciences

Dr. Jesse Johnson, Department of Computer Sciences

Contreras, M.A., Ph.D. December 2010 College of Forestry and Conservation
Spatio-Temporal Optimization of Tree Removal to Efficiently Minimize Crown Fire
Potential

Chairperson: Dr. Woodam Chung

High-intensity wildfires have resulted in large financial, social, and environmental costs in the western U.S. This trend is not expected to decline soon, as there are millions of overstocked hectares at medium to high risk of catastrophic wildfires. Thinning is being widely used to restore different types of overstocked forest stands. Typically, thinning prescriptions are derived from average stand attributes and applied to landscapes containing a large number of stands. Stand-level thinning prescriptions have thus limitations when applied for reducing the risk of high-intensity wildfires. They use indicators of crown fire potential (e.g., canopy base height and canopy bulk density) that ignore variability of fuels within stands, location of individual cut- and leave-trees after treatments, and the temporal effects of these prescriptions for reducing crown fire potential over time. To address the limitations of current stand-level thinning prescriptions, a computerized approach to optimize individual tree removal and produce site-specific thinning prescriptions was designed. Based on stem maps and tree attributes derived from light detection and technology (LiDAR), the approach predicts individual tree growth over time, quantifies tree-level fuel connectivity, and estimates skidding costs for individual trees. The approach then selects the spatial combination of cut-trees that most efficiently reduces crown fire potential over time while ensuring cost efficiency of the thinning treatment.

ACKNOWLEDGEMENTS

First and foremost, I want to thank and express my gratitude to my advisor Dr. Woodam Chung for giving me opportunity to continue my doctoral studies. Without his advice, guidance, correction and professional example, the completion of this dissertation would have not been possible.

I would like to extend my appreciation to my graduate committee members. Dr. David Affleck for his help with the development of several regression models and contributing in the preparation of the first chapter of this dissertation. Dr. Carl Seielstad for providing me with tree data and stem maps as well as many suggestions to improve the quality of this work. Dr. Mark Kayll and Dr. Jesse Johnson for their helpful discussions and comments about the general methods used in this research project.

I want to thank Dr. Russell Parsons for his help with WFDS open-source platform and running procedures, making available computer codes to generate WFDS inputs, and for his contribution to the development of the third chapter of my dissertation. I am also thankful to Dr. John Goodburn for his help with the preparation of trees cores that allowed me developing regression models to predict tree growth.

Last but not least, I want to express my immense gratitude to my parents, Belarmino Antonio and Luz Elena, for their endless support throughout these years, as well as many friends in Missoula for helping me keep my sanity.

TABLE OF CONTENTS

ABSTRACT	ii
ACKNOWLEDGEMENTS	iii
TABLE OF CONTENTS	iv
LIST OF TABLES	viii
LIST OF FIGURES	xi
GENERAL INTRODUCTION	1
LIMITATIONS OF STAND-LEVEL THINNING PRESCRIPTIONS	3
PREVIOUS WORK	5
Fire Behavior Modeling	5
Fire Behavior Models Considering Spatial Variability of Fuels	9
Tree-Level Thinning Prescriptions	10
Estimation of Harvesting Costs	11
Tree-Level Growth Models	13
STUDY OBJECTIVES	14
OUTLINE	15
REFERENCES	16
CHAPTER 1: EVALUATING DIFFERENT TREE-LEVEL COMPETITION	24
INDICES BY THEIR EFFECTIVENESS AS PREDICTORS OF BASAL	
AREA INCREMENT	
1.0 ABSTRACT	25
1.1 INTRODUCTION	26

1.2	METHODOLOGY	30
1.2.1	Study Area	30
1.2.2	Competition Indices	33
1.2.3	Evaluation of Competition Indices	39
1.2.4	Basal Area Increment Growth Model	40
1.3	RESULTS AND DISCUSSION	41
1.3.1	Competition Indices	41
1.3.2	Individual Tree Growth Model	48
1.4	CONCLUSIONS	52
1.5	REFERENCES	54
	CHAPTER 2: A MODELING APPROACH TO ESTIMATING SKIDDING COSTS OF INDIVIDUAL TREES FOR THINNING OPERATIONS	60
2.0	ABSTRACT	61
2.1	INTRODUCTION	62
2.2	METHODOLOGY	64
2.2.1	Log-Bunching Algorithm	67
2.2.2	Skid-Trail Network	69
2.3	MODEL APPLICATION – A CASE STUDY	73
2.4	RESULTS AND DISCUSSION	75
2.5	CONCLUSIONS	87
2.6	REFERENCES	89

CHAPTER 3: MODELING TREE-LEVEL FUEL CONNECTIVITY TO	95
EVALUATE THE EFFECTIVENESS OF THINNING TREATMENTS FOR	
REDUCING CROWN FIRE POTENTIAL	
3.0 ABSTRACT	96
3.1 INTRODUCTION	97
3.2 METHODOLOGY	100
3.2.1 LiDAR Data and Tree Attributes	100
3.2.2 Wildland-urban interface Fire Dynamics Simulator (WFDS)	104
3.2.2.1 Tree-level fuel representation	104
3.2.2.2 Weather scenarios and input data	105
3.2.3 Tree-Level Fuel Connectivity	108
3.2.3.1 Vertical fuel connectivity – crown fire initiation	108
3.2.3.2 Horizontal fuel connectivity – crown fire propagation	121
3.2.4 Regression Models	112
3.2.5 Thinning Scenarios	114
3.3 RESULTS AND DISCUSSION	118
3.3.1 Regression Models	118
3.3.1.1 Vertical fuel connectivity – crown fire initiation	118
3.3.1.2 Horizontal fuel connectivity – crown fire propagation	121
3.3.2 Evaluation of Alternative Thinning Scenarios	125
3.3.3 Capturing Spatial Variability of Fuels	131
3.4 CONCLUSIONS	135
3.5 REFERENCES	136

CHAPTER 4: DEVELOPING A COMPUTERIZED APPROACH FOR OPTIMIZING INDIVIDUAL TREE REMOVAL TO EFFICIENTLY REDUCE CROWN FIRE POTENTIAL	143
4.0 ABSTRACT	144
4.1 INTRODUCTION	145
4.2 METHODOLOGY	148
4.2.1 LiDAR Data and Tree Attributes	148
4.2.2 Individual Tree Fuel Connectivity	151
4.2.3 Individual Tree Distance-Dependent Growth Model	154
4.2.4 Individual Tree Timber Harvesting Cost	155
4.2.5 Individual Tree Removal Optimization	157
4.2.5.1 MVC algorithm	159
4.2.6 Model Application – A Case Study	165
4.3 RESULTS AND DISCUSSION	166
4.4 CONCLUSIONS	178
4.5 REFERENCES	180

LIST OF TABLES

Table 1.1	Diameter classes for selecting cored trees.	31
Table 1.2	Competition indices evaluated in this study.	34
Table 1.3	Log-transformed linear models selected from including each competition index and other selected growth predictors.	47
Table 1.4	Coefficients (a_1 , a_2 , a_3) and estimated variance parameter (s) from the final GLM with gamma distribution and log link fitted for individual tree growth.	50
Table 2.1	Target thinning intensities under each thinning scenario considered in the study.	75
Table 2.2	Results of the individual tree skidding cost model.	83
Table 2.3	Parameters used in the Fuel Reduction Cost Simulator (FRCS) to calculate skidding costs under each thinning scenarios.	85
Table 2.4	Comparison of average skidding cost results among various cost models including our individual-tree cost model, the Fuel Reduction Cost Simulator (FRCS), and six published regression models used in the FRCS for both thinning scenarios.	86
Table 3.1	LiDAR data acquisition parameters used for Lubrecht Experimental Forest	100
Table 3.2	Fuel moisture percentage values used to obtain surface fire intensity parameters.	107
Table 3.3	Weather and surface fire inputs used in WFDS fire simulations.	108

Table 3.4	Distance-dependent competition indices used to obtain measures of partial tree density.	114
Table 3.5	Proportion of trees expected to ignite for each target CBH value considered in the crown fire initiation simulations under both weather conditions.	118
Table 3.6	Correlation matrix showing the relationship between the three tree attributes and their relationship with percent DML.	120
Table 3.7	Logistic regression model predictive quality for crown fire initiation under average and severe weather conditions.	121
Table 3.8	Proportion of adjacent trees burned through crown fire propagation for each target spacing under both weather conditions.	122
Table 3.9	Correlation matrix of the six competition indices and their relationship with percent DML.	123
Table 3.10	Logistic regression model predictive quality for crown fire propagation under average and severe weather conditions.	125
Table 3.11	Tree-level fuel connectivity results from the logistic regression models under both weather conditions for each thinning scenario.	126
Table 3.12	Tree-level fuel connectivity results under the severe weather conditions for six alternative combinations of leave-trees under the same thinning intensity.	132
Table 3.13	Summary statistics for average stand attributes obtained after six alternative combinations of leave-trees.	133

Table 4.1	LiDAR data acquisition parameters used for Lubrecht Experimental Forest.	148
Table 4.2	Typical late summer surface fuel moisture values used in the development of tree-level fire crown initiation and propagation.	151
Table 4.3	Weather and surface fire input parameters used in the development of tree-level fire crown initiation and propagation.	152
Table 4.4	Steps required to obtain the MVC initialized with vertex number one.	161
Table 4.5	Tree-level fuel connectivity results from the logistic regression models for trees under the current stand condition and the projected future condition after a 20-year growing period.	167
Table 4.6	Current and future tree attributes predicted using the individual tree growth model over a 20 year period.	171
Table 4.7	Statistics on individual tree skidding costs estimated for the selected cut-trees in the study area.	173
Table 4.8	Comparisons on solution quality between the best tree selection found by the computerized approach and two alternative selections of cut- and leave-trees.	176

LIST OF FIGURES

Figure 1.1	Sample point with three cored trees (solid dots) and their respective competition plots.	32
Figure 1.2	Diameter at breast height (DBH) distribution of cored trees at Lubrecht Experimental Forest.	33
Figure 1.3	Area of influence-zone of a cored tree (Z) and areas of influence-zone overlap between the cored tree and each neighbor tree (O_i).	36
Figure 1.4	Schematic of horizontal angles from the cored tree center to the DBH of each neighbor tree within the competition plot used to compute CI_{10} and CI_{11} .	37
Figure 1.5	Schematic of the vertical angles from the base of the cored tree to the top of each neighbor within the competition plot used to compute CI_{12} and CI_{13} .	37
Figure 1.6	Discretization of a portion of the sky's hemisphere directly above the cored tree into 2160 light rays generated from a focal point at 60% of the cored tree's height.	39
Figure 1.7	Correlation matrix of the 16 competition indices showing global correlations on the lower diagonal and species-specific correlations on the upper diagonal (Douglas-fir = black dots; ponderosa pine = dark grey dots; western larch = light grey dots).	43
Figure 1.8	Scatter plots and least squares fit of growth versus three competition indices.	45

Figure 1.9	BAI ₁₀ as a function of DBH and CI ₁₁ for all species.	49
Figure 1.10	Residuals from the final GLM with gamma distribution and log link fitted for individual tree growth.	50
Figure 2.1	Flowchart of the log-bunching algorithm developed in this study.	68
Figure 2.2	Log-bunching simulation to identify log-pile locations.	69
Figure 2.3	Links connecting a cell with its eight adjacent cells.	70
Figure 2.4	Grid cells used to calculate the side slope and skid-trail gradient for a given skid-trail link.	70
Figure 2.5	Example of the skid-trail network created over an area with steep terrain and obstacles presented by two leave-tree buffers.	71
Figure 2.6	LiDAR-derived digital elevation model (a) and stem map (b) for the treatment unit selected for the model application area in the Lubrecht Experimental Forest.	73
Figure 2.7	Selected leave-trees locations under the two thinning scenarios with a target density of 400 and 300 trees per hectare, (a) and (b) respectively.	75
Figure 2.8	Cut-tree locations under thinning scenario I (a), and the corresponding log-pile locations identified by the log bunching algorithm (b).	77
Figure 2.9	Feasible skid-trail links created by the model for thinning scenario I (a), and the optimal skid-trail network identified by the model (b).	77

Figure 2.10	Optimal skid-trail network for thinning scenario I showing traffic levels in terms of volume traveled (a), and number of passes (b) over a given link.	78
Figure 2.11	Model results showing skidding cost per pile (a) and per individual cut-tree (b) for thinning scenario I.	78
Figure 2.12	Cut-tree locations under thinning scenario II (a), and the corresponding log-pile locations identified by the log bunching algorithm (b).	80
Figure 2.13	Feasible skid-trail links created by the model for thinning scenario II (a), and the optimal skid-trail network identified by the model (b).	80
Figure 2.14	Optimal skid-trail network for thinning scenario II showing traffic levels in terms of volume traveled (a), and number of passes (b) over a given link.	81
Figure 2.15	Model results showing skidding cost per pile (a) and per individual cut-tree (b) for thinning scenario II.	81
Figure 3.1	University of Montana’s Lubrecht Experimental Forest boundary and the selected forest stand for the study area.	101
Figure 3.2	Histogram and summary statistics of DBH distribution of LiDAR-derived trees in the study area	103
Figure 3.3	WFDS simulation design for crown fire initiation showing nine trees with different dimensions but similar CBH (i.e., 2 m).	109
Figure 3.4	WFDS simulation design for crown fire propagation. Examples show three, one, and two trees forming the flaming front (a, b, and c) and increasing spacing between the source and target tree.	111

Figure 3.5	LiDAR-derived stem map of trees in the study area (a), and location of leave-tree under thinning scenarios I through III, b) through d) respectively.	116
Figure 3.6	Schematic of the flaming front area used to estimate crown fire propagation between a source tree and a target tree.	117
Figure 3.7	Percent dry mass lost distribution from trees in the WFDS crown fire initiation simulations for average (a) and severe conditions (b).	119
Figure 3.8	Percent dry mass lost distribution from trees in the WFDS crown fire propagation simulations for average (a) and severe conditions (b).	123
Figure 3.9	Location and size of clusters formed by predicted tree-level fuel connections for thinning scenario I under average (a) and severe (b) weather conditions.	127
Figure 3.10	Location and size of clusters formed by predicted tree-level fuel connections for thinning scenario II under average (a) and severe (b) weather conditions.	128
Figure 3.11	Location and size of clusters formed by predicted tree-level fuel connections for thinning scenario III under average (a) and severe (b) weather conditions.	129
Figure 4.1	University of Montana’s Lubrecht Experimental Forest.	149
Figure 4.2	Schematic of the flaming front area used to search additional source trees (dashed lines) showing spacing between a source tree and a target tree (solid lines) (a) and the calculation of CI_1 (b) to estimate fuel connectivity.	153

Figure 4.3	Example of fuel connectivity network formed by 43 vertices and 9 clusters of connected trees.	159
Figure 4.4	LiDAR-derived digital elevation model (a) and stem map (b) for the 4.6-ha study area in LEF.	166
Figure 4.5	Location, size, and summary statistics of clusters formed by predicted tree-level fuel connections under the current conditions in the study area.	168
Figure 4.6	Changes in objective function value over 15,000 iterations. The best solution was found at iteration 12,023.	169
Figure 4.7	Leave-tree locations and summary statistics of clusters formed by remaining fuel connections found by the best solution.	170
Figure 4.8	Leave-tree locations and summary statistics of clusters formed by future fuel connections after a 20-year growth period.	172
Figure 4.9	Cut-tree locations (a) and log-piles (b), feasible skid-trail links (c), and optimal skid-trail network (d) for the selected cut-trees in the best solution found	174
Figure 4.10	Distribution of skidding costs over the study area showing cost per log-pile (a) and cost per individual cut-tree (b).	175

GENERAL INTRODUCTION

Historically, low-intensity fires burned frequently in the western United States (US) maintaining open forest structures and reducing forest fuel loads (Hessl et al. 2004, Allen et al. 2002). Over the last decades, successful fire exclusion has contributed to the accumulation of understory vegetation and increased forest stand density, creating greater continuity of fuels in stand structures and increasing the potential for high-intensity wildfires (Mutch 1994, Arno and Brown 1991). As a result, wildfires have burned more severely causing considerable financial, social, and environmental losses. In the last five years alone, high-intensity wildfires burned more than eight million hectares in the western US (NIFC 2010). Wildfires are expected to continue burning severely; some estimates indicate that more than 27 million hectares of forestlands have departed significantly from natural wildland fire conditions and are at medium to high risk of catastrophic wildfires (Schmidt et al. 2002).

Thinning is one of the most common silvicultural treatments used to reduce the risk of high-intensity wildfire (O'Hara et al. 1994). It has been widely applied to many types of forest stands to reduce fire intensity by changing stand structures and reducing fuel loads (Graham et al. 2004, Graham et al. 1999). Typically, thinning prescriptions are derived from average stand attributes and applied to landscapes containing a large number of stands. However, treating stands with varying site potentials and vegetation structures under similar thinning prescriptions is often inefficient for achieving fuel reduction goals throughout the treatment area (Parsons 2007, Graetz et al. 2007, Keyes and O'Hara 2002). Forest managers need tools to develop site-specific thinning

prescriptions for individual forest stands based on their current vegetation structures and wildfire potential. Such tools can improve the effectiveness of thinning practices for reducing stands' susceptibility to high-intensity wildfires, while considering cost efficiency of thinning operations and other forest management goals such as wildlife habitat and water conservation. Developing site-specific thinning prescriptions for individual stands requires tree-level forest inventory data as well as analytical approaches to guide the selection of cut-trees to best modify vegetation structures to efficiently and effectively reduce the risk of high-intensity wildfires.

Traditionally, decision-making in forest management is based on stand attribute information collected using stand examination. As field based inventory data are expensive and labor intensive to acquire, sampling intensity is limited providing average stand characteristics while ignoring large variability in vegetation and terrain within stands. Recent advances in remote sensing and geographic information systems technologies have drastically changed forest data acquisition by providing tree-level inventory data for large landscapes. These unprecedented high-resolution forest inventory data can be used to facilitate the transition of forest management from stand-level to a more detailed tree-level. Although these tree-level datasets are becoming more widely available, there is a need for decision support systems that integrate such data into decision-making to improve current forest management practices.

LIMITATIONS OF STAND-LEVEL THINNING PRESCRIPTIONS

Development and evaluation of thinning prescriptions for reducing the risk of crown fire using the existing fire management tools have four limitations. These tools use indicators of crown fire potential (i.e., canopy base height and canopy bulk density) that ignore the following four important factors:

i) Variability in tree sizes within a stand – Stand-level thinning prescriptions are designed to reduce the likelihood of crown fire initiation by increasing canopy base height. Crown base height, measured on an individual tree, is relatively easy to obtain; however, due to variability in tree sizes within a stand, it is difficult to represent an entire stand with a single canopy base height value (Scott and Reinhardt 2001). Stand-level thinning prescriptions are also designed to reduce the likelihood of crown fire propagation by decreasing canopy bulk density. Again, canopy depth is difficult to estimate for an entire stand and the calculation of canopy bulk density assumes that canopy fuels are distributed uniformly within a stand, which is unlikely the case even in stands with simple structures (Scott and Reinhardt 2001).

ii) Spatial distribution of leave-trees after treatment – Stand-level thinning prescriptions usually specify percentage of total tree removal or per size class in terms of number of trees and/or basal area. Hence, there are a countless number of combinations of cut-trees that meet the same thinning prescription for a given stand. Individual foresters, who select and mark the actual cut-trees on the ground, are likely unable to evaluate the effects on each cut-tree combination on reducing crown fire potential. However, the effectiveness of thinning treatments to mitigate the chance of fire transitioning to and

spreading through canopy fuels can vary widely depending on the spatial distribution of leave-trees after treatment (Parsons 2007).

iii) Spatial distribution of selected cut-trees – Estimation of harvesting costs for a thinning treatment is often simplified using average stand attributes such as skidding distance, ground slope, and harvestable timber volume, while ignoring the location of individual cut-trees relative to extraction points (either landing or road side) and detailed terrain conditions within a stand. For example, although two alternative combinations of cut-trees might have the same effect on reducing crown fire potential, the combination with cut-trees closer to the extraction points might be less costly than the other combination.

iv) Future tree growth and treatment longevity – Current thinning prescriptions rarely consider the longevity of treatments in terms of their effectiveness in altering fire behavior. Decisions on cut-tree selection affect micro conditions and future competition levels of remaining leave-trees, thus influencing tree growth and future stand conditions. However, individual tree growth and the associated temporal effects of cut-tree selection on the reduction of crown fire potential over time have not been incorporated into the development of thinning prescriptions.

Despite the limitations mentioned above, stand-level thinning prescriptions are still being considered for restoring different types of overstocked forest stands in need of fuel reduction treatments without being evaluated for their effectiveness at an individual tree level. This is mainly because of the way forest inventory data have been collected, which is through field-based sampling plots. Collecting more detailed tree-level data to quantify forest resources has been deemed impractical and economically infeasible.

However, in recent years, the Light Detection and Ranging (LiDAR) technology has been widely used to provide tree locations and attributes – tree height, crown width and derivative parameters such as diameter at breast height (DBH), volume, and crown base height over large landscapes (Maltamo et al 2006; Packalén and Maltamo 2006; Maltamo et al 2004). These tree-level data can be used to capture spatial variability in tree sizes and locations within a stand and develop more detailed tree-level thinning prescriptions to improve the efficiency and effectiveness of the current thinning practices for given forest management goals.

PREVIOUS WORK

Fire Behavior Modeling

Land managers have been using fire behavior models to predict fire intensity, identify stands with high risk of wildfire, and allocate resources for thinning treatments (Ager et al. 2006, Finney 2006). Available fire behavior models can be classified as empirical, semi-empirical, and physics-based models (Pastor et al. 2003). Empirical models are based on relationships between a response variable and explanatory variables without considering the controlling physical processes (Cheney et al. 1998, Cruz et al. 2004). These models usually predict spread rate of fire (and other quantities derived from spread rate) as a function of wind speed, terrain slope, and fuel characteristics (Mell et al. 2007). Semi-empirical models are based on conservation of energy theory, but

usually consider only one mode of heat transfer – conductive, convective, or radiative (Sullivan 2007). By assuming fuels homogeneity, most of these models can model fire behavior in two-dimensions (i.e., Van Wagner 1977, Alexander 1998, Butler et al. 2004, and Cruz et al. 2006a). Lastly, physics-based models are able to predict fine-scale time dependent fire behavior, fire-fuel, and fire-atmosphere interactions in three-dimensions by solving equations governing fluid dynamics, combustion, and heat transfer. All modes of heat transfer present in both fire-fuel and fire-atmosphere interactions are modeled (Sullivan 2007, Mell et al. 2005).

Several fire behavior models have been integrated into fire management tools developed to predict the risk of high-intensity wildfires on forest stands such as the FARSITE (Finney 1998), NEXUS (Scott 1999, Scott and Reinhardt 2001), FFE-FVS (Reinhardt and Crookston 2003), BehavePlus (Andrews et al. 2005), FMAplus (Carlton 2005), CFIS (Crown Fire Initiation and Spread; Cruz et al. 2005), and FlamMap (Finney 2006). These tools use different empirical and semi-empirical fire behavior models, but they are based on a common set of models including Rothermel's (1972) surface fire spread, Van Wagner's (1977) crown fire initiation, and Rothermel's (1991) crown fire spread models. Scott (2006) compared three widely-used fire management tools (i.e., NEXUS, FlamMap, and CFIS) in terms of their predictions of crown fire potential. Crown fires are of particular concern because they are difficult to control and have more lethal effects than other types of fires (Scott and Reinhardt 2001, Rothermel 1991). Scott (2006) found significant differences in crown fire potential under the same vegetation and weather conditions, but the relative risk of high-intensity wildfires was similar in all forest stands considered in his study. Although managers can rely on the relative crown

fire potential from any of these three tools, absolute crown fire potential is important to determine acceptable levels of fuels accumulation, prioritize areas for fuel treatments, and evaluate the benefits of such treatments for reducing crown fire potential (Scott 2006).

Several models are available to predict crown fire initiation, the transition of fire from surface fuels to the elevated canopy fuels (i.e., Van Wagner 1977, Cruz et al. 2004, and Cruz et al. 2006a). Van Wagner's (1977) is one of the oldest and most used models. It identifies the minimum amount of heat from a surface fire required to ignite canopy fuels as a function of canopy base height, fuel moisture, and an empirical constant derived from a single experimental fire conducted in a red plantation stand (Alexander 1998). Cruz et al. (2004) developed a logistic regression model to predict the probability of crown fire occurrence, which is the chance of observing a crown fire given certain fire burning conditions. Predictive variables include wind speed, fuel moisture, canopy base height, and available surface fuels. Cruz et al. (2006a and 2006b) later developed a semi-empirical model for predicting crown fire initiation based on heat transfer theory. In their model, surface fire characteristics (i.e., rate of spread, flame depth and height) and canopy fuels characteristics (area-to-volume ratio, density, specific heat, and fuel moisture) are used to determine fuel temperature at the base of the canopy considering radiative and convective heat transfer from the surface fire. Crown fire initiation is predicted to occur when estimated fuel temperature exceeds 600 K, at which piloted ignition occurs and fire propagates vertically into the canopy (Cruz et al. 2006a).

There are also several models available for predicting crown fire propagation, the spread of fire throughout canopy fuels. Van Wagner (1977) empirically determined from

a single fire experiment that solid flames would form and propagate through the canopy when the horizontal mass-flow rate of fuels exceeds $3.0 \text{ kg}\cdot\text{m}^{-2}\cdot\text{min}^{-1}$. Based on the stand's canopy bulk density, the minimal rate of spread required to sustain crown fire propagation is then determined. Rothermel (1991) developed an empirical model for predicting the spread rate of crown fires based on eight crown fires in the northern Rocky Mountains. Crown fire spread rate is estimated to be 3.34 times faster than surface fire spread rate predicted with the Rothermel's (1972) model considering surface fuels described by fuel model 10 (Anderson 1982) and a midflame wind speed of 40% of the observed wind speed at 6.1 meters above ground. Cruz et al. (2005) developed another empirical model for predicting crown fire spread rate using data from 25 small-scale experimental crown fires in plantations of three different conifer species. In their model, crown fire spread rate is predicted based on wind speed, canopy bulk density, and fuel moisture content. Butler et al. (2004) developed a semi-empirical model for predicting the spread rate of crown fires based on radiative heat transfer theory. Considering radiative heat transfer from free flame above the canopy, burning zone below the canopy, and available canopy fuels (i.e., canopy bulk density) ahead of the flaming front, the model iteratively describes an ignition isotherm (set at 600 K) from which spread rate is computed.

For given surface fuel and weather conditions, existing models predict crown fire initiation solely based on crown base height, which represents the vertical distance from the top of the surface fuels to the lower limit of canopy fuels that can sustain and vertically propagate fire. Similarly, crown fire propagation is predicted only based on canopy bulk density, which is usually computed as the available canopy fuels divided by

canopy depth (Keane et al. 1998). Consequently, existing fire management tools use average attributes values of forest stands for stand-level predictions of crown fire potential, and forest managers rely on such tools to design stand-level thinning prescription for reducing crown fire potential over large areas containing multiple forest stands.

Fire Behavior Models Considering Spatial Variability of Fuels

As mentioned above, the widely-used existing fire behavior and simulation models have limitations in properly modeling crown fire initiation and propagation at an individual tree or stand level. However, recent research efforts have focused on the development of advanced physics-based numerical fire behavior models capable of considering spatial variability of fuels within a forest stand. Examples of such models include FIRETECH (Linn et al. 2002) and the wildland-urban interface fire dynamics simulator (WFDS) (Mell et al. 2005), developed by the Los Alamos National Laboratory and the National Institute for Standards and Technology, respectively. These models have received considerable research attention because of their potential to provide more reliable and detailed predictions over a wider range of conditions than the existing models (Mell et al. 2007, Linn et al. 2005). For example, WFDS is a model able to predict fine-scale, time-dependent fire behavior, fire-fuel, and fire-atmosphere interactions in three dimensions (Mell et al. 2005). The use of voxels to represent fuels distribution allows taking into account size, shape composition and spatial arrangement

of fuels (Parsons 2006). Fluid dynamics, combustion, and heat transfer equations are solved for each voxel to simulate fire behavior over the entire simulation domain.

This advanced fire behavior modeling approach can be a promising method to properly model crown fire initiation and propagation at a fine scale and can be used to evaluate stand level effects of fuel treatments. However, practical applications of the fine-scale fire behavior models to an entire stand have been limited due to the large amount of data and computation time required to represent detailed variability of fuels and model the time-dependent fine scale fire-fuel and fire-atmosphere interactions for an entire stand (Mell et al. 2007).

Tree-Level Thinning Prescriptions

Although there are a few fire behavior and simulation models capable of considering fuels variability within a stand, they have not been specifically used in developing tree-level thinning prescriptions for reducing crown fire potential. There are; however, two approaches developed to optimize the tree selection and design tree-level thinning prescriptions for the purpose of timber production. One approach formulates the tree selection process as a non-linear problem and solves it using the Hooke and Jeeve (1961) algorithm (Pukkala and Miina 1998). Based on decision variables such as minimum spacing between trees and target basal area per size class, the approach selects cut-trees based on their competitive status (trees facing the most competition are removed first). This approach has been used to generate tree-level thinning prescription based on sample plot data. Trees outside the plots are assigned arbitrary x- and y-coordinates

assuming sample plots are surrounded by trees in the same spatial pattern. Consequently, tree-level information is used to generate tree-level prescriptions that are extrapolated to entire stands and applied at the stand-level with no specific identification of cut- and leave-trees. Studies using this approach show that solution quality is largely sensitive to the number and type of decision variables, indicating that the correct set of decision variables (i.e., locations of individual trees) is critical to solution quality (Rautiainen et al. 2000).

The second approach uses integer programming to optimize the selection of cut- and leave-trees (Hof and Bevers 2000). A grid and grid cells are used to represent, respectively, a stand and individual trees within the stand. Each grid cell is then assigned an integer decision variable (i.e., 1 or 0) indicating a cut- or leave tree, and the tree selection problem is solved using integer programming to maximize the net present value of timber production over a planning horizon. Because individual trees are used as decision variables, spatially sensitive components of stand management (e.g., regeneration) can be incorporated into the problem formulation, yet extremely large combinatorial problems result. Due to the inefficient solving process of integer programming, this approach has been applied only to a hypothetical problem set with a maximum of 40 x 40 grid cells.

Estimation of Harvesting Costs

Thinning costs have been typically estimated per acre using average stand attributes such as average skidding distance, ground slope, and timber volume (Rummer

2008). There are several cost models developed to estimate cost of thinning operations for a harvest unit. For example the Fuel Reduction Cost Simulator (FRCS) (Hartsough et al. 2001) is currently used as a timber harvesting cost estimator for multiple MS Excel-based tools such as STHARVEST (Fight et al. 2003) and My Fuel Treatment Planner (Biesecker and Fight 2006). FRCS consists of a collection of published machine cost and productivity studies for different harvesting systems operating in western U.S. (i.e., Johnson 1998, Gardner 1979, Gebhardt 1977). FRCS considers average tree size (DBH and volume), tree removal per acre, harvest unit size, machine rental rate, and site variables such as average skidding distance and ground slope. Skog et al. (2006) used FRCS to estimate the alternative thinning prescription for reducing fire hazard in western U.S. states. Arriagada et al. (2008) also used FRCS to estimate thinning costs per acre, based on the number of trees removed per acre in two diameter classes (below and above 32.8 cm) and average ground slope for forest stands in 12 states in the western U.S. However, in the application tools of such models, target removable timber volume is assumed to be evenly distributed within stands and cut-tree locations are not considered. Similarly, skidding is assumed feasible throughout the harvest unit and an average skidding distance is used for cost estimation. Skidding obstacles presented by inaccessible areas such as stand boundaries, steep terrain, riparian zones, and leave-trees are not usually considered in the existing models although these obstacles could substantially increase skidding distances and thus skidding costs (Contreras and Chung 2007).

Tree-Level Growth Models

By removing trees, thinning treatments change competition levels of remaining trees, which is one of the most important factors conditioning tree growth. Competition measures described in the literature include distance-independent measures which use non-spatial information about the average tree size within a given area and distance-dependent measures which incorporate the relative locations of neighboring trees. Several tree-level growth models including different measures of competition have been developed (De Luis et al. 1998, Biging and Dobbertin 1992, Holmes and Reed 1991, Tomé and Burkhart 1989, Moore et al. 1973, Bella 1971). However, competition measures perform differently according to tree species and forest conditions (Biging and Dobbertin 1995, Daniels et al 1986). Currently, there are a few models available to predict individual tree growth for tree species in western Montana. Wykoff (1990) developed a basal area increment model for several conifer species in the northern Rocky Mountains as a function of tree size (DBH), site conditions (i.e., site index, slope, and aspect), and competition. Wykoff's (1990) growth model is included in the Northern Idaho/Inland Empire variant of the Forest Vegetation Simulator (Keyser 2008) and has been widely used to predict tree growth for several species western Montana. Uzoh and Oliver (2008) developed a diameter increment model that is also based on site conditions, tree size and competition for ponderosa pine trees throughout the western U.S. These models were developed from large scale studies that included various forest conditions found in various western states. In addition, these models use distance-independent competition measures (i.e, stand density and basal area of trees larger than the subject

tree) that have not been evaluated in western Montana forests. Developing tree growth models that incorporate appropriate competition measures for the specific species and conditions found in western Montana is still needed to increase accuracy of growth predictions.

STUDY OBJECTIVES

To address the limitations of current thinning practices, the main objective of this dissertation was to develop a computerized approach that optimizes individual tree removal for thinning treatments while considering spatial variability of fuels within a stand. The approach is designed to generate site-specific thinning prescriptions for individual stands that can most efficiently reduce crown fire potential over time while ensuring the economic efficiency of the thinning treatment. Based on LiDAR-derived stem map and tree attributes, the approach quantifies fuel connectivity among individual trees and makes a spatial selection of cut- and leave-trees to reduce the risk of crown fire initiation and propagation to and through the stand canopy. The approach design includes functional models covering four specific research objectives:

- i)* Select the most effective competition index for predicting radial increment and develop an individual tree distance-dependent growth model for three common tree species in western Montana;
- ii)* Design a model for estimating location-specific skidding costs of individual trees for thinning treatments;

- iii)* Develop regression models to predict crown fire initiation and propagation and quantify tree-level vertical and horizontal fuel connectivity, and;
- iv)* Design an algorithm to optimize tree removal for reducing crown fire potential by minimizing both tree-level fuel connectivity among leave-trees over time and skidding costs of selected cut-trees.

OUTLINE

This dissertation is composed of four additional chapters covering each of the specific objectives described above. Chapters 1 through 4 are in the format of manuscripts for submission to scientific journals. Chapter 1 covers the evaluation of different tree-level competition indices by their effectiveness as predictors of radial growth and the development of an individual tree growth model for three common tree species in western Montana. Chapter 2 describes a modeling approach developed to estimate skidding costs for individual tree for thinning operations. Chapter 3 presents the procedures developed to model tree-level fuel connectivity and evaluate the effectiveness of thinning treatments for reducing crown fire potential. Lastly, chapter 4 explains the computerized approach designed for optimizing individual tree removal for the purpose of reducing crown fire potential.

REFERENCES

- Ager, A., M. Finney, and A. McMahan. 2006. A wildfire risk modeling system for evaluating landscape fuel treatment strategies. In *Fuels Management – How to Measure Success Conference Proceedings*. 28-30 March 2006, Portland, OR. Edited by Andrews, P.L. and Butler, B.W. Proceedings RMRS-P-41. Fort Collins, CO: USDA, Forest Service, Rocky Mountain Research Station. 809 p.
- Alexander, M.E. 1988. Help with making crown fire hazard assessments. In: Fischer, W.C., and S.F. Arno. *Protecting people and homes from wildfire in the Interior West: proceedings of the Symposium and Workshop; 1988 October 6-8; Missoula, MT*. Proc. Gen. Tech. Rep. INT-251. Ogden, UT: USDA, Forest Service, Intermountain Forest and Range Experimental Station. 147-156.
- Allen, C.D., M. Savage, D.A. Falk, K.F. Suckling, T.W. Swetnam, T. Schulke, P.B. Stacey, P. Morgan, M. Hoffman, and J.T. Klingel. 2002. Ecological restoration of southwestern ponderosa pine ecosystems: a broad perspective. *Ecol. Appl.* 12(5):1418-1433.
- Andrews, P.L., C.D. Bevens, and R.C. Seli. 2005. BehavePlus fire modeling system, version 3: Users Guide. Gen. Tech. Rep. RMRS-GTR-106WWW Revised. Ogden, UT: USDA, Forest Service, Rocky Mountain Research Station. 134 p.
- Arno, S.F., and J.K. Brown. 1991. Overcoming the paradox in managing wildland fire. *Western Wildlands* 171:40-46.
- Arriagada, R.A., F.W. Cabbage, K.L. Abt, and R.J. Huggett Jr., Robert J. 2008. Estimating harvest costs of fuel treatments in the West. *Forest Prod. J.* 58(7/8):24-30.

- Biesecker, R.L., and R.D. Fight. 2006. My fuel treatment planner: a user guide. Gen. Tech. Rep. PNW-GTR-663. Portland, OR: USDA, Forest Service, Pacific Northwest Research Station. 31p.
- Biging, G.S., and M. Dobbertin. 1992. A comparison of distance-dependent competition measures for height and basal area growth of individual conifer trees. *For. Sci.* 38(3):695–720.
- Biging, G.S., and M. Dobbertin. 1995. Evaluation of competition indices in individual tree growth models. *For. Sci.* 41(2):360-377.
- Butler, B., M. Finney, P. Andrews, and F. Albin. 2004. A radiation-driven model for crown fire spread. *Can. J. For. Res.* 34(8):1588-1599.
- Cheney, N.P., J.S. Gould, and W.R. Catchpole. 1998. Prediction of fire spread in grassland. *Int. J. Wildland Fire* 8(1):1-13.
- Contreras, M. and W. Chung. 2007. A computer approach to finding an optimal log landing location and analyzing influencing factors for ground-based timber harvesting. *Can. J. For. Res.* 37(2):276-292.
- Cruz, M.G., M.E. Alexander, and R.H. Wakimoto. 2004. Modeling the likelihood of crown fire occurrence in conifer forest stands. *For. Sci.* 50(5):976-983
- Cruz, M.G., M.E. Alexander, and R.H. Wakimoto. 2005. Developing and testing of models for predicting crown fire rate of spread in conifer stands. *Can. J. For. Res.* 35(7):1626-1639
- Cruz, M.G., B. Butler, M. Alexander, J. Forthofer, and R. Wakimoto. 2006a. Predicting the ignition of crown fuel above a spreading surface fire. Part I: model idealization. *Int. J. Wildland Fire* 15(1):47-60.

- Cruz, M.G., B. Butler, M. Alexander, J. Forthofer, and R. Wakimoto. 2006b. Predicting the ignition of crown fuel above a spreading surface fire. Part I: model evaluation. *Int. J. Wildland Fire* 15(1):61-72.
- Daniels, R.F., H.E. Burkhart, and T.R. Clason. 1986. A comparison of competition measures for predicting growth of loblolly pine trees. *Can. J. For. Res.* 16(6):1230-1237.
- De Luis, M., J. Raventós, J. Cortina, M.J. Moro, and J. Bellot. 1998. Assessing components of a competition index to predict growth in an even-aged *Pinus nigra* stand. *New For.* 15(3):223–242.
- Fight, R.D., X. Zhang, and B.R. Hartsough. 2003. User guide for STHARVEST: software to estimate the cost of harvesting small timber. Gen. Tech. Rep. PNW-GTR-582. Portland, OR: USDA, Forest Service, Pacific Northwest Research Station. 12 p.
- Finney, M.A. 1998. FARSITE: Fire Area Simulator—model development and evaluation. Res. Pap. RMRS-RP-4. Fort Collins, CO: USDA, Forest Service, Rocky Mountain Research Station. 47 p.
- Finney, M.A. 2006. An overview of FlamMap fire modeling capabilities. In *Fuels Management – How to Measure Success Conference Proceedings*. 28-30 March 2006, Portland, OR. Edited by Andrews, P.L. and B.W. Butler, Proceedings RMRS-P-41. Fort Collins, CO: USDA, Forest Service, Rocky Mountain Research Station. 809 p.
- Gardner, R.B. 1979. Turn cycle time prediction for rubber tired skidders in the northern Rockies. Res. Note INT-257. USDA, Forest Service, Intermountain Forest and Range Expt. Sta., Ogden, UT.

- Gebhardt, P.D. 1977. Timber harvesting production rates in mixed-conifer stands of eastern Oregon and Washington. Master of Forestry thesis, Univ. of Washington, Seattle, WA.
- Graetz, D., J. Sessions, and S. Garman. 2007. Using stand-level optimization to reduce crown fire hazard. *Landscape Urban Plan.* 80(3):312-319.
- Graham, R.T., A.E. Harvey, T.B. Jain, and J.R. Tonn. 1999. The effects of thinning and similar stand treatments on fire behavior in Western forest. Gen. Tech. Rep. PNW-GTR-463. Portland, OR: USDA, Forest Service, Pacific Northwest Research Station. 27 p.
- Graham, R.T., S. McCaffrey, and T.B. Jain (tech. eds.) 2004. Science basis for changing forest structure to modify wildfire behavior and severity. Gen. Tech. Rep. RMRS-GTR-120. Fort Collins, CO: USDA, Forest Service, Rocky Mountain Research Station. 43 p.
- Hartsough, B.R., X. Zhang, and R.D. Fight. 2001. Harvesting cost model for small trees in natural stands in the Interior Northwest. *Forest Prod. J.* 51(4):54-61.
- Hessl, A.E., D. McKenzie, and R. Schellhaas. 2004. Drought and Pacific Decadal Oscillation linked to fire occurrence in the inland Pacific Northwest. *Ecol. Appl.* 14(2):425-442.
- Hof, J., and M. Bevers. 2000. Optimizing forest stand management with natural regeneration and single-tree choice variables. *For. Sci.* 46(2):168-175.
- Holmes, M.J., and D.D. Reed. 1991. Competition indices for mixed species northern hardwoods. *For. Sci.* 37(5):1338-1349.
- Hooke, R., and T. Jeeves. 1961. Direct search solution of numerical and statistical problems. *J. ACM* 8(2):212-219.

- Johnson, L.R., and H.W. Lee. 1988. Skidding and processing of forest residues for firewood. *Forest Prod. J.* 38(3):35-40.
- Keane, R.E., J.L. Garner, K.M. Schmidt, D.G. Long, J.P. Menakis, and M.A. Finney. 1998. Development of input data layers for the FARSITE fire growth model for the Selway-Bitterroot Wilderness complex, USA. Gen. Tech. Rep. RMRS-GTR-3. Ogden, UT: USDA, Forest Service, Rocky Mountain Research Station. 66 p.
- Keyes, C.R. and K.L. O'Hara. 2002. Quantifying stand targets for silvicultural prevention of crown fires. *West. J. Appl. For.* 17(2): 101-109.
- Keyser, C.E., comp. 2008. Northern Idaho / Inland Empire (NI/IE) Variants Overview – Forest Vegetation Simulator. Internal Rep. Fort Collins, CO: USDA, Forest Service, Forest Management Service Center. 49p. (revised February 3, 2010).
- Linn, R., J. Reisner, J.J. Colman, and J. Winterkamp. 2002. Studying wildfire behavior using FIRETEC. *Int. J. Wildland Fire* 11(3-4):233–246.
- Linn, R.R., and P. Cunningham. 2005. Numerical simulations of grass fires using a coupled atmosphere-fire model: basic fire behavior and dependence on wind speed. *Journal of Geophysical Research* 110(13):1-19.
- Maltamo, M., K. Mustonen, J. Hyypä, J. Pitkänen, and X. Yu. 2004. The accuracy of estimating individual tree variables with airborne laser scanning in a boreal nature reserve. *Can. J. For. Res.* 34(9):1791-1801.
- Maltamo, M., K. Eerikäinen, P. Packalén, and J. Hyypä. 2006. Estimation of stem volume using laser scanning-based canopy height metrics. *Forestry* 79(2):217-229.
- Mell, W., M.A. Jenkins, J. Gould, and P. Cheney. 2007. A physics-based approach to modelling grassland fires. *Int. J. Wildland Fire* 16(1):1-22.

- Mell, W.E., J.J. Charney, M.A. Jenkins, P. Cheney and J. Gould. 2005. Numerical simulations of grassland fire behavior from the LANL-FIRETEC and NISTWFDS models. East FIRE conference, May 11-13, 2005. George Mason University, Fairfax, VA.
- Moore, J.A., C.A. Budelsky, and R.C. Schlesinger. 1973. A new index representing individual tree competitive status. *Can. J. For. Res.* 3(4):495-505.
- Mutch, R.W. 1994. Fighting fire with prescribed fire: a return to ecosystem health. *J. Forest.* 92(11): 31-33.
- NIFC. 2010. National Interagency Fire Center. Fire Information – Wildland Fire Statistics. Historical Wildland Fire Summaries. URL: http://www.nifc.gov/fire_info/fire_stats.htm.
- O'Hara, K.L., R.S. Seymour, S.D. Tesch, and J.M. Guldin. 1994. Silviculture and our changing profession. *J. For.* 92(1):8-13.
- Pastor, E., L. Zarate, E. Planas, and J. Arnaldos. 2003. Mathematical models and calculation systems for the study of wildland fire behavior. *Progress in Energy and Combustion Science* 29(2):139-153.
- Packalén, P., and M. Maltamo. 2006. Predicting the plot volume by species using airborne laser scanning and aerial photographs. *For. Sci.* 52(6):611-622.
- Parsons, R. 2006. Fuels 3-D: A spatially explicit fractal fuel distribution model. In *Fuels Management – How to Measure Success Conference Proceedings*. 28-30 March 2006, Portland, OR. Edited by Andrews, P.L. and Butler, B.W. Proceedings RMRS-P-41. Fort Collins, CO: USDA, Forest Service, Rocky Mountain Research Station. 809 p.

- Parsons, R. 2007. Spatial variability in forest fuels: Simulation modeling and effects on fire behavior. PhD dissertation, University of Montana, Missoula, MT. 286 p.
- Pukkala, T., and J. Miina. 1998. Tree-selection algorithm for optimizing thinning using a distance-dependent growth model. *Can. J. For. Res.* 28(5):693-702.
- Rautiainen, O., T. Pukkala, and J. Miina. 2000. Optimising the management of even-aged *Shorea robusta* stands in Nepal using individual tree growth models. *For. Ecol. Manage* 126(3):417-429.
- Reinhardt, E.D., and N.L. Crookston (tech. eds.). 2003. The Fire and Fuels Extension to the Forest Vegetation Simulator. Gen. Tech. Rep. RMRS-GTR-116. Ogden, UT: USDA, Forest Service, Rocky Mountain Research Station. 209 p.
- Rothermel, R.C. 1972. A mathematical model for predicting fire spread in wildland fuels. Gen. Tech. Rep. INT-11. Ogden, UT: USDA, Forest Service, Intermountain Forest and Range Experiment Station. 40p.
- Rothermel, R.C. 1991. Predicting the behavior and size of crown fires in the northern Rocky Mountains. Res. Pap. INT-RP-438. Ogden, UT: USDA, Forest Service, Intermountain Forest and Range Experiment Station. 46p.
- Rummer, B. 2008. Assessing the costs of fuel reduction treatments: A critical review. *Forest Policy and Economics* 10(6):355-362.
- Schmidt, K.M., J.P. Menakis, C.C. Hardy, W.J. Hann, and D.L. Bunnell. 2002. Development of coarse-scale spatial data for wildland fire and fuel management. Gen. Tech. Rep. RMRS-GTR-87. Fort Collins, CO: USDA, Forest Service, Rocky Mountain Research Station. 41 p.

- Scott, J.H. 1999. NEXUS: a system for assessing crown fire hazard. *Fire Management Notes*. 59(2):20-24.
- Scott, J.H. 2006. Comparison of crown fire modeling systems used in three fire management applications. Res. Pap. RMRS-RP-58. Fort Collins, CO: USDA, Forest Service, Rocky Mountain Research Station. 25 p.
- Scott, J.H., and E.D. Reinhardt. 2001. Assessing crown fire potential by linking models of surface and crown fire behavior. Res. Pap. RMRS-RP-29. Fort Collins, CO: USDA, Forest Service, Rocky Mountain Research Station. 59 p.
- Skog, K, R. Barbour, K. Abt, E. Bilek, F. Burch, R. Fight, R. Hugget, P. Miles, E, Reinhardt, and W. Sheppard. 2006. Evaluation of silvicultural treatments and biomass use for reducing fire hazard in western states. Res. Pap. FPL-RP-634. Madison, WI: USDA Forest Service, Forest Products Lab. 29 pp.
- Sullivan, A. 2007. A review of wildland fire spread modelling, 1990-present, 1: Physical and quasi-physical models. arXiv:0706.3074v1[physics.geo-ph]. 46 p.
- Tomé, M, and H.E. Burkhart. 1989. Distance-dependent competition measures for predicting growth of individual trees. *For. Sci.* 35(3):816–831.
- Uzoh, F.C., and W.W. Oliver. 2008. Individual tree diameter increment model for managed even-aged stands of ponderosa pine throughout the western United States using a multilevel linear mixed effects model. *For. Ecol. Manage.* 251(3):438-445.
- Van Wagner, C.E. 1977. Conditions for the start and spread of crown fire. *Can. J. For. Res.* 7(1): 23–34.
- Wykoff, W.R. 1990. A basal area increment model for individual conifers in northern Rocky Mountains. *For. Sci.* 36(4):1077-1104.

CHAPTER 1:

EVALUATING DIFFERENT TREE-LEVEL COMPETITION INDICES BY THEIR
EFFECTIVENESS AS PREDICTORS OF BASAL AREA INCREMENT

1.0 ABSTRACT

Inter-tree competition is commonly one of the most important predictors of individual tree growth. Numerous studies have developed indices to quantify the level of competition an individual tree experiences and evaluated how these indices condition tree growth. Results from these studies suggest that neither a single competition index nor a single class of indices is universally superior; indices perform differently according to tree species and forest conditions. We chose several widely used distance-independent and distance-dependent competition indices, and also developed distance- and orientation-dependent competition indices from estimates of light reception by tree crowns. We evaluated these measures of tree competition by their effectiveness as growth predictors for three common tree species in western Montana, USA. It was found that the best distance-dependent competition indices were more strongly correlated with tree growth and could explain a larger amount of growth variation than the best distance-independent indices (64% versus 56%). Our results suggest that competition is important and intense in these forests. Further, weak correlations between light values and basal area growth suggest that trees in this study region are competing primarily for resources other than light. To accommodate a log-linear relationship between radial growth and the growth predictors as well as a positive mean-variance relationship we used a gamma regression model that incorporated the best competition index to predict individual tree basal area increment.

Keywords: individual-tree growth, gamma regression, Montana, Douglas-fir, ponderosa pine, western larch.

1.1 INTRODUCTION

Traditionally, decision-making in forest management has been based on stand attribute information collected using sample-based stand examination. Because field-based inventory data are expensive and labor-intensive to acquire, sampling intensity is usually limited. However, new technologies in remote sensing and geographic information systems such as Light Detection and Ranging (LiDAR) are becoming more available and can provide inventory data at the tree level for entire stands. LiDAR has been widely used to estimate tree locations and dimensions such as height, crown width, diameter at breast height (DBH), and volume (Packalén and Maltamo 2006, Maltamo et al. 2006, Maltamo et al. 2004). The complete spatial coverage of these more-detailed inventory data can better capture variability in vegetation within natural stands. The tree location and dimension information that comprise these data also offer the potential for more efficient planning and management of forest resources. However, to realize that potential more accurate individual tree growth models are needed to assess the effects of management actions over time.

Tree competition is one of the most important growth predictors commonly used in individual tree growth models. Competition can be defined as the negative effect of one tree on another by consuming, or controlling access to, limiting resources such as light, water, and nutrients (Keedy 1989). Numerous studies have developed indices to quantify the level of competition an individual tree experiences and have evaluated how these indices condition tree growth (De Luis et al. 1998, Biging and Dobbertin 1992, Holmes and Reed 1991, Tomé and Burkhart 1989, Moore et al. 1973, Bella 1971).

Traditionally, competition indices described in the literature can be divided into two main classes: i) distance-independent that use only non-spatial information about the average tree size within a given area (e.g., a plot or stand), and ii) distance-dependent that also incorporate the relative locations of neighboring trees within the area. Recently, a new class of competition measures called semi-distance-independent has been developed (Lederman 2010, Stage and Lederman 2008). Broadly, these measures apply distance-independent index calculations to a spatially-defined group of trees centered around the subject tree but also within the confines of an inventory plot. The motivation for semi-distance-independent indices stems from the fact that sample-based inventory data are typically populated from sets of trees in plots and include no information on off-plot trees that are competing with subject trees. Yet when the inventory data include the locations and dimensions of all trees in the stand, distance-dependent and -independent indices can be evaluated for every tree using a true tree-centered spatial neighborhood.

Comparisons of different competition indices in terms of their effectiveness as predictors of growth in individual tree models have been conducted for several species and forest conditions. Martin and Ek (1984) found that including distance-independent competition indices considerably improved the fit of a diameter growth model for red pine (*Pinus resinosa* Ait.) plantations in northern Wisconsin. After comparing several competition indices, Daniels et al. (1986) reported that the best distance-dependent indices showed slightly higher R^2 values associated with basal area growth regression models than the best distance-independent indices for loblolly pine (*Pinus taeda* L.) plantations in northern Louisiana. Pukkala and Kolström (1987) evaluated several distance-dependent competition indices and found that the best indices could explain

about 50% of the variation of radial growth for Scots pine (*Pinus sylvestris* L.) in Finland. Working with mixed hardwood species in upper Michigan, Holmes and Reed (1991) also evaluated various competition indices of both main types and, based on their correlation with annual diameter growth, found that size ratio distance-independent indices performed as well or better than distance-dependent indices. Biging and Dobbertin (1995) evaluated various competition indices for mixed conifer species of northern California. They found that distance-independent indices considering crown cross-sectional area, crown volume, and crown surface area performed slightly better than the best distance-dependent indices. Rivas et al. (2005) evaluated different competition indices for mature even-aged stand of *Pinus cooperi* Blanco in Mexico and found that both types of competition indices performed similarly in terms of mean squared error reduction in basal area growth models. Lederman (2010) compared several distance-dependent and semi-distance-independent competition indices on an even-aged 110-year-old mixed conifer and hardwood species, and a 150-year-old mixed conifer stand Vienna, Austria. He found that the best competition indices of both types could explain similar levels of variation in basal area increment. Results from these various studies suggest that neither a single competition index nor a single class of indices is universally superior; indices perform differently according to tree species, forest conditions and sites (Biging and Dobbertin 1995, Daniels et al 1986).

Most competition indices are independent of the directional distribution of competitors and only a few attempts have been made to consider the orientation of competitor trees from a subject tree (i.e., Miina and Pukkala 2002, Newton and Jolliffe 1998). However, these attempts do not account for the position of the sun, which directly

affects light availability and potentially growth. A number of models have been developed to simulate the amount of light received by individual trees in spatially-explicit stand representations (Groot 2004, Brunner 1998, Korzukhin et al. 1995). Nevertheless, only a few studies have evaluated the relationship between light availability, in addition to competition indices, and tree growth (Stadt et al. 2007, Mailly et al. 2003).

The studies mentioned above have developed competition indices for individual tree growth models for many distinct species and forest conditions. However, to our knowledge, no previous study has evaluated the utility of distance-dependent and -independent competition indices for the commercial tree species and forest conditions of western Montana, nor have light availability indices been evaluated in this context. Currently, there are few models available to predict individual tree growth for tree species in western Montana (but see Uzoh and Oliver 2008, Wykoff 1990, Dixon 1989). The existing models were developed from regional studies or studies in nearby states, and use competition measures that have not been evaluated in western Montana forests. Therefore, developing a tree growth model that incorporates a competition measure appropriate for the species and conditions of western Montana has the potential to increase the accuracy of growth predictions.

The main objective in this study was to select the competition index most effective for predicting radial growth in three common conifer species in western Montana. For this purpose, we chose several widely used distance-independent and distance-dependent indices. We also characterized light reception by individual tree crowns and used derived light values as competition indices. A total of 16 different competition indices were evaluated based on their relationship with basal area increment,

and on the goodness of fit of log-transformed linear models incorporating competition and other growth predictors. Additionally, we developed a growth model incorporating the selected competition index to predict individual tree basal area increment. Owing to a log-linear relationship between radial growth and the predictors, as well as to a positive mean-variance relationship in the growth measurements, this objective was addressed using a log-link gamma regression model.

1.2 METHODOLOGY

1.2.1 Study Area

The study was conducted in the University of Montana's Lubrecht Experimental Forest (LEF), located approximately 48 km northeast of Missoula, Montana in the Blackfoot River drainage. Across this 8,500-ha forest, sample points were located systematically on a square grid of approximately 1,000 meters. Tree growth measurements were completed at 57 of these points. Within a 17.8 m search radius of each point, the first tree of each species in each of the diameter classes in Table 1.1 was selected and an increment core sample was taken at breast height.

Table 1.1. Diameter classes for selecting cored trees.

Diameter Class	Minimum Diameter (cm)	Maximum Diameter (cm)
1	12 (5 in.)	25 (9.9 in.)
2	26 (10 in.)	37 (14.9 in.)
3	38 (15 in.)	50 (19.9 in.)
4	51 (20 in.)	62 (24.9 in.)
5	63 (25 in.)	N/A

In the summer of 2008, neighborhood information was collected in 11 m fixed-radius competition plots centered on each cored tree. This plot radius is approximately 3.5 times the average estimated radius of the tree crowns, as recommended by Lorimer (1983). Other studies have used similar plot dimensions for quantifying inter-tree competition in Montana (Woodall et al. 2003). Inside these competition plots, DBH, height, species, and azimuth and horizontal distance from the cored tree were collected on all neighbor trees above 10 cm DBH. Figure 1.1 shows an example of a sample point with three competition plots centered at each cored tree: neighbor trees were always within 11 m of the cored tree but potentially more than 17.8 m from the sample point. Additionally, site information (i.e., average slope, aspect, and elevation) was collected at each sample point location.

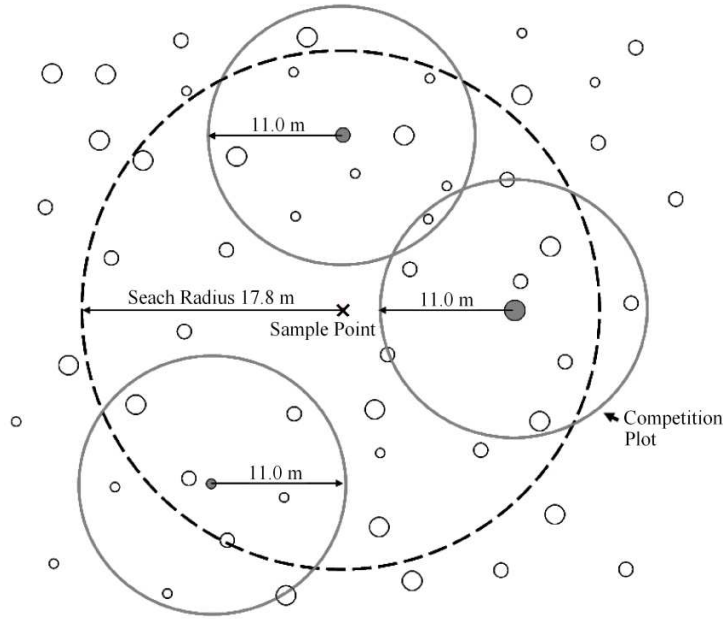


Figure 1.1. Sample point with three cored trees (solid dots) and their respective competition plots.

In this study, we considered the three most abundant species at LEF: Douglas-fir (*Pseudotsuga menziesii*), ponderosa pine (*Pinus ponderosa*) and western larch (*Larix occidentalis*). The tree growth measurements dataset consisted of 285 cored trees; 145 Douglas-fir (DF), 99 ponderosa pine (PP), and 41 western larch (WL). Figure 1.2 shows the DBH distribution for each species. Annual radial increments over the last 10 years was measured on the increment cores to the nearest 0.001 mm, using a microscope mounted on a dendrochronometer with a Velmex sliding stage and Accurite measuring system. From the radial increments we computed the average annual basal area increment (cm^2/year) of the last 10 years (BAI₁₀), which was used in this study as the response variable.

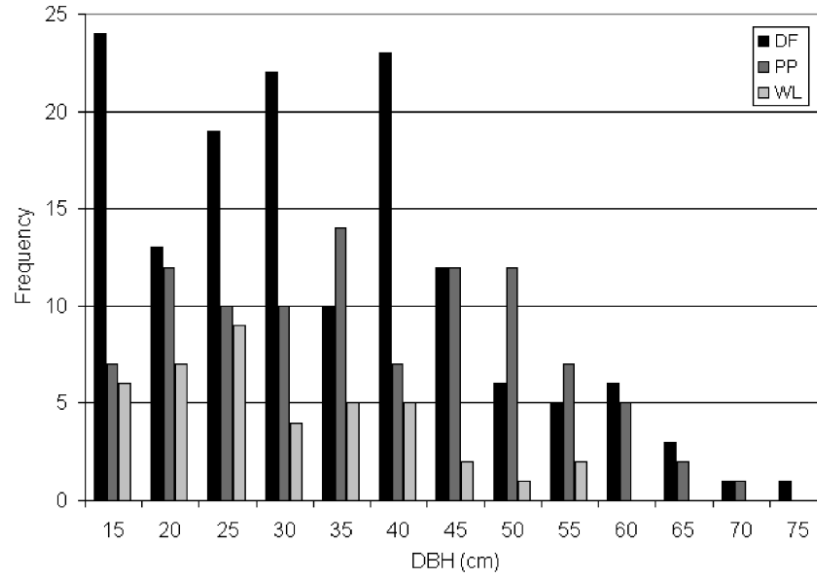


Figure 1.2. Diameter at breast height (DBH) distribution of cored trees at Lubrecht Experimental Forest.

1.2.2 Competition Indices

In this study, we describe the competition level experienced by each of the 285 individual cored trees using 16 different competition indices (see Table 1.2). The first four indices (CI₁-CI₄) are distance-independent, nine are distance-dependent (CI₅-CI₁₃), and three are light values used as competition indices (CI₁₄-CI₁₆).

Table 1.2. Competition indices evaluated in this study.

Index	Source	Equation
Distance-independent competition indices:		
CI ₁	Reineke (1933)	$10^{(\log N + 1.605 \times \log dg - 1.605)}$
CI ₂	Referred as canopy closure in Rivas et al. (2005)	$(\sum_{i=1}^n (\pi \times cw_i^2) / 4) / S$
CI ₃	Wykoff et al. (1982)	$(\sum_{j=1}^n (\pi \times d_{\max j}^2) / 4) = BAL$
CI ₄	Schröder and Gadov (1999)	$(1 - [1 - (BAL / G)]) / RS$
Distance-dependent competition indices:		
CI ₅	Number of neighbors	n
CI ₆	Gerrard (1969)	$\sum_{i=1}^n O_i / Z$
CI ₇	Bella (1971)	$\sum_{i=1}^n (O_i \times d_i) / (Z \times d)$
CI ₈	Hegyí (1974)	$\sum_{i=1}^n d_i / (d \times dist_i)$
CI ₉	Baathe (1980), cited in Pukkala and Kolström (1987)	$\sum_{i=1}^n h_i / (h \times dist_i)$
CI ₁₀	Rouvinen and Kuuluvainen (1997)	$\sum_{i=1}^n \arctan(d_i / dist_i)$
CI ₁₁	Rouvinen and Kuuluvainen (1997)	$\sum_{i=1}^n (d_i / d) \times \arctan(d_i / dist_i)$
CI ₁₂	Rouvinen and Kuuluvainen (1997)	$\sum_{i=1}^n \arctan(h_i / dist_i)$
CI ₁₃	Rouvinen and Kuuluvainen (1997)	$\sum_{i=1}^n (h_i / h) \times \arctan(h_i / dist_i)$
Light values:		
CI ₁₄	Sky's hemisphere	$(\sum_{i=1}^{2160} B_i) / 2160$
CI ₁₅	Sky's hemisphere / Sun position	$(\sum_{i=1}^{1080} B_{N_i}) + (\sum_{i=1}^{1080} 2 \times B_{S_i}) / 3180$
CI ₁₆	Sun position	$(\sum_{i=1}^{63} B_i) / 108$

N trees per ha in the plot; dg quadratic mean diameter (cm); n number of neighbors within the 11 meter radius competition plot; cw_i crown width of the i^{th} neighbor tree (m); S plot size (m^2); $d_{\max j}$ DBH of the j^{th} neighbor tree larger than the cored tree (m); BAL basal area of neighbor trees larger than the cored tree ($\text{m}^2 \text{ha}^{-1}$); G total basal area of the trees within the 11 meter radius plot ($\text{m}^2 \text{ha}^{-1}$); RS relative spacing index of the plot; O_i area of the influence-zone overlap between the i^{th} neighbor tree and the cored tree (m^2); Z area of the influence-zone of the cored tree (m^2); d_i DBH of the i^{th} neighbor tree (cm); d DBH of the cored tree (cm); $dist_i$ horizontal distance from the i^{th} neighbor tree to the cored tree (m); h_i height of the i^{th} neighbor tree (m); h height of the cored tree (m); B_i binary variable that is 1 if the i^{th} light ray is blocked, or 0 otherwise; B_{N_i} binary variable associated with north-oriented light rays (azimuths from 270° to 90°), 1 if blocked and 0 otherwise; B_{S_i} binary variable associated with south-oriented light rays (azimuths from 90° to 270°), 1 if blocked and 0 otherwise.

The four distance-independent indices are some of the most widely used measures found in the literature. CI_1 is Reineke's (1933) stand density index, which is based on the number of trees per ha in the competition plot (N) and their quadratic mean diameter. CI_2 is the canopy closure which represents the area of the crowns projected on the horizontal plane as a fraction of the competition plot area. CI_3 is the sum of basal areas of neighbor trees larger than the cored tree (BAL) as proposed by Wykoff et al. (1982). CI_4 is a modification of the previous index, proposed by Schröder and Gadow (1999), which incorporates the relative spacing index (RS) calculated as follows:

$$[1.1] \quad RS = \frac{\sqrt{10,000 \times N}}{H}$$

where, H is the dominant height (m) in the plot, considered in this study as the average height of the 20% tallest trees. It should be noted that these distance-independent indices were calculated from the dimensions of the distinct sets of trees within 11 m of each cored tree – some neighbor trees were further than 17.8 m from a sample point, and some trees within 17.8 m of a cored tree's sample point were not considered (see Figure 1.1).

The 9 distance-dependent competition indices were selected due to their observed utility in previous studies. CI_5 is a simple measure of competition calculated as the number of neighbor trees inside the competition plot. CI_6 (Gerrard 1969) and CI_7 (Bella 1971) are widely used influence-zone overlap indices which assume that the area (projected on the horizontal plane) over which trees compete for resources can be represented by a circle (Figure 1.3). The radius of the circle is usually a function of tree size and is thought to be equal to the expected growing space of open-grown trees (Rivas et al. 2005). To estimate the latter, we used species-specific maximum crown width equations from the Northern Idaho / Inland Empire variant of the Forest Vegetation

Simulator (Dixon 1989 – revised version, June 2009). CI_8 (Hegyí 1974) and CI_9 (Baathe 1980) are size-ratio competition indices which are based on the hypothesis that the competition effect of a neighbor tree increases with increasing size and decreasing distance (Tomé and Burkhart 1989). These two indices use DBH and height as indicators of size, respectively. CI_{10} through CI_{13} are also size-ratio indices but employ sums of subtended angles (Rouvinen and Kuuluvainen 1997). CI_{10} is the sum of horizontal angles originating from the cored tree center and spanning the DBH of each neighbor tree within the competition plot (Figure 1.4). CI_{11} is the sum of the horizontal angles multiplied by the ratio of the DBHs of the neighbor and the cored tree. CI_{12} is the sum of vertical angles from the cored tree base to the top of each neighbor tree within the competition plot (Figure 1.5). Similar to CI_{11} , CI_{13} includes the ratio of the heights between the neighbor and the cored tree. All 9 distance-dependent indices were calculated from the full set of trees within 11 m of each cored tree.

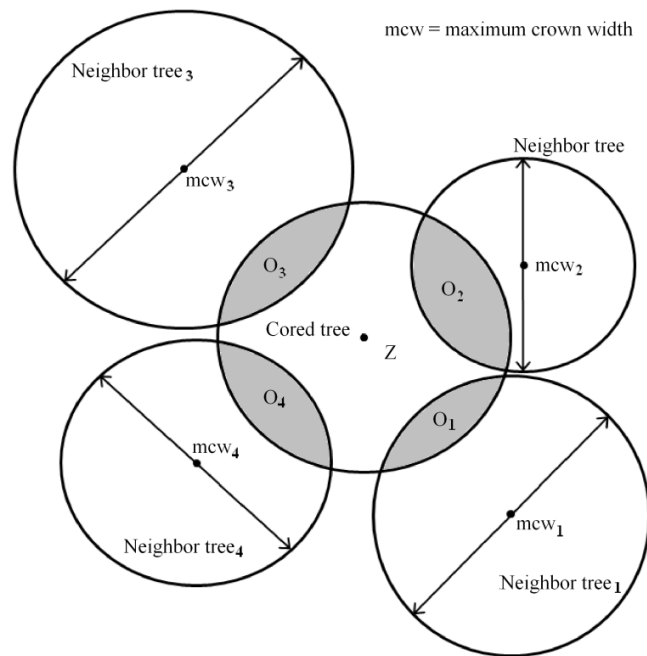


Figure 1.3. Area of influence-zone of a cored tree (Z) and areas of influence-zone overlap between the cored tree and each neighbor tree (O_i).

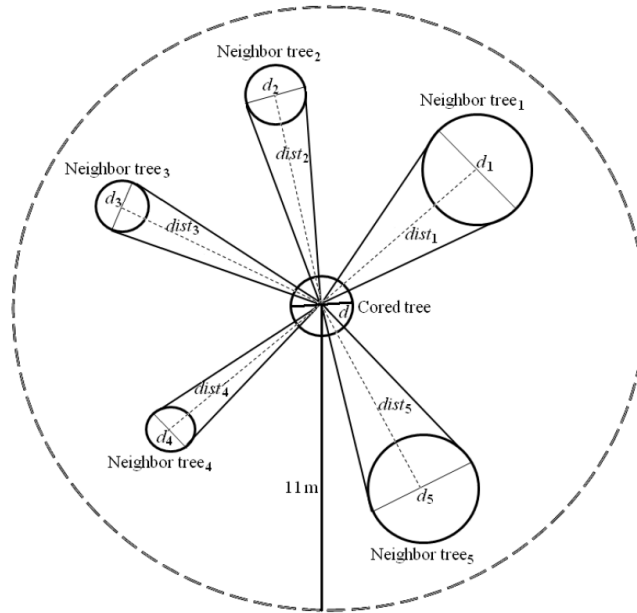


Figure 1.4. Schematic of horizontal angles from the cored tree center to the DBH of each neighbor tree within the competition plot used to compute CI_{10} and CI_{11} .

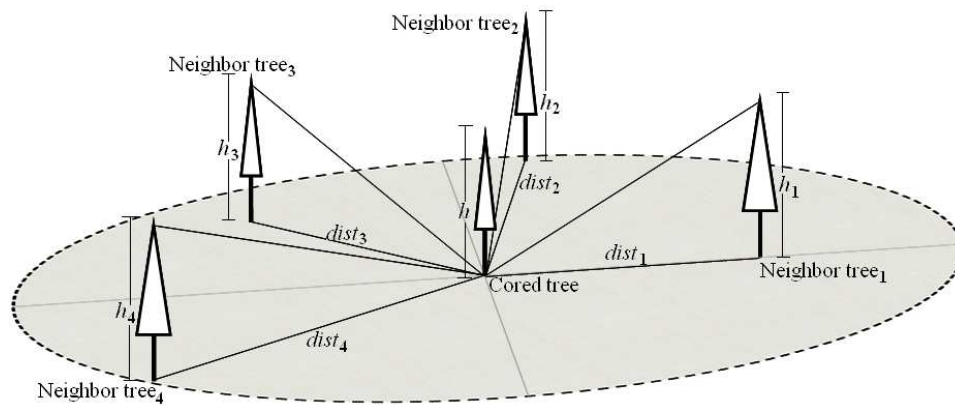


Figure 1.5. Schematic of the vertical angles from the base of the cored tree to the top of each neighbor within the competition plot used to compute CI_{12} and CI_{13} .

CI_{14} through CI_{16} are derived from models that estimate the amount of light intercepted by tree crowns (Groot 2004, Brunner 1998, Korzukhin et al. 1995). The portion of the sky's hemisphere directly above the cored tree was discretized by generating light rays from a focal point at 60% of the cored tree's height to the sky with

vertical angles running from 60° to 85° at intervals of 5° (Figure 1.6). These six light rays were generated in 360 directions (at every 1° azimuth from 0° to 359°) resulting in a total of 2160 light rays. We assume that neighbor tree crowns are completely opaque and cone-shaped with basal crown widths estimated from the crown width equations in Dixon (1989). CI_{14} was then computed as the percentage of total light rays blocked by neighbor tree crowns. Because the study area is located at latitude of approximately 46° north, the position of the sun is generally south of any given tree, thus CI_{15} indirectly incorporates the position of the sun by giving twice as much weight to those blocked light rays in directions between azimuths 90° to 270° . To compute CI_{16} , we used the average position of the sun at different dates within a typical growing season in LEF. We considered the sun position every 15 days starting from the May 1st to the September 1st (9 dates) at 12 different hours of the day from 7am to 6pm. A total of 108 sun position estimations consisting of azimuth and elevation were obtained from charts generated by the Solar Radiation Monitoring Laboratory of the University of Oregon¹.

¹ <http://solardat.uoregon.edu/SunChartProgram.html>

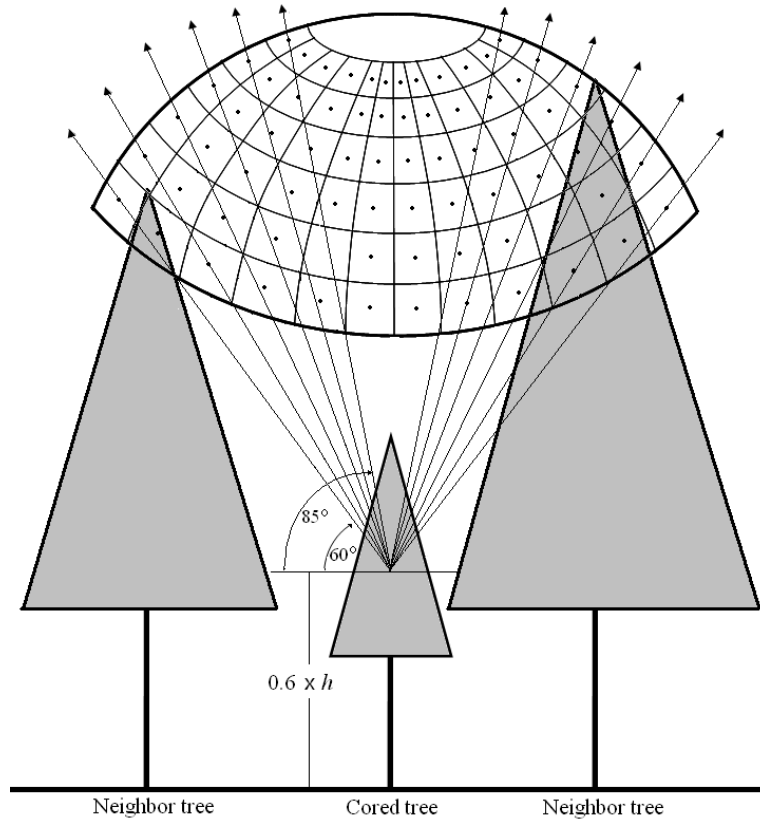


Figure 1.6. Discretization of a portion of the sky's hemisphere directly above the cored tree into 2160 light rays generated from a focal point at 60% of the cored tree's height.

1.2.3 Evaluation of Competition Indices

As mentioned above, we collected neighborhood information for the 285 cored trees using competition plots centered at each cored tree. Competition indices were then computed based on the tree-centered competition plot data. Although distance-independent competition indices are typically plot-centered, we believe that using a tree-centered measure can better represent the competition level experienced by a particular tree and thus make comparisons with distance-dependent measures more appropriate. In addition, having tree-centered competition plots for each cored tree avoided edge effect problems when computing distance-dependent competition indices. Furthermore, we

plan to use these indices with stem-mapped inventory data with complete stand coverage, not with mapped plot data.

After the 16 competition indices were computed for the 285 cored trees, we calculated the Pearson correlation coefficients (r) between all pairs of indices to examine the overall dependence structure and determine species-specific relationships among indices. We also calculated the correlation between each competition index and $\ln(\text{BAI}_{10})$ to identify the indices' pairwise linear relationships and potential effectiveness as growth predictors. We fit several log-transformed linear models considering each individual competition index along with other potential growth predictors. The latter included the two tree variables DBH (d) and tree height (h) at present time (year 2008), as well as the 4 average site characteristics slope (S), aspect (A), elevation (E), and dominant height (H). For model selection purposes, we started with all potential predictors and through a backward selection method we removed all insignificant variables ($\alpha = 0.05$). Models were compared using the adjusted coefficient of determination (adj-R^2).

1.2.4 Basal Area Increment Growth Model

These models described above were used as an exploratory analysis to select the competition index that, along with other significant growth predictors, provided the best fit for all three species. However, instead of using these log-transformed linear models, we used generalized linear models (GLM) to fit the individual tree basal area increment growth models. GLMs are able to accommodate mean functions that are linear in the

predictors on a transformed scale and can be applied to data that conform to any probability distribution in the exponential family such as the normal, gamma, or inverse Gaussian functions (McCullagh and Nelder 1989). GLMs directly describe the mean of the dependent variable, thus avoiding the biases introduced by log-transformed models that require subsequent correction using elements of the error structure (McCullagh and Nelder 1989). Because our data exhibited increasing variance with increasing scores of our dependent variable (BAI_10), we used a GLM with a gamma distribution, which is a flexible 2-parameter probability density function able to model heteroscedastic continuous data (see also Gea-Izquierdo and Cañellas 2009).

1.3 RESULTS AND DISCUSSION

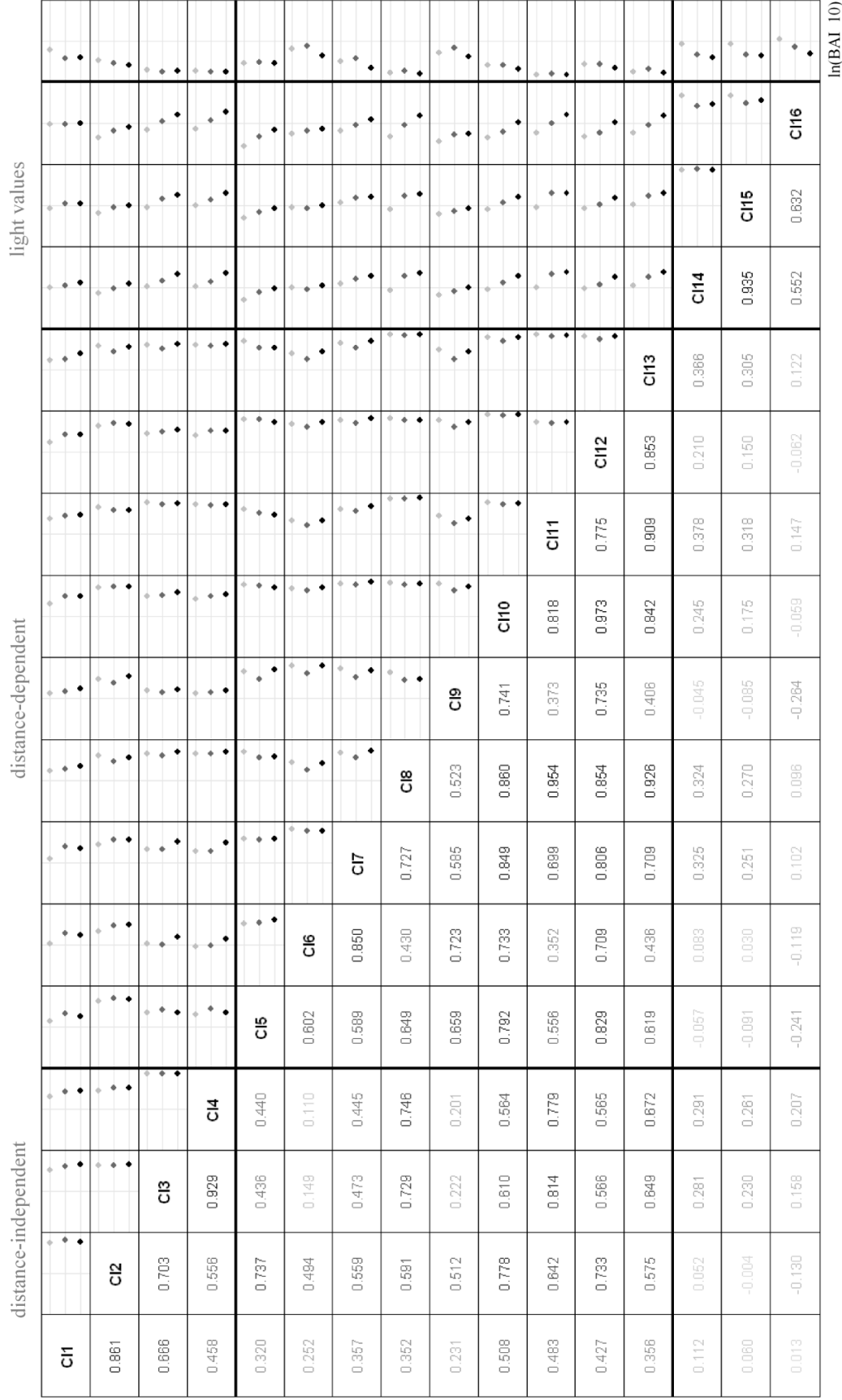
1.3.1 Competition Indices

The correlation structure of the 16 competition indices is presented in Figure 1.7. The correlation matrix shows global correlations on the lower diagonal and species-specific correlations on the upper diagonal. Each panel on the upper diagonal runs from -1 to 1 (left to right) with a vertical line in the middle at zero. In viewing these results, we can notice a broad range of correlation values among the different indices but, in general, correlation values seem to be consistent for all three species. Most competition indices of the same class present stronger correlations among themselves than with indices of different classes. For example, distance-independent indices CI_1 - CI_2 and CI_3 - CI_4 ;

distance-dependent indices CI₆-CI₇, CI₁₀-CI₁₁, CI₁₀-CI₁₂, and CI₁₁-CI₁₃; and light value pairs CI₁₄-CI₁₅, and CI₁₅-CI₁₆, are all strongly correlated regardless of species. These results are expected because of the similarities in the formulations (see Table 1.2).

Although certain pairings of distance-dependent and distance-independent indices are strongly correlated (i.e. CI₃-CI₁₁ and CI₄-CI₁₁), correlations are stronger within than across classes.

The light values are poorly correlated with competition indices of other classes. The low ($|r| < 0.38$) and sometimes negative correlations suggest that these light values describe competition differently than the other indices. Most distance-dependent and distance-independent competition indices utilize tree size (i.e. DBH, crown width, height) as a measure current growth, with overall size being the result of all factors affecting growth (i.e. availability of light, water, and nutrients). In contrast, light values only capture one of these factors, light availability, which might partially explain the low correlations. This distinction between light values and other competition indices was also apparent from a principal component analysis of the 16 indices (not shown). For all species, the first component effectively averaged all the distance-dependent and distance-independent indices, with slightly heavier weights given to the distance-dependent indices. On the other hand, the second component was primarily composed of the three light values, with only small contributions from other indices.



ln(BAL_10)

Figure 1.7. Correlation matrix of the 16 competition indices showing global correlations on the lower diagonal and species-specific correlations on the upper diagonal (Douglas-fir = black dots; ponderosa pine = dark grey dots; western larch = light grey dots).

Correlations between each competition index and growth are also shown in Figure 1.7 (right-most column). As expected, for all three species most competition indices are negatively correlated with basal area increment. Thus, trees under high levels of competition exhibit low growth rates. Consistently, for all species CI_3 and CI_4 are the distance-independent indices most strongly correlated with growth ($-0.75 < r < -0.71$). The distance-dependent indices with strongest correlations are CI_8 and CI_{11} ($-0.82 < r < -0.72$). Overall, light-values are the least correlated with growth ($-0.38 < r < 0.09$). This poor correlation suggests that light is less of a limiting factor and that trees may be competing primarily for soil resources such as water and nutrients. We also evaluated light availability at other height percentiles. However, we selected 60% of the height because we wanted to measure light availability at some point within the trees' crowns and, when evaluating light-values at higher focal points, most trees yielded zero values (100% light availability).

Figure 1.8 shows the relationships between growth and competition indices of each class for the three species. These plots show the negative growth response to increasing competition as measured by CI_3 (distance-independent index of Wykoff et al. 1982) and CI_{11} (sum of horizontal angles distance-dependent index of Rouvinen and Kuuluvainen 1997). As evidenced by the correlation values in Figure 1.7, CI_{11} can explain a larger amount of the observed variation in growth than CI_3 , with across-species R^2 values of 0.52 and 0.64, respectively. On the other hand, there is no discernible pattern between growth and competition as measured by CI_{16} . As suggested by Weldon et al. (1988), the relatively flat slope and low R^2 value of this relationship indicates that competition for light is neither intense nor important. Similar results have been found in

other forest conditions (Stadt et al. 2007, Mailly et al. 2003). Interestingly, our data show only minor differences in growth rates among different species, with all three having similar slopes and intercepts.

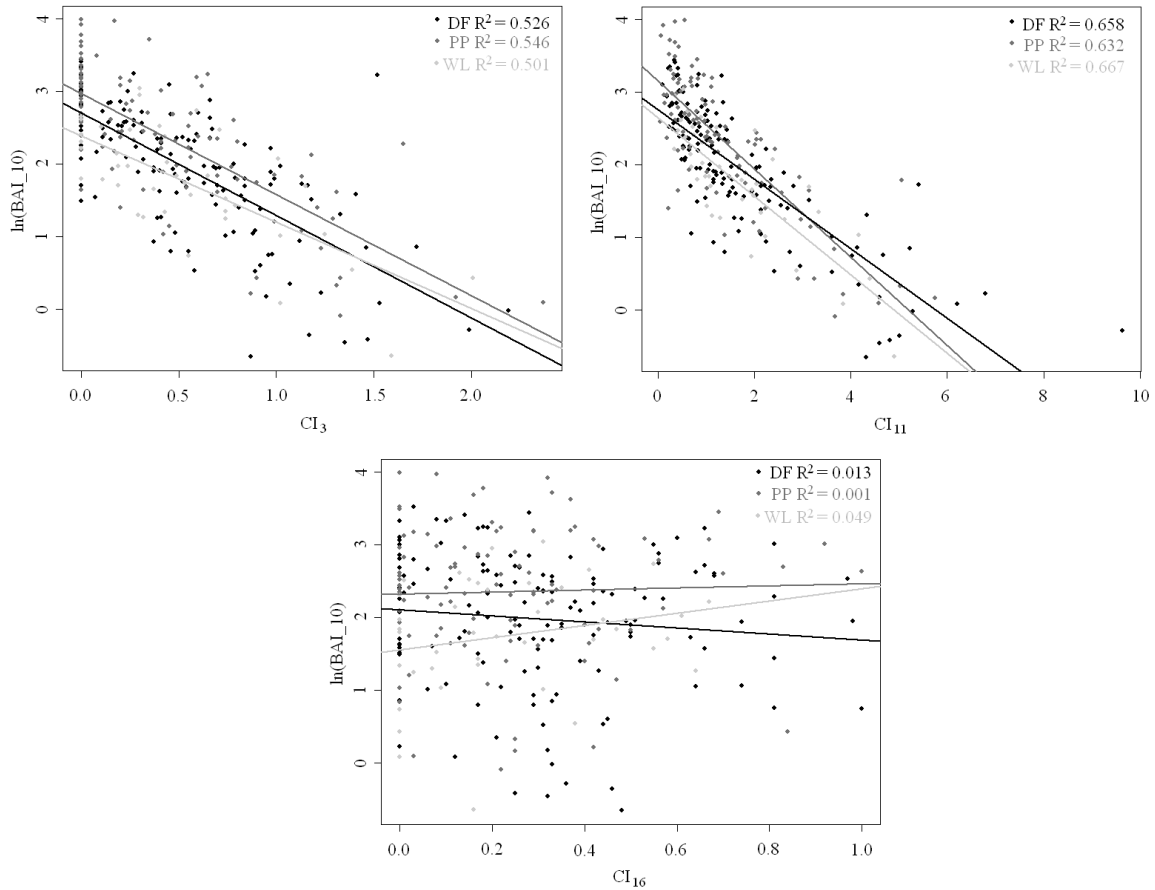


Figure 1.8. Scatter plots and least squares fit of growth versus three competition indices.

Selected log-transformed linear models are given in Table 1.3. In general, for Douglas-fir and western larch, DBH and competition were the only significant growth predictors. However, site variables such as E and H were also significant predictors of growth for ponderosa pine. This indicates that growth rates of ponderosa pine are more variable across LEF, thus site variables also explain growth variability. For the three

species, all 4 distance-independent indices (CI₁ through CI₄) and most distance-dependent indices (CI₅ through CI₁₃), except for CI₆ and CI₉ for ponderosa pine and western larch, were significant growth predictors. As expected because of the low correlations, light values (CI₁₄ through CI₁₆) were insignificant predictors and were dropped from models for Douglas-fir, western larch, and ponderosa pine.

Based on the adj-R² values, some of the best distance-dependent indices (i.e. CI₈, CI₁₁, and CI₁₃) performed better across all species than the best distance-independent indices (i.e. CI₂ and CI₃). However, these latter indices have higher adj-R² values than some widely known distance-dependent indices (i.e. Gerrard's (1969) CI₆ and Bella's (1971) CI₇). Among the distance-dependent indices, those including sums of angles (CI₁₀ through CI₁₃) explained a larger proportion of growth variation than most of the other size-ratio and influence-zone overlap competition indices, with the exception of Hegyi (1974)'s competition index, CI₈. The log-transformed linear model with CI₁₁ provided the best fit for all three species. For Douglas-fir and western larch, DBH and CI₁₁ together could explain about 70% and 72% of the total variation in annual growth. For ponderosa pine, DBH, CI₁₁ and H explained approximately 71% of the total growth variation.

Table 1.3. Log-transformed linear models selected from including each competition index and other selected growth predictors.

Competition Index	Douglas-fir		Ponderosa pine		Western larch	
	Explanatory variables	Adj-R ²	Explanatory variables	Adj-R ²	Explanatory variables	Adj-R ²
1	DBH, CI ₁	0.528	DBH, CI ₁	0.619	DBH, CI ₁	0.585
2	DBH, CI ₂	0.598	DBH, E, H, CI ₂	0.653	DBH, CI ₂	0.602
3	DBH, E, CI ₃	0.588	DBH, S, CI ₃	0.652	DBH, CI ₃	0.607
4	E, CI ₄	0.594	DBH, E, CI ₄	0.626	H, CI ₄	0.583
5	DBH, CI ₅	0.553	DBH, E, H, CI ₅	0.614	DBH, H, CI ₅	0.555
6	DBH, CI ₆	0.519	DBH, E, H	0.573	DBH	0.464
7	DBH, CI ₇	0.608	DBH, E, H, CI ₇	0.609	DBH, CI ₇	0.509
8	DBH, CI ₈	0.688	DBH, E, H, CI ₈	0.666	DBH, CI ₈	0.645
9	DBH, CI ₉	0.535	DBH, E, H	0.573	DBH	0.464
10	DBH, CI ₁₀	0.651	DBH, E, H, CI ₁₀	0.644	DBH, CI ₁₀	0.552
11	DBH, CI ₁₁	0.700	DBH, H, CI ₁₁	0.713	DBH, CI ₁₁	0.716
12	DBH, CI ₁₂	0.631	DBH, E, H, CI ₁₂	0.626	DBH, CI ₁₂	0.523
13	DBH, CI ₁₃	0.677	DBH, E, H, CI ₁₃	0.645	DBH, CI ₁₃	0.639
14	DBH	0.452	DBH, E, H	0.573	DBH	0.464
15	DBH	0.452	DBH, E, H	0.573	DBH	0.464
16	DBH	0.452	DBH, E, H	0.573	DBH	0.464

1.3.2 Individual Tree Growth Model

Although the best log-transformed linear model for ponderosa pine growth included H as a significant predictor, the contribution of this variable to the overall predictive quality of that model was marginal. By removing H from the model the amount of variation explained is reduced by only 1%. Therefore, we used DBH and CI₁₁ as the only two predictors of growth to fit a more parsimonious GLM for all species. Figure 1.9 shows the relationships between BAI_10 and the predictors where in both plots we can see an increasing variance for increasing scores of BAI_10. This heterogeneous variance was addressed by using a gamma GLM. We initially included species-specific intercepts, DBH, and competition terms in this model. However, as suggested by Figures 1.7 and 1.8 where no appreciable differences in growth rates among species are evident, deviance partitioning tests showed that these species-specific terms were insignificant ($\alpha = 0.05$). Thus, only one intercept and one global coefficient for each of DBH and CI₁₁ were retained. Also, there was no evidence of a significant interaction between CI₁₁ and DBH so only additive effects were retained.

The final individual tree growth model

$$[1.2] \quad \text{BAI}_{10} = \exp^{[a_1 + (a_2 \times d) + (a_3 \times \text{CI}_{11})]}$$

had a scale parameter estimate of 0.2736, a mean bias of 0.0645 cm²/year, and a root mean square error (RMSE) of 6.418 cm²/year. The model coefficient estimates are presented in Table 1.4. A plot of the deviance residuals against fitted values from the model (Figure 1.10) shows no appreciable structure; however, a loess smooth through the plot shows that the model slightly underestimates growth. The mean bias and RMSE

associated with the model that included the insignificant species-specific DBH and CI_{11} terms were $0.0532 \text{ cm}^2/\text{year}$ and $6.0145 \text{ cm}^2/\text{year}$, respectively, which indicates only a marginal improvement in accuracy associated with this use of four additional degrees of freedom. In addition, we anticipate applying this model to stem-mapped data derived from LiDAR acquisitions for LEF. Initial analyses of these stem maps indicate that tree location and dimension attributes are relatively reliable but that species identification is weak or lacking. Thus, the inclusion of species-specific terms in the basal area increment model [Eq. 2] would be of no practical advantage.

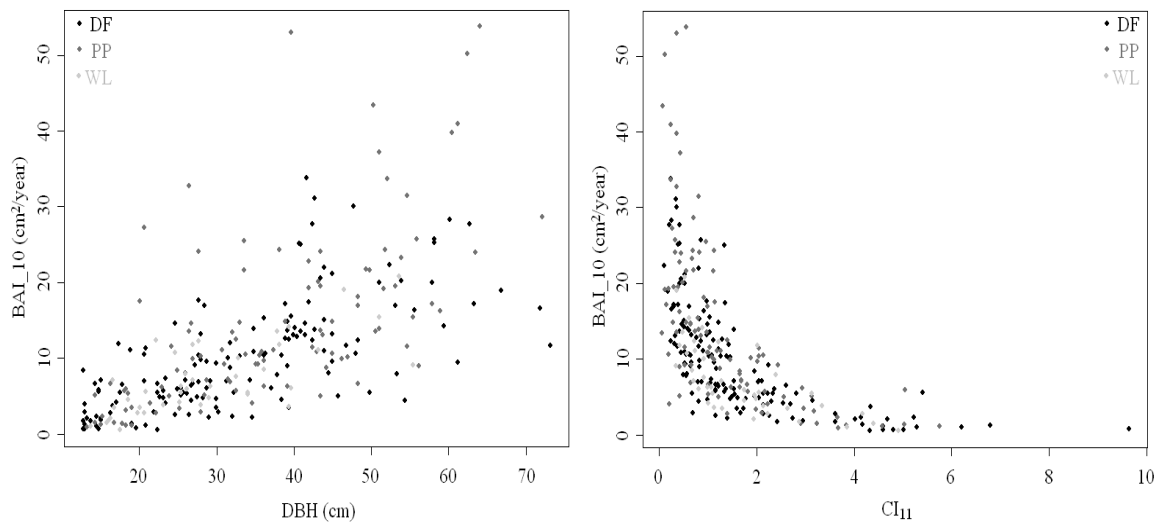


Figure 1.9. BAI_10 as a function of DBH and CI_{11} for all species.

Table 1.4. Coefficients (a_1 , a_2 , a_3) and estimated variance parameter (s) from the final GLM with gamma distribution and log link fitted for individual tree growth.

Coefficients			
	Estimate	Std. Error	Pr(> t)
a_1 - (Intercept)	1.974503	0.132216	< 2.00 e-16
a_2 - DBH	0.022768	0.002846	3.23 e-14
a_3 - CI_{11}	-0.361392	0.028753	< 2.00 e-16
S	0.273628		
Bias	0.064474		
RMSE	6.418001		

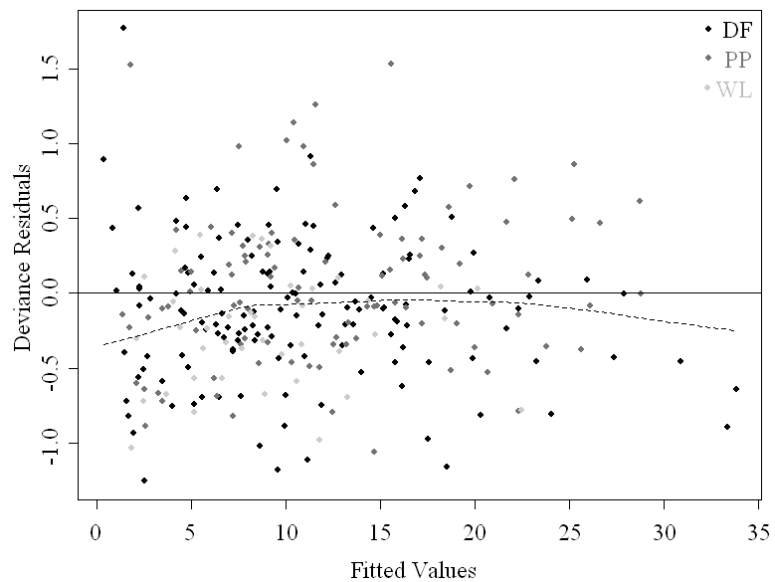


Figure 1.10. Residuals from the final GLM with gamma distribution and log link fitted for individual tree growth.

Typically, growth models are built to condition on the state of the forest at the beginning of a growth period and to project that state forward. In this study, we examined the relationship between competition indices based on state variables measured in 2008 and annualized radial growth over the period 1998-2007. It was not possible to estimate competition levels in LEF in 1998 because of the lack of a permanent plot database. Furthermore, where permanent plots have been established elsewhere in

western Montana requisite information on the locations and dimensions of neighbor trees outside the permanent plot boundaries is lacking. Regarding our primary objective of assessing the relative predictive power of the 16 competition indices in Table 1.2, we believe our retrospective modeling approach is sound. Approaches both prospective and retrospective that estimate the effects of competition on multi-year growth will suffer a comparable lack of precision due to changes in the competitive regime throughout the growth period. Yet it is necessary to study growth over several years to distinguish between competitive effects and the effects of annual climatic fluctuations. Evaluation of the competition indices for each cored tree using 1998 neighborhood data would produce values different from those used in this study, but the tree growth and tree mortality processes that produce this difference have continuously changed the competition regime of each tree throughout the period. Thus, we believe that the relative magnitudes of the correlations of the 16 competition indices against basal area increment would be similar to those observed if 1998 neighborhood data had been available. In contrast, we recognize that our retrospective approach to quantifying competitive effects in model (Eq. 1.2) will likely bias downwards the estimates of future periodic growth if the model is applied in a prospective manner (i.e., if values for CI_{11} are obtained from state variables at the start of the projection period). The imputation of 1998 values for CI_{11} using 2007 neighborhood data can be viewed as an introduction of measurement error into the competition predictor. This type of measurement error generally leads to attenuation biases in parameter estimation (Carroll et al. 2006). Bias notwithstanding, there is a need for individual tree growth models for these commercial species in western Montana and model (Eq. 1.2) provides a provisional instrument. The sample points

used in this study were selected to establish a permanent plot network, and in time will supply data for modeling growth prospectively and assessing the accuracy of the model developed above.

Finally, when applying model (Eq. 1.2) to project the growth of trees measured in a plot-based inventory, edge correction procedures will need to be applied unless off-plot data are available. As our competition measures and basal area growth model are based on tree-centered definitions of competition intensity, the model is best suited for growing trees in stands with complete spatial inventory information derived from technologies such as LiDAR.

1.4 CONCLUSIONS

In this study, we evaluated several measures of tree competition by their effectiveness as growth predictors for three common tree species in western Montana. It was found that for all species the best distance-dependent competition indices were more strongly correlated with tree growth and could explain a larger amount of growth variation than the best distance-independent indices. Our results suggest that competition exists and that it is important and intense for all three species, as measured by several competition indices. However, the low correlations between light values and growth suggest that trees might not be competing primarily for light. These results are in concordance with other studies reporting soil moisture as the most important growth

limiting factor for tree species in western Montana (Littell et al. 2008, Sala et al. 2005, Nagel and O'Hara 2002).

Based on the goodness of fit of a series of log-transformed linear models, Rouvinen and Kuuluvainen's (1997) distance-dependent competition index based on the sum of horizontal angles (CI_{11}) performed the best. Together with DBH this competition index explained approximately 70% of the total growth variation in all three species. Consequently, to predict the growth of an individual tree, the basal area growth model ultimately uses only the subject tree's DBH as well as the DBHs and distances of trees within 11 m. This enhances the practicality of the model because DBHs are commonly available and between-tree distances can be easily obtained from stem maps. Additionally, the use of a gamma GLM allowed us to directly model the mean annual basal area increment, thus avoiding biases associated with transformations, and to account for the increasing variance in growth rates among larger or more open-grown trees.

Although CI_{11} performed the best for all three species considered in this study, the log-transformed linear model including CI_{13} , which is based on tree heights and between-tree distances, provided the second best fit. This is particularly important for estimating individual tree growth across entire stands using LiDAR-derived stem maps and tree dimensions because tree height is the native measure obtained from LiDAR data. In those applications, because of the unexplained variation associated with height-DBH allometries, it would be of interest to examine a growth model considering CI_{13} and evaluate whether the quality of the model improves.

Finally, in this study we were interested primarily in modeling short-term tree growth and we ignored other more complex processes such as mortality and regeneration. These processes as well as other events such as fire occurrence and insect attack alter tree density and consequently inter-tree competition levels. For these reasons and the potential for changing climatic conditions moving forward, the model developed here from past growth records is not suited to long-term growth estimations.

1.5 REFERENCES

- Biging, G.S., and M. Dobbertin. 1992. A comparison of distance-dependent competition measures for height and basal area growth of individual conifer trees. *For. Sci.* 38(3):695–720.
- Biging, G.S., and M. Dobbertin. 1995. Evaluation of competition indices in individual tree growth models. *For. Sci.* 41(2):360-377.
- Brunner, A. 1998. A light model for spatially explicit forest stand models. *For. Ecol. Manage.* 107(1-3):19-46.
- Burton, P.J. 1993. Some limitations inherent to static indices of plant competition. *Can. J. For. Res.* 23(10):2141-2152.
- Carroll, R.J., D. Ruppert, LA. Stefanski, and C.M. Crainiceanu. 2006. *Measurement error in nonlinear models: a modern perspective (2nd edition)*. Chapman & Hall/CRC, Boca Raton.

- Daniels, R.F., H.E. Burkhart, and T.R. Clason. 1986. A comparison of competition measures for predicting growth of loblolly pine trees. *Can. J. For. Res.* 16(6):1230-1237.
- De Luis, M., J. Raventós, J. Cortina, M.J. Moro, and J. Bellot. 1998. Assessing components of a competition index to predict growth in an even-aged *Pinus nigra* stand. *New For.* 15(3):223–242.
- Dixon, G.E. 1989. Northern Idaho/Inland Empire (NI/IE) Variants Overview. Forest Vegetation Simulator. USDA For. Serv. Forest Management Service Center. 51 p. Revised version (June 2009).
- Gea-Izquierdo, G., and I. Cañellas. 2009. Analysis of Holm Oak intraspecific competition using gamma regression. *For. Sci.* 55(4):310-322.
- Gerrard, D.I. 1969. Competition quotient: a new measure for the competition affecting individual forest trees. Michigan State University, Agric. Res. Station Res. Bull 20:1–32.
- Groot, A. 2004. A model to estimate light interception by tree crowns, applied to black spruce. *Can. J. For. Res.* 34(4):788-799.
- Hegyí, F. 1974. A simulation model for managing jackpine stands. P. 74-90 in *Proceeding of Growth models for tree and stand simulation conference*: Fries, J. (ed.). IUFRO meeting S4.01.04, Royal College of Forestry, Stockholm.
- Holmes, M.J., and D.D. Reed. 1991. Competition indices for mixed species northern hardwoods. *For. Sci.* 37(5):1338-1349.
- Keddy, P.A. 1989. *Competition*. Chapman and Hall, London.

- Korzukhin, M.D., and M.T. Ter-Mikaelian. 1995. An individual tree-based model of competition for light. *Ecol. Model.* 79(1-3):221-229.
- Lederman, T. 2010. Evaluating the performance of semi-distance-independent competition indices in predicting the basal area growth of individual trees. *Can. J. For. Res.* 40(4):796-805.
- Ledermann, T., and A.R. Stage. 2001. Effects of competitor spacing in individual-tree indices of competition. *Can. J. For. Res.* 31(12):2143-2150.
- Littell, J.S., D.V. Peterson, and M. Tjolkner. 2008. Douglas-fir growth in mountain ecosystem: water limits tree growth from stand to region. *Ecol. Monogr.* 78(3):349-368.
- Lorimer, C.G. 1983. Tests of age-independent competition indices for individual trees in natural hardwood stands. *For. Ecol. Manage* 6(4):343-360.
- Mailly, D., S. Turbis, and D. Pothier. 2003. Predicting basal area increment in a spatially explicit, individual tree model: a test of competition measures with black spruce. *Can. J. For. Res.* 33(3):435-443.
- Maltamo, M., K. Mustonen, J. Hyypä, J. Pitkänen, and X. Yu. 2004. The accuracy of estimating individual tree variables with airborne laser scanning in a boreal nature reserve. *Can. J. For. Res.* 34(9):1791-1801
- Maltamo, M., K. Eerikäinen, P. Packalén, and J. Hyypä. 2006. Estimation of stem volume using laser scanning-based canopy height metrics. *Forestry* 79(2):217-229.
- Martin, G.L., and A.R. Ek. 1984. A comparison of competition measures and growth models for predicting plantation red pine diameter and height growth. *For. Sci.* 30(3):731-743.

- McCullagh, P., and J.A. Nelder. 1989. Generalized linear models. Chapman & Hall, London, UK.
- Miina, J., and T. Pukkala. 2002. Application of ecological field theory in distance-dependent growth modeling. *For. Ecol. Manage* 161(1-3):101-107.
- Moore, J.A., C.A. Budelsky, and R.C. Schlesinger. 1973. A new index representing individual tree competitive status. *Can. J. For. Res.* 3(4):495-505.
- Nagel, L.M, and K.L. O'Hara. 2002. Diurnal fluctuations in gas exchange and water potential in different stand structure of *Pinus ponderosa*. *Trees* 16(4-5):281-290.
- Newton, P.F, and P.A. Jolliffe. 1998. Assessing processes of interspecific competition within spatially heterogeneous black spruce stands. *Can. J. For. Res.* 28(2):259-275.
- Packalén, P., and M. Maltamo. 2006. Predicting the plot volume by species using airborne laser scanning and aerial photographs. *For. Sci.* 52(6):611-622
- Pukkala, T., and T. Kolström. 1987. Competition indices and the prediction of radial growth in Scots pine. *Silva Fenn.* 21(1):55-67.
- Reineke, L.H. 1933. Perfecting a stand density index for even-aged forest. *J. Agric. Res.* 46:627-638.
- Rivas, J.J.C., J.G. González, O. Aguirre, and F.J. Hernández. 2005. The effect of competition on individual tree basal area growth in mature stands of *Pinus cooperi* Blanco in Durango (Mexico). *Eur. J. For. Res.* 124(2):133-142.
- Rouvinen, S., and T. Kuuluvainen. 1997. Structure and asymmetry of tree crowns in relation to local competition in a natural mature Scot pine forest. *Can. J. For. Res.* 27(6):890-902.

- Sala, A., G.D. Peters, L.R. McIntyre, and M.G. Harrington. 2005. Physiological responses of ponderosa pine in western Montana to thinning, prescribed burning, and burning season. *Tree Physiol.* 25(3):339-348.
- Schröder, J., and K.von Gadow. 1999. Testing a new competition index for Maritime pine in northwestern Spain. *Can. J. For. Res.* 29:280–283.
- Shao, G., and K. Reynolds. 2006. Computer applications in sustainable forest management: Including perspectives on collaboration and integration. Springer-Verlag New York, LLC. 277pp.
- Stadt, K.J., C. Huston, K.D. Coates, Z. Feng, M.R.T. Dale, and V.J. Lieffers. 2007. Evaluation of competition and light estimation indices for predicting diameter growth in mature boreal mixed forest. *Ann. For. Sci.* 64(5):477-490.
- Stage, A.R., and Ledermann, T. 2008. Effects of competitor spacing in a new class of individual-tree indices of competition: semi-distance-independent indices computed for Bitterlich versus fixed-area plots. *Can. J. For. Res.* 38(4): 890–898.
- Tomé, M, and H.E. Burkhart. 1989. Distance-dependent competition measures for predicting growth of individual trees. *For. Sci.* 35(3):816–831.
- Uzoh, F.C., and W.W. Oliver. 2008. Individual tree diameter increment model for managed even-aged stands of ponderosa pine throughout the western United States using a multilevel linear mixed effects model. *For. Ecol. Manage.* 251(3):438-445.
- Weldon, C.W., W.L. Slauson, and R.T. Ward. 1988. Competition and abiotic stress among trees and shrubs in northwest Colorado. *Ecology* 69(5):1566-1577
- Woodall, C.W., C.E. Fidler, and K.S. Milner. 2003. Intertree competition in uneven-aged ponderosa pine stands. *Can. J. For. Res.* 33(9):1719-1726.

Wykoff, W.R., N.L. Crookston, and A.R. Stage. (1982) User's guide to the stand prognosis model. USDA For. Serv. Gen. Tech. Rep. INT-133. 119 p.

Wykoff, W.R. 1990. A basal area increment model for individual conifers in northern Rocky Mountains. For. Sci. 36(4):1077-1104.

CHAPTER 2:

A MODELING APPROACH TO ESTIMATING SKIDDING COSTS OF INDIVIDUAL TREES FOR THINNING OPERATIONS

2.0 ABSTRACT

Thinning is a common silvicultural treatment used for different forest management purposes. Traditionally, thinning prescriptions are derived from sample plots and applied to stands with various vegetation conditions. A few studies have optimized cut-tree selection to create site-specific thinning prescriptions. However, these studies greatly simplify the estimation of harvesting costs by ignoring the location of the cut-trees relative to the extraction point. Consequently, resulting tree-level thinning prescriptions might not provide the most economically efficient selection of cut-trees. In this paper, we developed a model to estimate skidding costs of individual cut-trees based on size, location, and spatial distribution of selected cut-trees. The model uses a log-bunching algorithm to identify log-pile locations and then creates a skid-trail network that connects log-piles to the extraction point at a minimum skidding cost. We applied the model to a treatment unit, where LiDAR data was used to obtain terrain and tree data, considering two thinning scenarios with target densities of 400 and 300 leave-trees per hectare, respectively. Comparison of the model results with those obtained from the existing cost models indicates that our model results are within the reasonable range for skidding costs. As our model considers terrain slope to create skid-trails, it can be effectively used to delineate non-accessible or difficult terrain areas for skidding operations. The model can also be used to automatically generate optimal skid-trail networks connecting multiple log-piles to the extraction point.

Key words: selective harvesting, skid-trail networks, forest operations, forest management, LiDAR.

2.1 INTRODUCTION

Thinning is a common silvicultural treatment used for different purposes in forest management. It has been used for many decades to increase tree growth for timber production (Bailey and Tappeiner 1998, Barbour et al. 1994, Brodie et al. 1978), to lower the risk of high-intensity wildfires by reducing fuel loads (Agree and Skinner 2005, Pollet and Omi 2002, Graham et al. 1999), and increasingly in the last decade, to modify stand structure and introduce spatial heterogeneity for wildlife habitat improvement (Carey 2001, Hayes et al. 1997).

Independent of treatment objectives, thinning prescriptions are traditionally developed from ground sample plots. However, because sample plots do not usually capture the full range of variability in terrain and vegetation within each stand, thinning prescriptions might not produce the most desirable results when extrapolated and applied to multiple stands with different site potentials and vegetation structures (Pukkala and Miina 2005). Efforts to develop site-specific thinning prescriptions by optimizing cut-tree selection at the individual-tree level have yielded two approaches: the first one formulates the cut-tree selection process as a non-linear problem and solves it using the Hooke and Jeeve (1961) algorithm (Pukkala and Miina 1998, Valsta 1992), while the other approach uses an integer-programming model (Hof and Bevers 2000). Several studies have used the former approach to develop thinning prescriptions that maximize the economic return on different forest types (Cao et al. 2006, Hyytiäinen et al. 2005, Palahí and Pukkala. 2003, Rautiainen et al. 2000). However, when considering the economics of thinning operations, all of these studies greatly simplify the estimation of

harvesting costs by using average values of stand attributes, such as skidding distance, ground slope, and harvest volume, while ignoring the location of the individual cut-trees relative to extraction points (either road side or log landing). Consequently, tree-level thinning prescriptions developed by these past studies might not provide the most economically efficient selection of cut-trees. Additionally, these approaches for optimal tree-selection have only been applied to sample plots. Their application to entire stands has been limited due to a lack of individual tree-level information.

Recently, new remote sensing and geographic information systems (GIS) technologies such as light detection and ranging (LiDAR) have been used to provide inventory data at the individual tree-level. For example, tree heights, crown widths, and derivative parameters such as diameter at breast height (dbh) and volume are some of the tree characteristics that have been derived from LiDAR data (Packalén and Maltamo 2006, Maltamo et al. 2006, Maltamo et al. 2004). As this type of high-resolution spatial data becomes more available, there is increasing potential to use optimal tree selection algorithms to develop site-specific, tree-level thinning prescriptions that can be applied to an entire stand (Shao and Reynolds 2006). However, harvesting cost models that provide estimates for individual cut-trees still need to be developed and implemented into optimal tree selection algorithms to ensure cost efficiency of thinning operations for given management purposes.

In this paper, we present a computerized model to develop skid trail networks and estimate tree-level timber harvesting costs. The model considers size, location, and spatial distribution of individual cut-trees and is designed for ground-based harvesting

operations. If coupled with optimal cut-tree selection algorithms, this model is expected to develop cost-efficient thinning guidelines for given treatment objectives.

2.2 METHODOLOGY

A treatment unit is defined in this study as an area to be thinned by a ground-based harvesting system. All logs are assumed to be brought into one extraction point (log landing), where they are loaded onto log trucks for further transportation. A whole-tree harvesting is further assumed for this study as follows: *i*) cut-trees are felled at the stump location, *ii*) a cable skidder is used to bunch and skid nearby cut-trees within a maximum winching radius (MWR) to a given log landing, and *iii*) trees are then delimited and topped at the landing.

This study is based on the availability of a stem map, pre-selected cut- and leave-tree locations, and terrain information within the entire treatment unit. For this study, a stem map and a DEM derived from LiDAR data by Rowell et al. (2009) was used. In their study, the LiDAR raw data was processed to produce a high resolution 1-meter digital elevation model (DEM) and a canopy height model (CHM). Tree locations were obtained using a stem identification algorithm based on a combination of variable window local maxima filtering (Popescu and Wynne 2004) and neighborhood canopy height variance and return density (Rowell et al. 2006). Individual tree DBH were estimated using a log-linear model ($n = 1555$, $R^2 = 0.76$, Error = 7.6%) (Rowell et al. 2009).

$$[2.1] \quad \ln \text{dbh} = 1.732 + (0.041 \times h) + (0.798 \times rh) - (0.007 \times sd)$$

where h is the height of the tree (m), rh is the relative height (m) calculated as the tree height divided by the mean height of dominant and co-dominant trees in a 20 m × 20 m neighborhood, and sd is stem density of dominant and co-dominant stems in the neighborhood. Tree volumes were estimated using an equation from the Northern Idaho / Inland Empire of the Forest Vegetation Simulation (Keyser 2008).

$$[2.2] \quad \text{Vol} = \left[\left\{ 0.00171 \times (2.54 \times d)^2 \times h \right\} + \left\{ 0.00171 \times (2.54 \times d) \times h \right\} \right] \times 0.02831$$

where, vol is the tree volume (m³), and d is the tree DBH (cm). These LiDAR-derived DEM and stem map, as well as the location of the extraction point for the treatment unit are the main input datasets for our cost model.

To estimate the harvesting cost for individual trees, the model first uses a log-bunching algorithm to identify log-pile locations and volumes. The algorithm simulates a cable skidder operation which collects nearby cut-trees through a cable winch to complete a full load and skids trees together to a landing. The target maximum loading capacity (MLC) of the skidder was used to limit the volume of a log-pile that the skidder can carry during its travel to the landing, assuming log volume is the limiting factor on skidding capacity, not the number of log pieces. The model then designs the skid-trail network that connects each log-pile location to the extraction point while minimizing the total skidding cost. The model estimates the skidding cost for a given ith log-pile (PSC_i) using the following equation:

$$[2.3] \quad \text{PSC}_i = \left(\frac{\text{CT}_i}{60} \right) \times \text{RR}$$

where, CT_i is the skidding cycle time in minutes for a round trip between the extraction point and the i^{th} log-pile location and RR is the rental rate of the skidder in \$/hr. Cycle times can be estimated using regression models that appropriately capture the interaction between the skidding equipment and the terrain conditions such as slope and distance. However, there exist no regression models that accurately provide estimations of cycle time for short distances such as those obtained from a high-resolution DEM. Therefore, for demonstration purposes we modified the skidding cycle time models introduced by Han and Renzie (2005) and used them in our model applications to estimate downhill and uphill skidding cycle times that are proportional to skidding distances (Eqs. 2.4 and 2.5). We also assumed that the uphill skidding cycle time is 20% larger than downhill cycle time for equal skidding distance.

$$[2.4] \quad CT_{ds} = 3.9537 + (0.0215 \times D)$$

$$[2.5] \quad CT_{us} = 3.9537 + (0.0258 \times D)$$

where, CT_{ds} is the cycle time for downhill skidding, CT_{us} is the cycle time (min) for uphill skidding, and D is the skidding slope distance (m) from a given log-pile location to the treatment unit extraction point.

To estimate the skidding cost of an individual tree, the model prorates the skidding cost based on the volume ratio of the individual tree to the entire log-pile (Eq. 2.6). Thus, bigger cut-trees entail a larger skidding cost than smaller cut-trees in the same pile.

$$[2.6] \quad TSC_j = \left(\frac{\text{vol}_j \times PSC_i}{P\text{vol}_i} \right)$$

where, TSC_j is the skidding cost of the j^{th} individual cut-tree, vol_j is the volume of the j^{th} cut-tree, PSC_i is the skidding cost of the i^{th} log-pile containing cut-tree j , and $Pvol_i$ is the volume of the i^{th} log-pile.

2.2.1 Log-Bunching Algorithm

The log-bunching algorithm identifies the number, volume, and location of log-piles based on the three-dimensional coordinates of each cut-tree provided by the DEM and stem map. Figure 2.1 shows a flowchart describing the log-bunching process. The process begins with sorting all cut-trees based on their slope distance from the treatment unit extraction point. Starting with the first log-pile ($i=1$), the algorithm selects the closest cut-tree to the extraction point. This closest cut-tree is identified as the i^{th} log-pile location (Figure 2.1), assigned to the log-pile, and its volume is added to the i^{th} log-pile. After the i^{th} log-pile location has been identified, the algorithm re-sorts all remaining unassigned cut-trees based on their slope distance from the i^{th} log-pile. The closest cut-tree to the i^{th} log-pile is selected and labeled as a candidate neighbor (CN) cut-tree to be added to the log-pile. If the CN cut-tree is beyond the MWR, the algorithm stops assigning cut-trees to the i^{th} log-pile, the current CN cut-tree is unlabeled, and the process continues for the next pile ($i = i + 1$). If the CN cut-tree is within the MRW, the algorithm checks whether the current volume of the i^{th} log-pile plus the CN cut-tree volume exceeds the MLC of the skidder. If the combined volume is greater than the MLC, the current CN cut-tree is unlabeled and the next closest cut-tree to the i^{th} log-pile is selected and labeled as a CN cut-tree. On the other hand, when the combined volume is less than the MLC of

the skidder, the CN tree is assigned to the i^{th} log-pile and the pile volume is updated. When no more cut-trees can be assigned to the i^{th} log-pile because of MLC, the algorithm moves to the next ($i = i + 1$) log-pile location. Figure 2.2 shows a log-bunching example for a log-pile including five cut-trees with a combined volume of 2.1 m^3 , when the MLC is 2.5 m^3 . The algorithm stops the log-bunching process when all cut-trees in the treatment unit have been assigned to a log-pile.

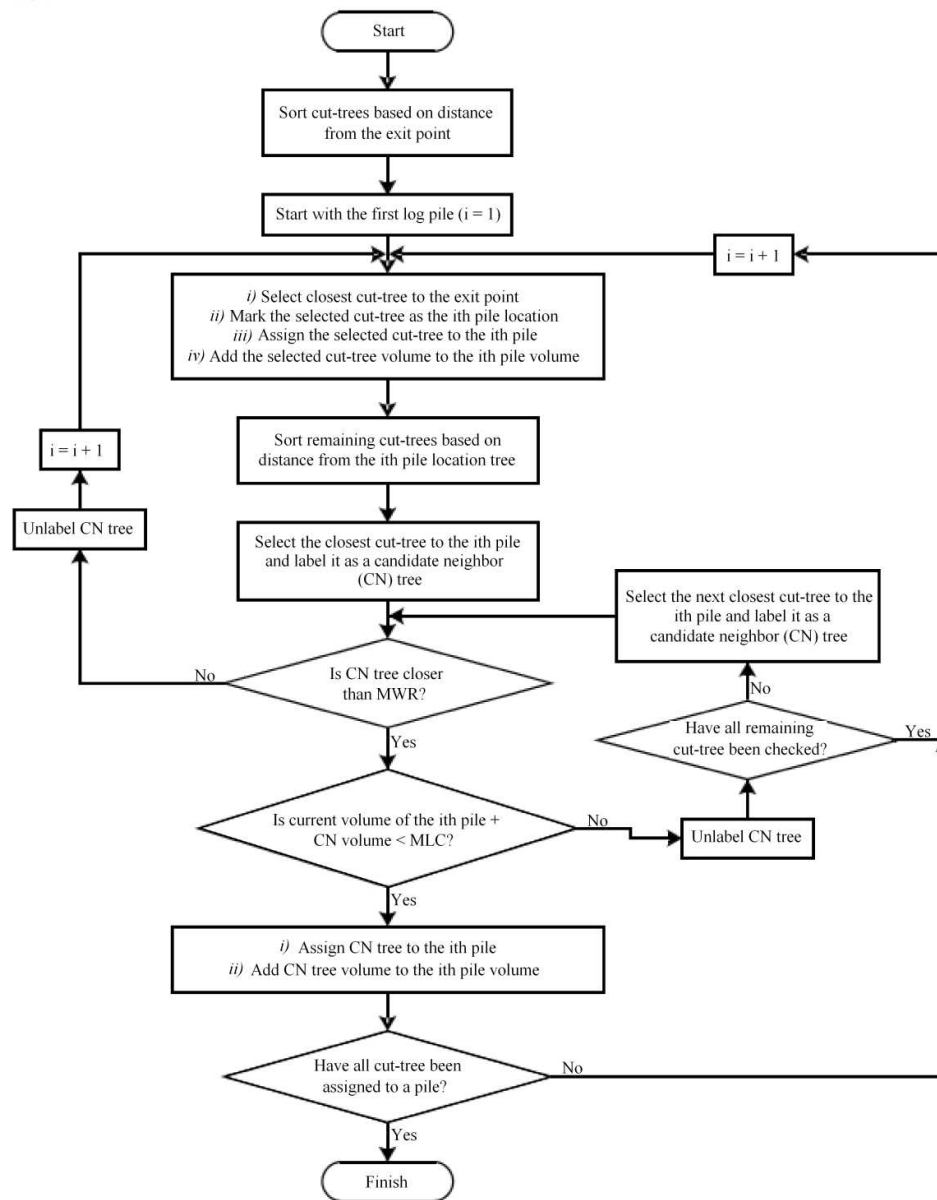


Figure 2.1. Flowchart of the log-bunching algorithm developed in this study.

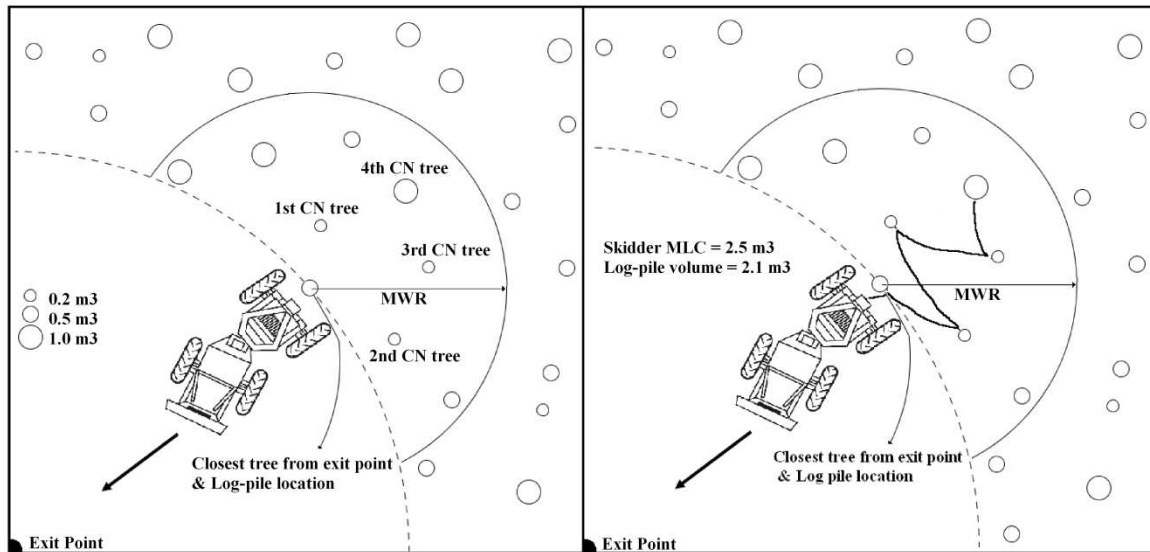


Figure 2.2. Log-bunching simulation to identify log-pile locations.

2.2.2 Skid-Trail Network

To estimate the skidding cycle time for a given log-pile, it is necessary to know the route the skidder will follow between the log-pile location and the treatment unit extraction point. Our model identifies the route that connects each log-pile to the extraction point at a minimum cycle time. To determine the least cycle time route location, the model creates a skid-trail network consisting of a set of nodes and links. Nodes represent the center of DEM grid cells, log-pile locations, and the treatment unit extraction point, and links represent connections to adjacent nodes (Figure 2.3). In our model, each node is connected to its eight adjacent neighbors. A skid-trail network generated from all possible nodes in the 1-meter DEM has a very large number of nodes and links even for a small treatment unit. To reduce the size of the problem of finding minimum cycle time routes, we created a skid-trail network with nodes spaced at 5 meters.

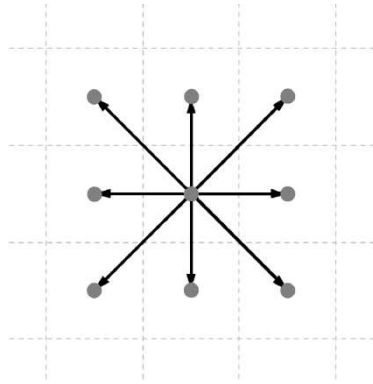


Figure 2.3. Links connecting a cell with its eight adjacent cells.

Before creating a link, the model checks whether skidder traffic is feasible over the link representing a skid-trail segment. Typically, because of safety and productivity reasons, skidder operations are limited to areas with gentle slopes. Therefore, a link is only created when the link gradient and side slopes are both below a pre-defined maximum skid-trail gradient (MSTG) and maximum skid-trail side slope (MSTSS). Skid-trail gradient is calculated based on the elevation difference of the two cells forming the link (solid line in Figure 2.4). Side slope is calculated based on the elevation difference and horizontal distance between the two grid cells of the front grid cell of a link (shaded line in Figure 2.4).

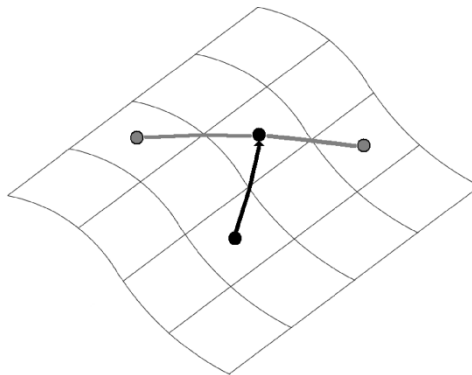


Figure 2.4. Grid cells used to calculate the side slope and skid-trail gradient for a given skid-trail link.

To avoid damage to the residual stand, we set a safety buffer distance (SBD) for each leave-tree in the treatment unit where no skid-trails are allowed to pass through. Figure 5 shows an example of a skid-trail network on an area with three pile locations, steep terrain (shaded grid cells in Figure 2.5), and obstacles presented by leave-trees. Any other zones where heavy machinery traffic should be limited such as wetlands or unstable soils, can be specified and included in the model.

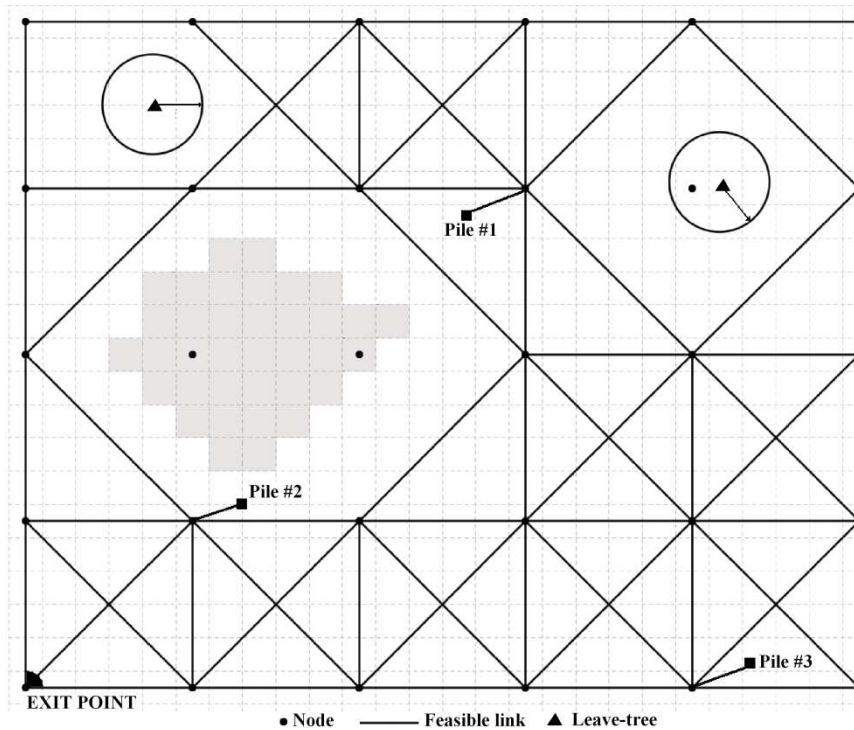


Figure 2.5. Example of the skid-trail network created over an area with steep terrain and obstacles presented by two leave-tree buffers.

After the skid-trail network has been created, the model estimates the variable cycle time associated to each link. We assumed the first term in Equations 2.4 and 2.5 is an estimate of the fixed cycle time due to activities such as hooking and unhooking logs to the winch line, and the second term estimates the skidder travel time on a skid-trail.

Thus, because the fixed cycle time is independent of the skid-trail route location, the model estimates the variable cycle time for each link using only the second term in Equations 2.4 and 2.5.

Once the variable cycle time is calculated for each link, a network problem is formulated to find a set of routes that has the least variable cycle time from each log-pile location to the treatment unit extraction point. The variable cycle time per link is used as the link attribute value, and the objective function is to minimize the total variable cycle time. The model uses Dijkstra's shortest path algorithm (Dijkstra 1959) to find the set of routes connecting each log-pile to the extraction point with the least variable cycle time, and then estimate the total variable cycle time for each log-pile. The shortest path algorithm used in the model is known to be efficient and is widely used to determine the shortest paths between a destination node and a set of origin nodes in a given network (Chung et al. 2004, Anderson and Nelson 2004, Tan 1999;).

Once the minimum variable cycle time route has been found for a given log-pile, the model adds the fixed cycle time (first term in Equations 2.4 and 2.5) to obtain the total cycle time for the log-pile (CT in Equations 2.4 and 2.5). CT is then used to compute the skidding cost for the pile, and estimate skidding cost of individual cut-trees included in the log-pile.

2.3 MODEL APPLICATION – A CASE STUDY

We applied our model to a treatment unit in the University of Montana’s Lubrecht Experimental Forest (LEF), located approximately 48 km northeast of Missoula, Montana in the Blackfoot River drainage. The treatment unit is 4.6 ha in size with elevations ranging from 1,270 to 1,310 m. and an average slope of 13.5% (0.0 - 36.3% slope range) (Figure 2.6a). For the purpose of fuel reduction, we considered a thinning prescription that cuts, piles and burns all trees with DBH less than 12.7 cm (5 inches), and selects and harvests some merchantable trees for cost recovery. The LiDAR-derived stem map identified 2,645 individual stems with a DBH larger than 12.7 cm. Figure 2.6b shows the locations of these trees in the treatment unit.

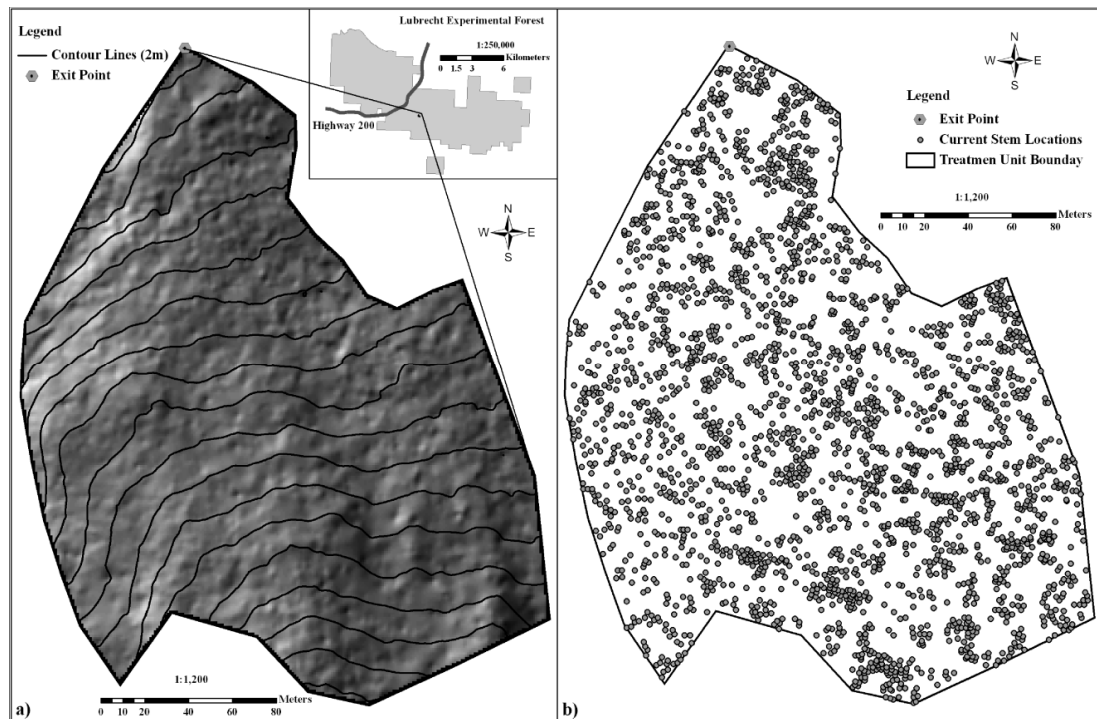


Figure 2.6. LiDAR-derived digital elevation model (a) and stem map (b) for the treatment unit selected for the model application area in the Lubrecht Experimental Forest.

The selection of leave-trees (and thus cut-trees) in the treatment unit was done manually simulating the marking process carried out by markers on the ground based on tree sizes and spacing between trees. Because of residual stand protection requirements, skid trails within the SBD of any leave-tree are not allowed. Thus, depending on the number and location of leave-trees, the resulting skid-trail network might not be fully connected, leaving piles isolated from the extraction point. In this situation, we assumed the isolated piles are left on the site without being skidded to the landing

We considered two thinning intensities scenarios to explore the performance of our cost model. For scenario I, cut-trees were selected from the treatment unit (see Figure 2.6b) until a target tree density of 400 leave-trees per hectare was met. For scenario II, additional cut-trees were selected among the trees left by scenario I until a target tree density of 300 leave-trees per hectare was met. Figures 2.7a and 2.7b show the locations of the leave-tree for scenarios I and II, respectively. Table 2.1 shows the number of cut- and leave-trees, average spacing between trees, and target cut and leave volume on the treatment unit after both selective harvesting scenarios are simulated.

The cost model was applied to the treatment unit for both scenarios considering the following link feasibility parameters; SBD = 1.5 m, MSTG = 35%, and MSTSS = 35%. The model also considered the following harvesting equipment parameters; MLC = 2.5 m³, RR = 85 \$/hr, and MWR = 10 m, which approximately correspond with a small-sized cable skidder used in thinning operations (Bustos-Letelier 2010). The extraction point was located on the lower elevation part of the treatment unit (see Figure 2.6a).

Table 2.1. Target thinning intensities under each thinning scenario considered in the study.

Target conditions	Scenario I (400 trees per ha)	Scenario II (300 trees per ha)
Number of leave-trees	1,840	1,380
Number of cut-trees	805	1,265
Average tree spacing (m)	5.0	5.8
Leave volume (m ³)	573.74	406.58
Cut volume (m ³)	200.32	367.48



Figure 2.7. Selected leave-trees locations under the two thinning scenarios with a target density of 400 and 300 trees per hectare, (a) and (b) respectively.

2.4 RESULTS AND DISCUSSION

The model identified log-pile locations as well as the optimal skid-trail network connecting log-piles to the treatment unit extraction point for both simulated selective

harvesting scenarios. For scenario I, based on the location of the 805 selected cut-trees (Figure 2.8a), the log-bunching algorithm identified a total of 215 log-pile locations (Figure 2.8b). Then, based on the location of the 1,840 leave-trees and the identified log-piles, the model created a skid-trail network composed of 2,710 feasible skid-trail links between nodes. Figure 2.9a shows the skid-trail network, where the model identified 11 of the 215 log-piles as isolated without a way out to the extraction point, and considered the cut-trees belonging to these log-piles as non-harvestable. These isolated log-piles are caused mainly by the leave-tree buffers where no skidder access is allowed. For the remaining 204 connected piles, the model determined the optimal skid-trail network that minimized the variable cycle time from each log-pile to the extraction point (Figure 2.9b). Figures 2.10a and 2.10b present the optimal skid-trail network with traffic levels on each skid-trail link in terms of timber volume and number of passes (turns). The model estimated the skidding costs for each connected log-pile using the variable cycle time obtained from the optimal skid-trail network. Figure 2.11a shows range of skidding costs per log-pile, where log-piles located farther away from the extraction point have larger harvesting costs. The model also estimated skidding costs for individual cut-trees (Figure 2.11b). Cut-trees with large cost can be found throughout the treatment unit because cost is a function of both distance from the extraction point and individual cut-tree volume.

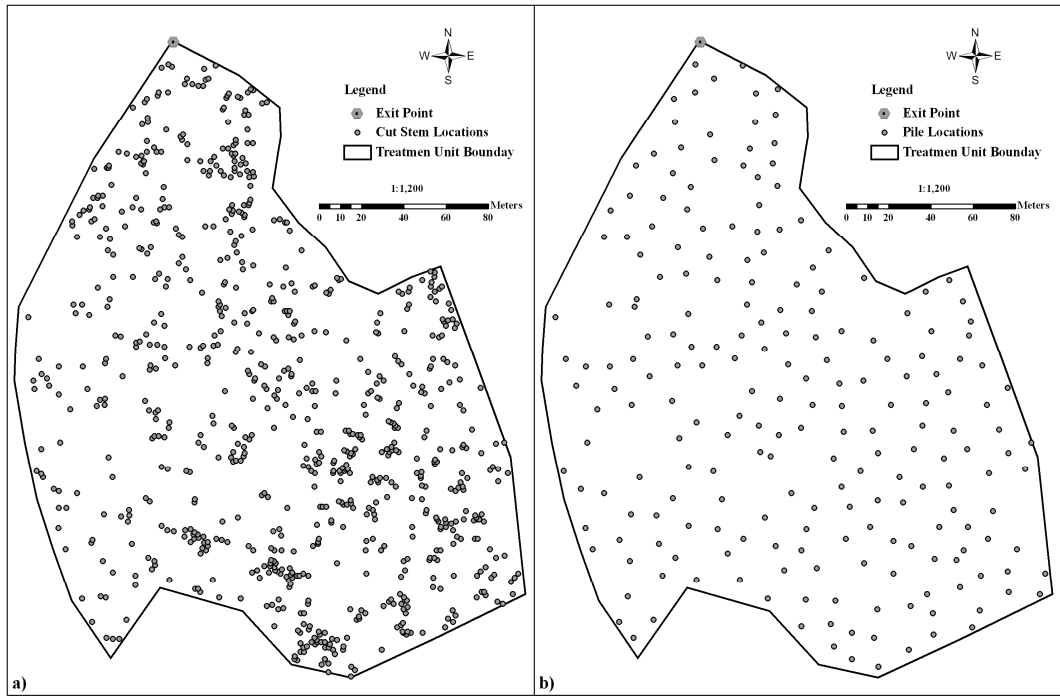


Figure 2.8. Cut-tree locations under thinning scenario I (a), and the corresponding log-pile locations identified by the log bunching algorithm (b).

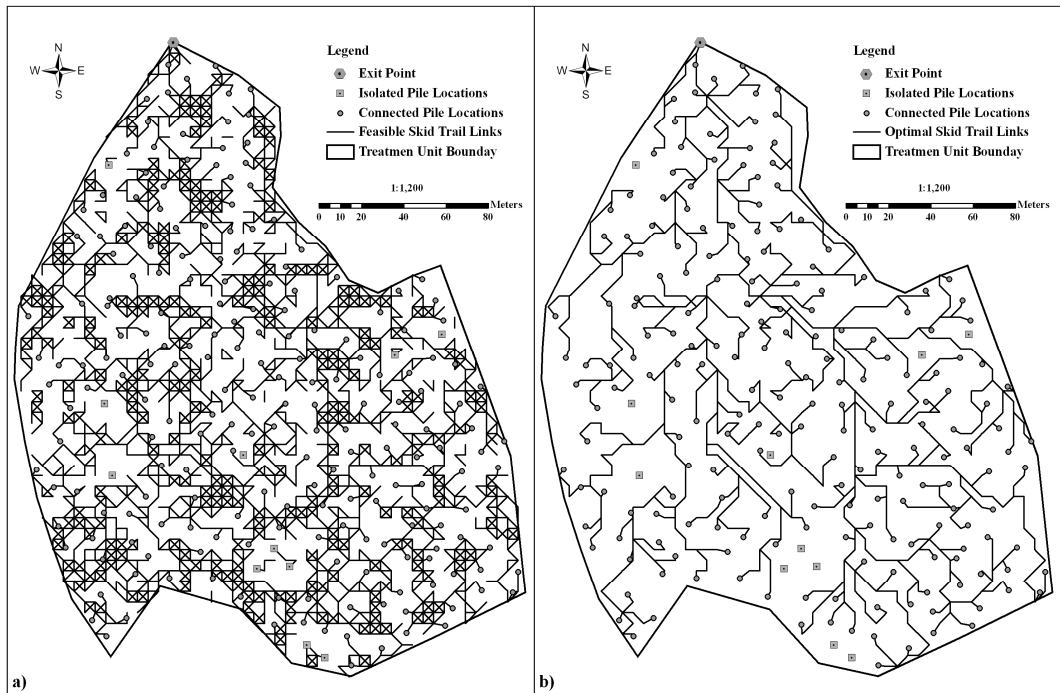


Figure 2.9. Feasible skid-trail links created by the model for thinning scenario I (a), and the optimal skid-trail network identified by the model (b).

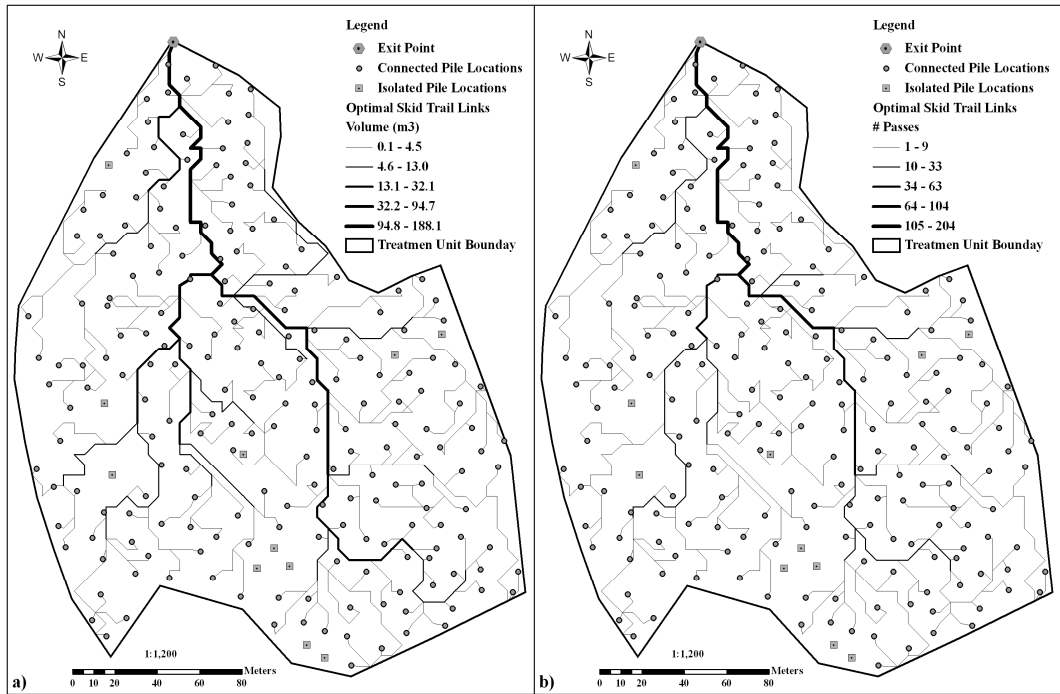


Figure 2.10. Optimal skid-trail network for thinning scenario I showing traffic levels in terms of volume traveled (a), and number of passes (b) over a given link.

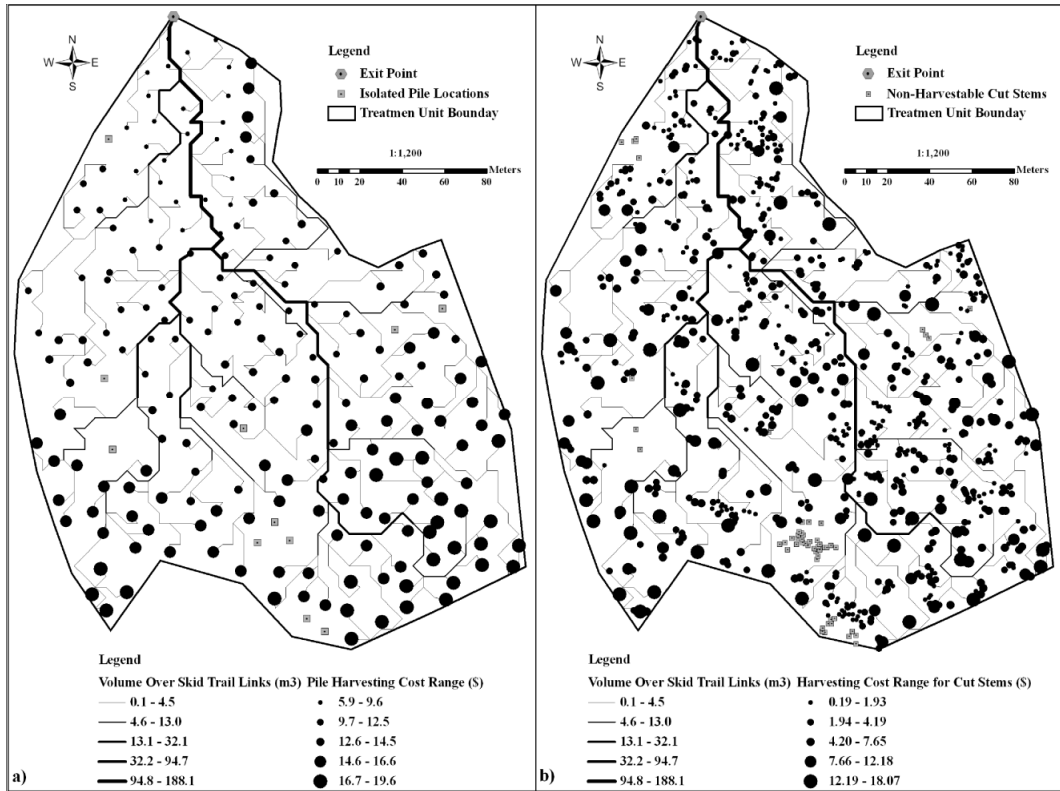


Figure 2.11. Model results showing skidding cost per pile (a) and per individual cut-tree (b) for thinning scenario I.

For scenario II, which considered 1,265 cut-trees (Figure 2.12a), the log-bunching algorithm identified 278 log-pile locations (Figure 2.12b). The model created a skid-trail network composed of 3,414 feasible skid-trail links (Figure 2.13a). Because of the smaller number of obstacles presented by fewer leave-trees, there were no isolated log-piles identified by the model. Using the variable cycle time of each link, the model determined the optimal skid-trail network connecting each log-pile to the extraction point at a minimum cycle time (Figure 2.13b). The optimal skid-trail network showing traffic levels in terms of volume traveled, and the number of passes is presented in Figures 2.14a and 2.14b, respectively. The model also estimated the skidding costs of the 278 log-piles, as well as skidding costs of the 1,265 individual cut-trees in the treatment unit (Figures 2.15a and 2.15b). Similar to scenario I, log-piles located closer to the extraction point have smaller skidding costs than distant log-piles.



Figure 2.12. Cut-tree locations under thinning scenario II (a), and the corresponding log-pile locations identified by the log bunching algorithm (b).

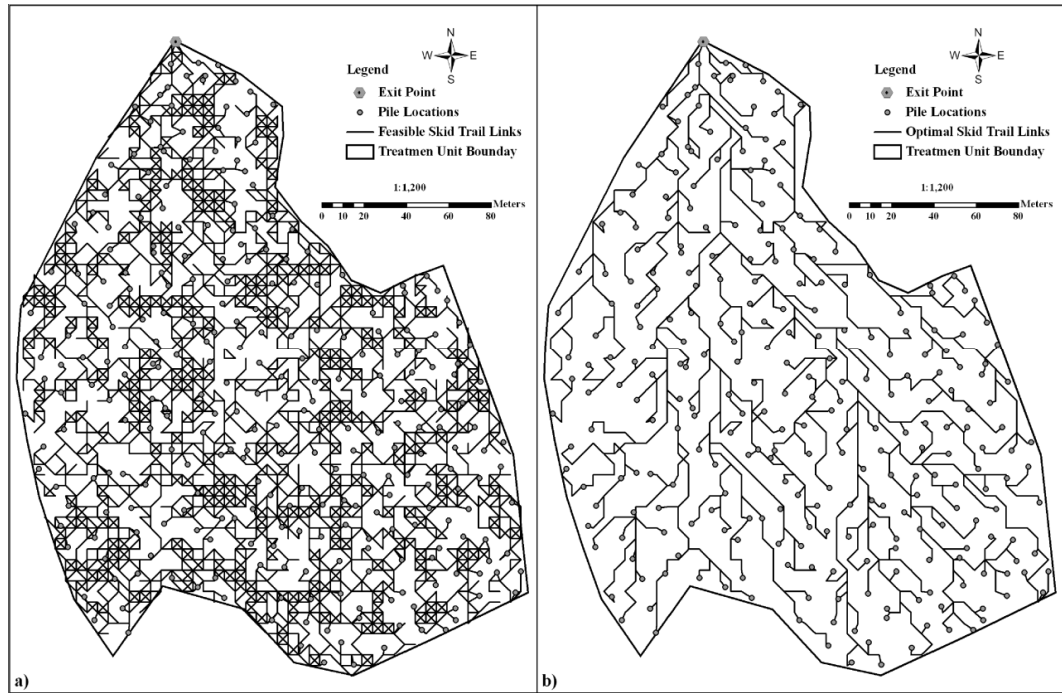


Figure 2.13. Feasible skid-trail links created by the model for thinning scenario II (a), and the optimal skid-trail network identified by the model (b).

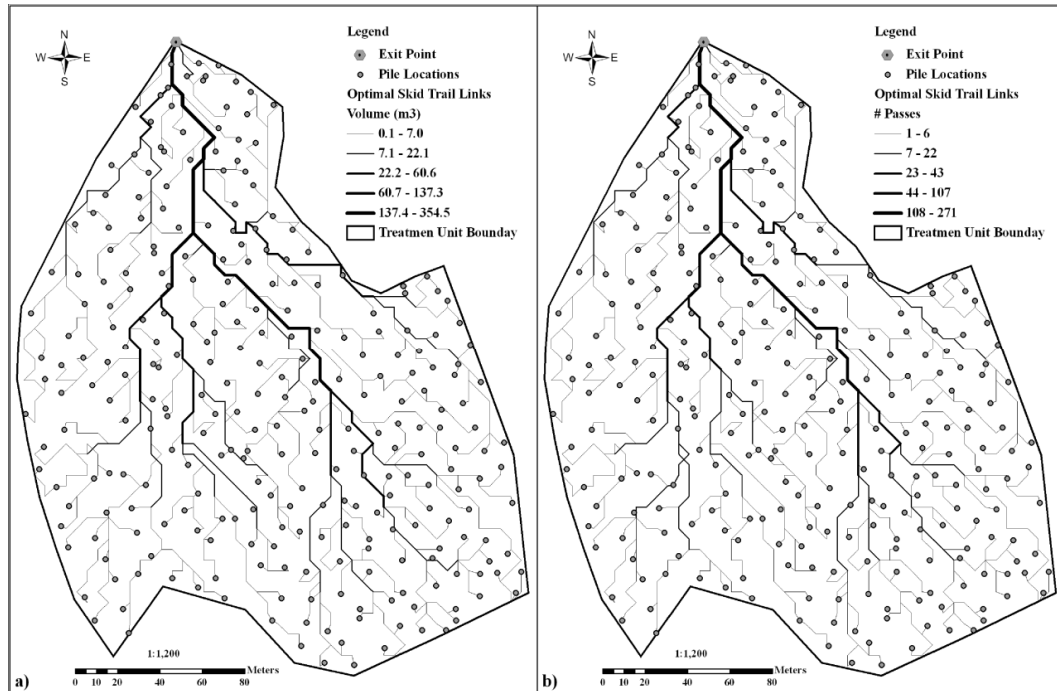


Figure 2.14. Optimal skid-trail network for thinning scenario II showing traffic levels in terms of volume traveled (a), and number of passes (b) over a given link.

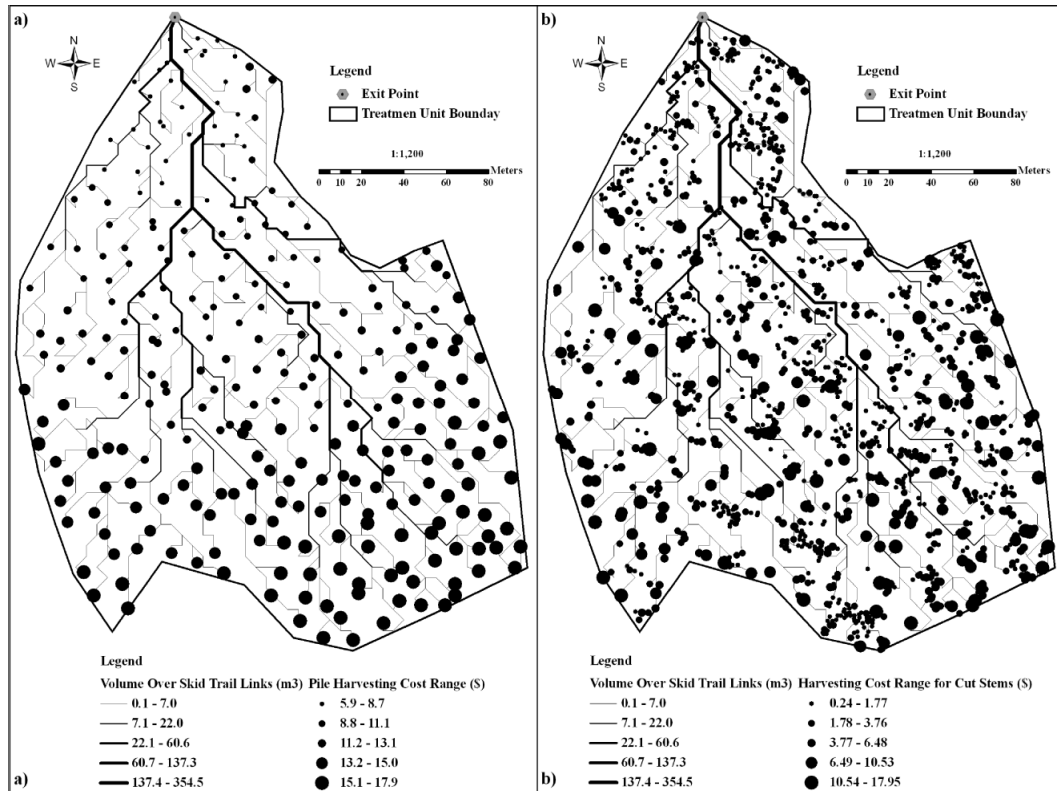


Figure 2.15. Model results showing skidding cost per pile (a) and per individual cut-tree (b) for thinning scenario II.

Table 2.2 summarizes the model results for both harvesting scenarios. As mentioned above, a total of 55 cut-trees (6.8% of the total selected cut-trees) were identified as non-harvestable in scenario I mainly because of leave-tree buffers. However, the combination of other factors related to the harvesting equipment and skid-trail network design can also affect the number and location of isolated log-piles. For example, MLC and MWR influence the number of cut-trees included in a log-pile, thus affecting the number and location of log-piles. Likewise, the spacing between nodes can also determine if a log-pile is either connected to the network or isolated. In our model, a log-pile location is defined as the location of the closest available cut-tree to the extraction point, and if its location is within a leave-tree SBD then the log-pile and all cut-tree forming it are considered isolated. However, in practice cut-trees inside a leave-tree SBD can be winched out of the no-traffic zone and the log-pile location can be shifted allowing these isolated trees to be extracted. Our model will need to be further refined to reflect this practical aspect of log piling. Additionally, leave-trees were selected based on tree sizes and spacing; however, if access is considered when selecting leave-trees, the number of isolated log-piles identified by the model in this study can be significantly reduced thus increasing timber recovery.

Table 2.2. Results of the individual tree skidding cost model.

Model Results	Scenario I (400 trees per ha)	Scenario II (300 trees per ha)
Harvesting Feasibility		
Harvestable Piles	204	278
Harvestable Cut-trees	750	1265
Harvestable Volume (m ³)	188	367
Non-Harvestable Piles	11	---
Non-Harvestable Cut-trees	55	---
Non-Harvestable Volume (m ³)	12.3	---
Harvestable Piles		
Minimum Number of Trees per Pile	1.00	1.00
Average Number of Trees per Pile	3.70	4.60
Maximum Number of Trees per Pile	11.00	15.00
Minimum Pile Volume (m ³)	0.05	0.05
Average Pile Volume (m ³)	0.92	1.32
Maximum Pile Volume (m ³)	2.48	2.64
Minimum Pile Distance (m)	11.11	11.11
Average Pile Distance (m)	259.13	225.15
Maximum Pile Distance (m)	443.59	395.64
Minimum Pile Cost (\$)	5.94	5.94
Average Pile Cost (\$)	13.64	12.53
Maximum Pile Cost (\$)	19.57	17.95
Harvestable Cut-trees		
Minimum Tree Volume (m ³)	0.05	0.05
Average Tree Volume (m ³)	0.25	0.29
Maximum Tree Volume (m ³)	1.71	2.64
Minimum Tree Cost (\$)	0.20	0.24
Average Tree Cost (\$)	3.71	2.75
Maximum Tree Cost (\$)	18.07	17.95

Log-pile characteristics between the two scenarios were slightly different. The average number of trees per log-pile is smaller for scenario I than for scenario II (3.7 versus 4.6) because fewer trees are available within the MWR to complete a full load. For the same reason, scenario I had a smaller average volume per log-pile than scenario II (0.92 m³ versus 1.32 m³). The maximum number of trees per log-pile is relatively high in both scenarios (i.e., 11 and 15 trees) because of the large number of small trees in the treatment unit. In this study, we did not restrict the number of trees per log-pile, which

could be included as another limiting factor on the carrying capacity of cable skidders. Additionally, because tree size was not considered in the cycle time equations (Eqs 2.4 and 2.5), our skidding cost estimates are independent of tree size. However, because small trees require more piling time than large trees to complete a full load, reducing tree sizes typically results in increases skidding costs per m³. Further research should consider evaluating skidding cycle time equations that account for such factors to obtain more realistic skidding cost estimates. The average distance from a log-pile to the extraction point was approximately 260 m and 225 m for scenarios I and II, respectively. The higher average distance for scenario I was caused by the presence of more leave-trees, which present obstacles to skidding paths. Due to this longer skidding distance in scenario I, the average skidding cost in scenario I is slightly higher than scenario II (\$13.6 versus \$12.5). Likewise, the average skidding cost for individual cut-trees is higher in scenario I than scenario II (\$3.46 versus \$2.75).

To ensure that our model results are comparable to those that can be obtained from the existing skidding cost models, we first aggregated the individual tree skidding costs estimated from the application results described above to calculate the average skidding cost per unit of timber volume (\$/m³). The average cost was then compared with average skidding costs estimated by conventional cost regression models that use average values of stand attributes (i.e. harvest volume per ha, average skidding distance, etc.) as explanatory variables.

For this comparison, we selected the Fuel Reduction Cost Simulator (FRCS) (Hartsough et al. 2001) that is currently used as timber harvest cost estimator for multiple MS Excel-based tools such as STHARVEST (Fight et al. 2003) and My Fuel Treatment

Planner (Biesecker and Fight 2006). We compared our model results with the skidding cost component of FRCS, which is calculated as a weighted average of skidding costs estimated by six published regression models. These regression models were developed for cable skidders of various sizes operating in different areas of the western US such as western Montana, Idaho, Oregon, and Washington (Johnson 1998, Gardner 1979, Gebhardt 1977). The skidder rental rate, cut-tree characteristics, and thinning intensities entered into FRCS as input parameters were the same as those used in our model applications. The average skidding distance (ASD) calculated as the slope distance from the centroid of the treatment unit to extraction point. Other characteristics of the treatment unit, such as size and average slope were also entered into FRCS (Table 2.3).

Table 2.3. Parameters used in the Fuel Reduction Cost Simulator (FRCS) to calculate skidding costs under each thinning scenarios.

FRCS parameters	Scenario I	Scenario II
Skidder rental rate (\$/hr)	85.00	85.00
Average slope (%)	13.50	13.50
Average skidding slope distance (m)	184.17	184.17
Area (ha)	4.60	4.60
Removal (trees per ha)	164.13	275.00
Average cut-tree volume (m ³)	0.25	0.29
Average cut-tree dbh (cm)	20.57	21.64
Maximum cut-tree volume (m ³)	1.71	2.64

Table 2.4 summarizes cost estimates resulted from our individual tree skidding cost model, FRCS, and the six cost regression models used in FRCS for both thinning scenarios. The skidding costs from our model are about 33% higher and 5% lower than the FRCS cost estimates for scenarios I and II, respectively. However, our model results are within the range of estimates produced by the six regression models. All models

estimated skidding costs of scenario I higher than scenario II, but the difference between the two scenarios was larger in the results of our model than in those of the existing models, which indicates that our cost model is more sensitive to thinning intensities than the existing models. This is mainly because thinning intensity does not affect ASD used in the existing models considered, while in our model ASD is calculated as the average distance from all log-piles to the extraction point along the optimal skid-trail network. However, modern skidding cost models should consider thinning prescriptions to better capture the interactions between thinning intensity and skidding operations and obtain more realistic estimates of the associated skidding costs.

Table 2.4. Comparison of average skidding cost results among various cost models including our individual-tree cost model, the Fuel Reduction Cost Simulator (FRCS), and six published regression models used in the FRCS for both thinning scenarios.

Skidding cost models	Skidding Cost (US\$/m ³)	
	Scenario I	Scenario II
Individual-tree cost model	14.80	9.48
FRCS (Hartsough et al. 2001)	11.12	9.93
Gebhardt (1977)	5.99	5.21
Johnson (1988)	12.59	11.49
Anderson and Young (1998)	10.46	9.70
Gardner (1979)	17.16	15.33
Gibson and Egging (1973)	13.38	11.94
Johnson and Lee (1988)	14.72	13.51

Although our model provides reasonable average cost estimates (\$/m³) compared with traditional methods, the accuracy of individual tree cost estimates largely depends on the accuracy of the input tree locations. There are several ways to obtain stem map information varying from traditional field measurements to advanced remote sensing and

GIS technologies such as high-resolution aerial photo (Hirschmugl et al. 2007), multispectral imaging (Popescu and Wynne 2004), and LiDAR (Maltamo et al. 2004). The algorithms used to derive LiDAR-derived stem maps in our study area have provided stem detection accuracies of approximately 53 % when considering all forest types (Suratno et al. 2009). However, stem detection accuracy increases significantly on dominant trees. In similar forest conditions to those of our treatment unit, the stem detection algorithm provided an accuracy of about 90% when considering only dominant trees (Rowell et al. 2006). In this study, we considered only dominant trees with DBH larger than 12.7 cm, thus we expect the stem map used for our study has a high stem detection accuracy level.

As our model considers terrain slope to create feasible skid-trail links, it can be effectively used to delineate non-accessible or difficult terrain areas for skidding operations. Our model can also be used to automatically generate optimal skid-trail networks connecting multiple log-piles to the extraction point. Additionally, soil recovery costs associated with amelioration of soil disturbances caused by skidder traffic can also be incorporated into our model to generate skid-trail networks that minimize both skidding costs and soil disturbances (Contreras and Chung 2009).

2.5 CONCLUSIONS

Due to advanced remote sensing and GIS technologies that have brought us to an unprecedented level of precision in terrain and vegetation mapping, high resolution

DEMs and individual tree stem maps are now available for forest resources management applications. With such stem maps, silvicultural prescriptions can be developed and implemented at the individual tree level, which can potentially help meet desired management goals more effectively than the conventional way of developing and applying prescriptions. To facilitate individual tree-level decision-making, we have developed a cost model that estimates skidding costs for individual cut-trees for thinning operations based on tree volume and locations.

The model was applied to a treatment unit where merchantable trees were to be selectively harvested under two hypothetical thinning scenarios. Comparison of the model results with those obtained from the existing cost models indicates that our model results are within the reasonable range for skidding costs but more sensitive to thinning intensities than the existing models. In addition, our model can be potentially used as a tool to develop skidding trail networks and delineate difficult terrain areas for skidding operations.

The model should be further validated through field tests to ensure that the results are applicable on the ground. There is also a need to develop appropriate cycle time regression equations for the model. The model currently employs two regression equations for uphill and downhill skidding cycle times, but they do not directly account for the effects of ground slopes, number of logs, log-pile volume, and wide range of skidding distances, on cycle times. The simple skid-trail network design is another limitation of the model. Many sharp turns and skid-trail crossings exist in the optimal skid-trail because only the second-order neighborhood system (eight adjacent grid cells) was considered. More realistic skid-trails can be obtained by reducing node spacing,

increasing the number of neighbor cells considered, or both. However, other skid trail designs factors such as the skidder's minimum turning radius should also be considered for link feasibility to ensure the skid-trails identified by the model can be implemented on the ground.

2.6 REFERENCES

Agree, J.K., and C.N. Skinner. 2005. Basic principles of forest fuel reduction treatments. *For. Ecol. Manage.* 211(1-2):83-96.

Anderson, A.E., and J. Nelson. 2004. Projecting vector-based road networks with a shortest path algorithm. *Can. J. For. Res.* 34(7):1444-1457.

Anderson, B., and G. Young 1998. Harvesting coastal second growth forests: summary of harvesting system performance. *FERIC Technical Report TR-120.*

Bailey, J.D., and J.C. Tappeiner. 1998. Effects of thinning on structural development in 40- to 100-year-old Douglas-fir stands in western Oregon. *For. Ecol. Manage.* 108(1-2):99-113.

Barbour, R. J., D. Fayle, G. Chauret, J. Cook, M.B. Karsh, and S. Ran. 1994. Breast-height relative density and radial growth in mature jack pine (*Pinus banksiana*) for 38 years after thinning. *Can. J. For. Res.* 24(12): 2439–2447.

Biesecker, R.L., and R.D. Fight. 2006. My fuel treatment planner: a use guide. *Gen. Tech. Rep. PNW-GTR-663.* Portland, OR: USDA, Forest Service, Pacific Northwest Research Station. 31p.

- Brodie, J.D., D.M. Adams, and C. Kao. 1978. Analysis of economic impacts on thinning and rotation for Douglas-fir using dynamic programming. *For. Sci.* 24(4):513–522.
- Bustos-Letelier, O. 2010. A comparison of production, costs and stand impacts among four yarding methods. PhD dissertation, University of Maine, Orono. ME, 124p.
- Cao, T., K. Hyytiäinen, O. Tahvonen, and L. Valsta. 2006. Effects of initial stand states on optimal thinning regime and rotation of *Picea abies* stands. *Scan. J. For. Res.* 21(5):388-398.
- Carey, A.B. 2001. Induced spatial heterogeneity in forest canopies: response of small mammals. *J. Wildl. Manage* 65(4):1014-1027.
- Contreras, M. and W. Chung. 2009. Designing skid-trail networks to minimize skidding cost and soil disturbances. Proceeding: “Environmentally Sound Forest Operations”. Council of Forest Engineering (COFE). 32th Annual Meeting. Kings Beach (Lake Tahoe), California, USA.
- Chung, W., J. Sessions, and H. Heinimann. 2004. An application of heuristic network algorithm to cable logging layout design. *Int. J. For. Eng.* 15(1):11-24.
- Dijkstra, E. 1959. A note on two problems in connexion with graphs. *Numerische Math.* 1:269-271.
- Fight, R.D., X. Zhang, and B.R. Hartsough. 2003. User guide for STHARVEST: software to estimate the cost of harvesting small timber. Gen. Tech. Rep. PNW-GTR-582. Portland, OR: USDA, Forest Service, Pacific Northwest Research Station. 12 p.
- Gardner, R.B. 1979. Turn cycle time prediction for rubber tired skidders in the northern Rockies. Res. Note INT-257. USDA, Forest Service, Intermountain Forest and Range Expt. Sta., Ogden, UT.

- Gebhardt, P.D. 1977. Timber harvesting production rates in mixed-conifer stands of eastern Oregon and Washington. Master of Forestry thesis, Univ. of Washington, Seattle, WA.
- Gibson, D.F., and L.T. Egging. 1973. A location model for determining the optimal number and location of decks for rubber-tires skidders. Pap. No. 73-1534. Am. Soc. of Agri. Engineers, St. Joseph, MI.
- Graham, R.T., A.E. Harvey, T.B. Jain, and J.R. Tonn. 1999. The effects of thinning and similar stand treatments on fire behavior in western forests. Gen. Tech. Rep. PNW-GTR-463. Portland, OR: USDA, Forest Service, Pacific Northwest Research Station. 27 p.
- Hartsough, B.R., X. Zhang, and R.D. Fight. 2001. Harvesting cost model for small trees in natural stands in the Interior Northwest. *Forest Prod. J.* 51(4):54-61.
- Han, H.-S., and C. Renzie. 2005. Productivity and cost of partial harvesting method to control mountain pine beetle infestation in British Columbia. *West. J. Appl. For.* 20(2):128-133
- Hayes, J.P., S.S. Chan, W.H. Emmingham, J.C. Tappeiner, L.D. Kellogg, and J.D. Bailey. 1997. Wildlife response to thinning young forests in the Pacific Northwest. *J. For.* 95(8):28-33.
- Hirschmugl, M., M. Ofner, J. Raggam, and M. Schardt. 2007. Single tree detection in very high resolution remote sensing data. *Remote Sens. Environ.* 110(4):533-544.
- Hof, J., and M. Bevers. 2000. Optimizing forest stand management with natural regeneration and single-tree choice variables. *For. Sci.* 46(2):168-175.

- Hooke, R., and T. Jeeves. 1961. Direct search solution of numerical and statistical problems. *J. ACM* 8(2):212-219.
- Hyytiäinen, K., O. Tahvonen, and L. Vasta. 2005. Optimum juvenile density, harvesting, and stand structure in even-aged Scot pine stands. *For. Sci.* 51(2):120-133.
- Johnson, L.R. 1988. Final report: summary of production and timber studies of mechanized harvesting equipment in the Intermountain West. Forest Prod. Dept., University of Idaho. Moscow, ID.
- Johnson, L.R., and H.W. Lee. 1988. Skidding and processing of forest residues for firewood. *Forest Prod. J.* 38(3):35-40.
- Keyser, C.E., comp. 2008. Northern Idaho / Inland Empire (NI/IE) Variants Overview – Forest Vegetation Simulator. Internal Rep. Fort Collins, CO: USDA, Forest Service, Forest Management Service Center. 49p. (revised February 3, 2010).
- Maltamo, M., K. Mustonen, J. Hyyppä, J. Pitkänen, and X. Yu. 2004. The accuracy of estimating individual tree variables with airborne laser scanning in a boreal nature reserve. *Can. J. For. Res.* 34(9):1791-1801.
- Maltamo, M., K. Eerikäinen, P. Packalén, and J. Hyyppä. 2006. Estimation of stem volume using laser scanning-based canopy height metrics. *Forestry* 79(2):217-229.
- Packalén, P., and M. Maltamo. 2006. Predicting the plot volume by species using airborne laser scanning and aerial photographs. *For. Sci.* 52(6):611-622.
- Palahí, M., and T. Pukkala. 2003. Optimizing the management of Scot pine (*Pinus sylvestris* L.) stands in Spain based on individual-tree models. *Annals of Forest Science* 60:105-114.

- Pollet, J., and P.N. Omi. 2002. Effect of thinning and prescribed burning on crown fire severity in ponderosa pine forests. *Int. J. Wildl. Fire* 11(1):1-10.
- Popescu, S.C., and R.H. Wynne. 2004. Seeing the trees in the forest: Using LIDAR and multispectral data fusion with local filtering and variable window size for estimating tree height. *Photogrammetric Engineering & Remote Sensing* 70(5):589-604.
- Pukkala, T., and J. Miina. 1998. Tree-selection algorithm for optimizing thinning using a distance-dependent growth model. *Can. J. For. Res.* 28(5):693-702.
- Pukkala, T., and J. Miina. 2005. Optimizing the management of a heterogeneous stand. *Silva Fennica* 39(4):525-538.
- Rautiainen, O., T. Pukkala, and J. Miina. 2000. Optimising the management of even-aged *Shorea robusta* stands in Nepal using individual tree growth models. *For. Ecol. Manage* 126(3):417-429.
- Rowell, E., C. Seielstad, L. Vierling, L. Queen, and W. Shepperd. 2006. Using laser altimetry-based segmentation to refine automated tree identification in managed forests of the Black Hills, South Dakota. *Photogrammetric Engineering & Remote Sensing* 72(12):1379-1388
- Rowell, E., C. Seielstad, J. Goodburn, and L. Queen. 2009. Estimating plot-scale biomass in a western North American mixed-conifer forest from lidar-derived tree stems. *Silvilaser 2009. Proceedings of the 9th International Conference on Lidar Applications for Assessing Forest Ecosystems*. Texas A&M University. October 15, 2009.
- Shao, G., and K. Reynolds. 2006. Computer applications in sustainable forest management: Including perspectives on collaboration and integration. Springer-Verlag New York, LLC. 277pp.

- Suratno, A., C. Seielstad, and L. Queen. 2009. Tree species identification in mixed coniferous forest using laser scanning. *ISPRS Journal of Photogrammetry and Remote Sensing* 64(6):683-693.
- Tan, J. 1999. Locating forest roads by a spatial and heuristic procedure using microcomputers. *Int. J. For. Eng.* 10:91-100.
- Valsta, L. 1992. An optimization model for Norway spruce management based on individual-tree growth models. *Acta Forestalia Fennica* 232.

CHAPTER 3:

MODELING TREE-LEVEL FUEL CONNECTIVITY TO EVALUATE THE
EFFECTIVENESS OF THINNING TREATMENTS FOR REDUCING CROWN FIRE
POTENTIAL

3.0 ABSTRACT

Land managers have been using fire behavior and simulation models to assist in several fire management tasks. These widely-used models use average attributes to make stand-level predictions without considering spatial variability of fuels within a stand. Consequently, as the existing models have limitations in adequately modeling crown fire initiation and propagation, the effects of fuel treatments can only be evaluated based on average conditions, where the effects of thinning design (e.g., cut-tree locations) on changing fire behavior are largely ignored. To overcome these limitations, we coupled an advanced physics-based fire behavior model with light detection and ranging (LiDAR) technology to capture spatial variability of fuels within stands and properly model crown fire initiation and propagation. Advanced physics-based fire behavior models are computationally demanding, and it is not currently feasible to run such models for large landscapes (thousands of hectares) at which fuel treatments are often considered. Thus, to extend the capabilities of these fine scale models to larger landscapes, we developed logistic regression models based on tree data and fire behavior model output to predict crown fire initiation and propagation for given tree locations and attributes for two weather scenarios, representing average and severe conditions, for our study area. We applied these regression models and used tree-level fuel connectivity prediction as measures to evaluate the effectiveness of thinning treatments for reducing crown fire potential. We demonstrate this method using LiDAR-derived stem map and tree attributes developed for a 4.6-ha forest stand in western Montana, USA.

Keywords: Fire behavior, fire simulation modeling, WFDS, LiDAR, thinning treatments.

3.1 INTRODUCTION

Historically, low intensity fires burned frequently in the western U.S., with ignitions caused by lightning and humans (Hessl et al. 2004, Allen et al. 2002). These fires functioned to control regeneration of fire sensitive species, promote fire tolerant species, maintain open forest structures, and reduce forest fuel loads (Arno and Allison-Bunnell 2002, Swetnam et al. 1999). Over the last decades, successful fire exclusion has contributed to the accumulation of understory vegetation and increased stand densities, creating a greater vertical and horizontal continuity of fuels in stand structures, which has increased the potential for high-intensity wildfires in the western U.S. (Mutch 1994, Arno and Brown 1991). Some estimates suggest that more than 27 million ha of forestland in the western U.S. have departed significantly from natural wildland fire conditions and are at medium to high risk of catastrophic wildfires (Schmidt et al. 2002). In response to the continuing threat of severe wildfires, the National Fire Plan (USDA and USDI 2001) and the Healthy Forest Restoration Act (2003) mandate that land managers restore forest habitats and reduce the risk of wildfires in federal forests.

Land managers and decision makers have been using fire behavior and simulation models as a tool to predict fire potential, identify stands with high risk of wildfires, and allocate resources for fuel treatments (Chung et al. 2009, Ager et al. 2006, Finney 2006, Cruz 2004). However, the widely-used existing fire behavior and simulation models, such as FARSITE (Finney 1998), NEXUS (Scott 1999), FFE-FVS (Reinhardt and Crookston 2003), BehavePlus (Andrews et al. 2005), and FlamMap (Finney 2006) use the average attribute values of a forest stand for stand-level predictions without considering spatial

variability in fuels and vegetation within a stand. For example, the existing models for predicting crown fire initiation (i.e., Van Wagner 1977, Cruz et al. 2006a, and Cruz et al. 2006b) and crown fire occurrence (Cruz et al. 2004) are based solely on the stand canopy base height that represents the vertical distance from the top of the surface fuels to the lower limit of canopy fuels that can sustain and vertically propagate fire. However, due to variability within a stand, it is difficult to represent an entire stand with a single canopy base height value (Scott and Reinhardt 2001). In addition, the existing models predict crown fire propagation through canopy fuels (i.e., Van Wagner 1977) based only on the stand canopy bulk density (CBD). The calculation of CBD assumes that canopy fuels are distributed uniformly throughout the stand, but this is unlikely the case even in stands with simple structures (Scott and Reinhardt 2001). Consequently, the widely-used existing fire behavior models have limitations in properly modeling crown fire initiation and propagation, as well as assessing fire-atmosphere interactions that influence the initiation and cessation of rapid and intense fires within a stand (Rothermel 1991, Potter 2002). Furthermore, the effects of fuels treatments, such as fuel reduction thinning, can only be evaluated based on average conditions (Van Wagendonk 1996), where the effects of thinning design (e.g., cut-tree locations) on changes in fire behavior are largely ignored.

To overcome the limitations of the existing fire behavior models, recent effort has been put into the development of advanced physics-based numerical fire behavior models capable of considering spatial variability of fuels within forest stands as well as fire-fuel and fire-atmosphere interactions (Mell et al. 2007). The wildland-urban interface fire dynamics simulator (WFDS) developed by the National Institute for Standards and

Technology is one of the models that simulate crown fire initiation and propagation as a fine-scale, physics-based process that takes into account size, shape, composition and spatial arrangement of fuel particles (Mell et al. 2005). WFDS can be coupled with the Light Detection and Ranging (LiDAR) technology, which has been widely used to obtain tree locations and attributes (Maltamo et al. 2004, Packalén and Maltamo 2006, Maltamo et al. 2006), to provide spatial arrangement and characteristics of fuels within stands. The advanced, fine-scale fire behavior modeling approach can be a promising method to properly model crown fire initiation and spread, as well as evaluate stand level effects of fuel treatments. However, practical applications of the fine-scale fire behavior models have been limited due to the large amount of data and computation time required to represent detailed variability of fuels within a stand and model the time-dependent fine scale fire-fuel and fire-atmosphere interactions (Mell et al. 2007).

In this study, we developed an alternative method to use a fine-scale fire behavior model (i.e., WFDS) for the purpose of improving evaluation of fuel treatment effects on changes in fire behavior. Instead of running WFDS on an entire forest stand, which is a very computationally intensive process, we run the model on different combinations of tree arrangements to represent various spatial distributions of trees and tree attributes. We then developed logistic regression models to predict crown fire initiation and propagation for given tree locations (spacing) and attributes. If crown fire initiation is predicted for given tree location and weather condition, then the tree crown fuels are considered vertically connected with surface fuels under the same weather condition. If fire is predicted to propagate from a burning tree crown to an adjacent tree crown, then both trees are considered horizontally connected. We apply these regression models and

use tree-level fuel connectivity predictions as a measure to evaluate the effectiveness of thinning treatments for reducing crown fire potential. We demonstrated this method using LiDAR-derived stem map and tree attributes developed for a 4.6-ha forest stand in the University of Montana’s Lubrecht Experimental Forest (LEF) in western Montana, USA.

3.2 METHODOLOGY

3.2.1 LiDAR-Derived Stem Map and Tree Attributes

In the summer of 2005, the National Center for Landscape Fire Analysis (NCLFA) acquired LiDAR data over the LEF located approximately 48 km northeast of Missoula, Montana in the Blackfoot River drainage (N 46°53’30”, W -113°26’3”) (Figure 3.1). Table 3.1 shows the LiDAR data acquisition parameters used for LEF. These parameters provided an average return density of ~ 1 return per 2.29 m² on the ground with a vertical accuracy of 0.15 m and a horizontal accuracy 0.25 m (Suratno et al. 2009).

Table 3.1. LiDAR data acquisition parameters used for Lubrecht Experimental Forest¹.

Elevation	1100 – 1900 m
Average flight height above surface	1900 m
Average flight speed	70.76 ms ⁻¹
Scan frequency	25.5
Laser pulse frequency	36200 Hz
Scan angle	±35°
Sidelap	50%
Average swath width	1150 m
Average return density	0.44 m ²
Average footprint	1 m ²

¹ Taken from Suratno et al. (2009)

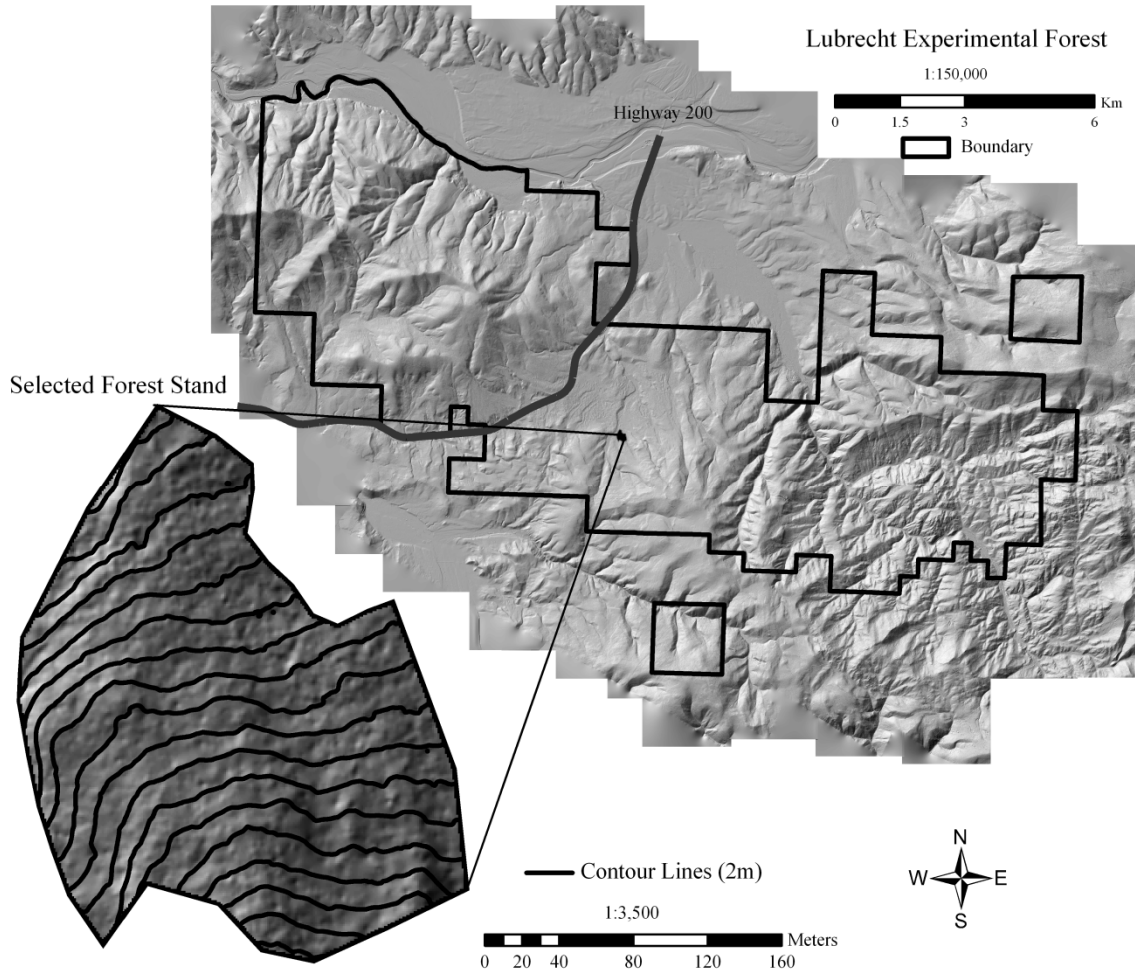


Figure 3.1. University of Montana's Lubrecht Experimental Forest boundary and the selected forest stand for the study area.

Researchers at the NCLFA separated the raw three-dimensional LiDAR points into vegetation (aboveground) and bare earth points using a triangulated irregular network densification method available in the TerraScan software suite (Terrasolid 2004). Ground points were used to create a digital elevation model (DEM) using inverse distance weighted interpolation at 1 m resolution. The DEM and aboveground points were used to calculate the canopy height model (CHM) using the spot elevation method

(Daniels 2001). This approach computed the canopy height (elevation above ground level) at each point by subtracting the DEM height from the CHM (Suratno et al. 2009).

NCLFA researchers delineated individual trees using a stem identification algorithm based on a combination of variable window local maxima filtering (Popescu and Wynne 2004) and neighborhood canopy height variance and return density (Rowell et al. 2006). This approach anticipated crown width (CW) as a function of canopy height and stand structure, and searched for a circle with dimensions of expected CW for points higher than the candidate point. If no circles are found, the candidate point was assumed to be a tree top. This process was conducted for every point in the CHM to produce a stem map (Suratno et al. 2009). For trees species at LEF, CW was expected to be 33% of the tree height for trees in stands with canopy cover less than 35%, 16% of tree height for trees in stands with moderately closed canopy cover ranging between 35% and 65%, and 11% of tree height for trees in stands with closed canopy cover greater than 65%. After a tree location and expected CW were estimated, crown base height (CBH) was estimated using a square search window of $2 \times CW$ m centered at the tree location. CBH was then estimated as the mean height of all CHM points inside the search window divided by the associated standard deviation of the heights. Individual tree diameter at breast height (DBH) were estimated using the following log-linear model ($n=1555$, $R^2= 0.76$, Error = 7.6%) (Rowell et al. 2009).

$$[3.1] \quad \ln DBH = 1.732 + (0.041 \times HT) + (0.798 \times RH) - (0.007 \times SD)$$

where, HT is the height of the tree (m), RH is the relative height (m) calculated as the tree height divided by the mean height of dominant and co-dominant trees in a $20 \text{ m} \times 20 \text{ m}$

neighborhood, and SD is stem density of dominant and co-dominant stems in the neighborhood.

For the applications of this study, we selected a forest stand in LEF (see Figure 3.1). The stand is 4.6 ha in size with elevations ranging from 1,270 to 1,310 m, on a north-facing aspect, and an average slope of 13.5% (0.0 – 36.3% slope range). Douglas-fir is the dominant species with a small amount of ponderosa pine. The stand has an established under- and middle-story creating continuous canopy fuels from the ground to the top of the canopy, resulting from logging in the mid-1940s and thinning in the mid-1970s. The LiDAR-derived stem map identified 11,213 stems, most of which are small, suppressed trees (Figure 3.2).

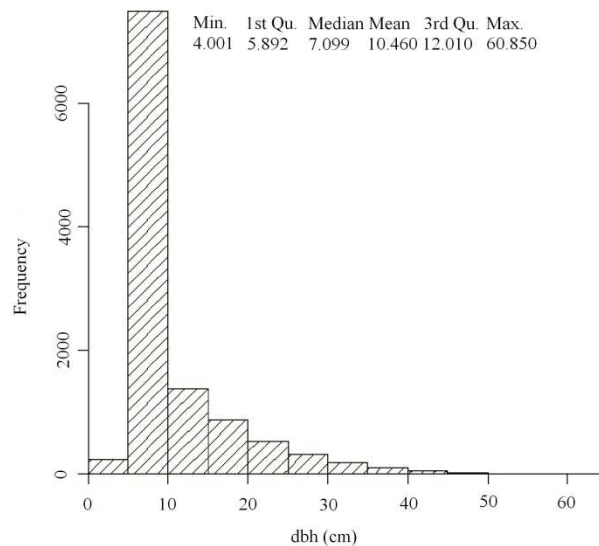


Figure 3.2. Histogram and summary statistics of DBH distribution of LiDAR-derived trees in the study area.

3.2.2 Wildland-urban interface Fire Dynamics Simulator (WFDS)

WFDS is an extended version of the Fire Dynamics Simulator developed by the Building and Fire Research Laboratory at the National Institute of Standards and Technology designed to include fire spread in vegetative fuels (Mell et al. 2007). WFDS is a fully three-dimensional model that, in recent years, has received considerable research attention because it can provide more reliable and detailed predictions of fire behavior and its effect over a wider range of conditions than existing widely-used models (Mell et al. 2005, Linn et al. 2002). WFDS is a physics-based computational fire model able to predict fine-scale time-dependent fire behavior, fire-fuel, and fire-atmosphere interactions in three dimensions (Mell et al. 2005). WFDS attempts to solve in some approximation equations governing fluid dynamics, combustion, and heat transfer, where all modes of heat transfer (conduction, convection, and radiation) present in both fire-fuel and fire-atmosphere interactions are modeled (Mell et al. 2005). WFDS uses voxels to represent the spatial distribution of fuels. Voxel dimensions might vary from centimeters to meter based on the scale of the fire simulation and level of detail. Fluid dynamics, combustion, and heat transfer equations are solved for each voxel to simulate fire behavior over the entire simulation domain.

3.2.2.1 Tree-level fuel representation

We used LiDAR-derived stem map and tree attribute inputs to represent the spatial distribution of canopy fuels in WFDS fire simulations. Each tree is defined by its x-, y-, and z-coordinates as well as DBH (cm), HT (m), CBH (m), crown length (m), and

CW (m). Tree crowns are represented as frusta of right circular cones where the bottom (larger) diameter equals the crown width at CBH and the top (smaller) diameter equals a single voxel size. WFDS can then determine the three-dimensional location and volume of each tree crown, identify all voxels inside tree crowns, and assign them canopy fuels characteristics such as bulk density and fuel moisture content (FMC). Although fuel density is likely to change within a tree crown, we assumed a homogeneous fuel density that is sufficient to initiate and sustain fire propagation within the crown. Additionally, moisture content is also likely to vary according to the fuels position inside the crown. For simplicity, we assumed a constant FMC throughout the tree crown volume. Amount and arrangement of surface fuels can have a significant effect on fire behavior. Although field sampling can be used to estimate the amount and type of surface fuels, detailed spatial distribution is rarely available. Typically, for the purpose of modeling fire behavior, surface fuels are classified according to fuels models (Anderson 1982) and assumed to be homogeneously distributed over the study area (Scott 2006). In this study, we assumed a homogeneous surface fuel bed represented by fuel model 10 (FBFM10), which we believe best describes the surface fuel conditions present in the study area at LEF.

3.2.2.2 Weather scenarios and input data

Weather conditions can have a significant effect on fire behavior (Cruz et al. 2006b, Scott and Reinhardt 2001, Rothermel 1972). For the purpose of evaluating the effects of fuel removal on fire behavior, either a range of values for weather parameters such as wind speed and FMC or values representing some condition of interest are

usually considered (Scott 2006, Scott and Reinhardt 2001). In this study, we considered two cases representing the average and severe weather conditions of a typical fire season in western Montana (June to September), defined by the 50th and 90th percentiles, respectively. More extreme weather conditions were not considered in this study because most fuel treatments are not likely effective in changing fire behavior under such conditions (Finney and Cohen 2003). In WFDS, weather conditions are defined by wind speed (m/s), ambient temperature (°C), ambient relative humidity (%), and FMC (%). We used historical observation data from the Seeley Lake (N 47°10'58", W -113°26'50") weather station, located approximately 30 km north of LEF, obtained from the National Fire and Aviation Management web application (<http://famtest.nwcg.gov/fam-web/>). Weather records consist of daily observations recorded at 13:00 hrs from July 1st 1954 to January 4th 2010. From these observations, we selected weather parameter values associated with the average and severe weather conditions.

In the WFDS model, the complex dynamics of a fire burning in crown fuels can produce significant fluctuations in the rate of spread and energy released in the surface fire, particularly at fine scales. As this highly dynamic (although realistic) behavior made it difficult to produce consistent surface fire conditions at the individual tree scales of our simulations, we chose to use a less dynamic, but more predictable, approach for characterizing the surface fire behavior. This can be accomplished in WFDS with a user-assigned surface fire, in which, the rate of spread (ROS) in m/s, heat release rate per unit area (HRRPUA) in kW/m², and residence time in seconds are all set as model inputs. Residence time is the time required for the flame to pass a stationary point at the top of the surface fuel (Anderson 1969). The same residence time was used for both weather

scenarios because it is a function only of the characteristic surface-area-to-volume ratio of the fuel particles (Anderson 1969). We used a residence time of 20 seconds based on Rothermel (1983) fuel particle sizes and residence time relationship for FBFM10. We adapted Rothermel's (1991) fuel moisture values typical of normal and late summer in the Northern Rocky Mountains (Table 3.2) and used NEXUS (Scott 1999) to obtain expected surface fire burning characteristics for FBFM10 surface fuels corresponding to our average and severe weather conditions, respectively. Table 3.3 shows the weather and surface fire inputs for the two weather conditions used in WFDS fire simulations. The intent of the user-assigned surface fire burning conditions was to provide consistent surface fire burning conditions for our fine scale crown fire initiation and tree-to-tree propagation simulations. This consistency facilitated our statistical modeling approach for prediction of crown fire initiation and propagation because the surface fire conditions could be described as a single set of conditions, rather than a complex and variable, time and space dependent evolution of surface fire conditions.

Table 3.2. Fuel moisture percentage values used to obtain surface fire intensity parameters.

Fuel type	Average conditions (normal summer)	Severe conditions (late summer)
1-h	4	2
10-h	5	3
100-h	6	4
Live woody	100	75

Table 3.3. Weather and surface fire inputs used in WFDS fire simulations.

	Average conditions (50 th percentile)	Severe conditions (90 th percentile)
Wind speed	2.22 (m/s)	3.56 (m/s)
Adjusted wind speed ¹	0.66 (m/s)	1.07 (m/s)
Max. ambient temperature	26.1 °C	32.1 °C
Ambient relative humidity	26 %	14 %
FMC	100 %	100 %
ROS	0.05 (m/s)	0.1 (m/s)
HRRPUA	650 (kW/m ²)	700 (kW/m ²)
Residence time	20 (s)	20 (s)

¹ After applying a wind reduction factor of 0.3, the ratio of midflame to open windspeeds (Rothermel 1983)

3.2.3 Tree-Level Fuel Connectivity

We designed WFDS simulations to model crown fire ignition and propagation independently because the transition of fire from surface to crown fuels and the propagation of fire through adjacent tree crowns are separate processes influenced by different tree and fuel characteristics. (i.e., CBH and tree spacing, respectively).

3.2.3.1 Vertical fuel connectivity – crown fire initiation

WFDS simulations were designed to determine a critical CBH that allows crown fire initiation given the burning characteristics of each weather condition. A simulation domain was set up within a small area of 0.24 ha, 60 m long × 40 m wide × 30 m high (Figure 3.3). For fire computations this area was divided into 120 × 80 × 60 voxels of 0.5 m resolution. Surface fuels that burn with the characteristics defined by HRRPUA, ROS, and residence time were simulated within the spatial domain. A fire ignition point was placed in the middle of the left edge of the simulation domain. Nine trees were placed systematically in a grid starting at 20 m from the left edge of the simulation domain. We

arbitrarily selected 15-meter spacing between trees to avoid the propagation of fire through adjacent crowns. Figure 3.3 shows an example of a WFDS simulation for crown fire initiation. Trees in a given simulation were set to have varying sizes (i.e., DBH, HT) but a similar CBH. For a given WFDS simulation, a target CBH was determined, and nine trees with CBH within 0.25 m from the target CBH were randomly selected from the LiDAR dataset and placed in the simulation domain. Fourteen different CBH values were considered in this study, ranging from 0 m to 6.5 m at intervals of 0.5 m. For each target CBH value, we developed 10 repetitions resulting in a total of 140 crown fire initiation simulations under each weather condition.

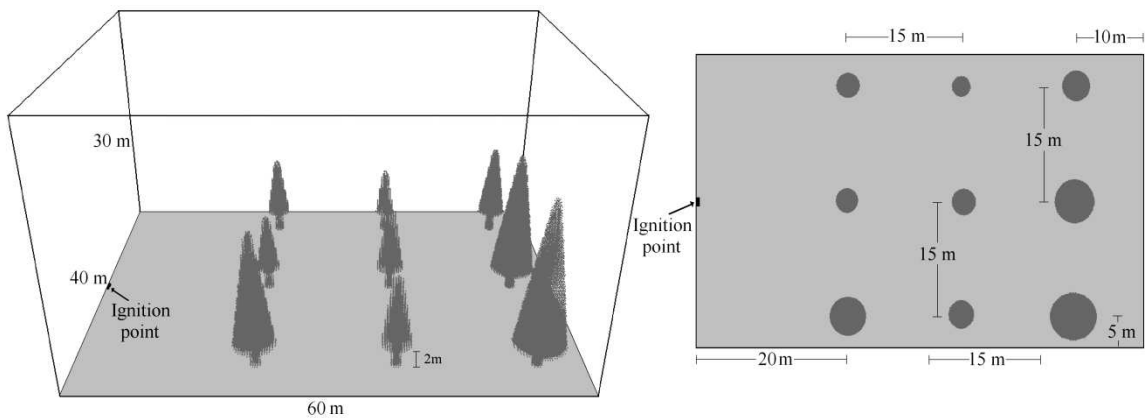


Figure 3.3. WFDS simulation design for crown fire initiation showing nine trees with different dimensions but similar CBH (i.e., 2 m).

3.2.3.2 Horizontal fuel connectivity – crown fire propagation

WFDS simulations were designed to predict crown fire propagation from a burning tree crown to an adjacent tree crown in front of the flaming front. A simulation domain was set to 30 m long \times 20 m wide \times 30 m high, which resulted in $60 \times 40 \times 60$ voxels with a 0.5 m resolution. As in the crown fire ignition simulations, surface fuels

burning with the characteristics defined by HRRPUA, ROS, and residence time were simulated within the spatial domain, and a fire ignition point was located in the middle of the left edge. One source tree representing the flaming front with crown fuels expected to ignite was placed at the center of the domain and a target tree ahead of the flaming front was placed to the right (Figure 3.4). Spacing between these two trees (SP) was defined as the horizontal gap distance between their crown projections (edge to edge). We simulated crown fire propagation with several SP values ranging from 0 m to 3.5 m at intervals of 0.5 m. To account for wider flaming fronts formed by more than one tree, we also considered one and two additional source trees. When considering two trees forming the flaming front, one additional source tree was placed next to the first source tree on a randomly selected side. The horizontal distance between both source trees was set to provide a crown overlap at 10% of the distance between the tree centers to ensure a continuous flaming front. When considering a flaming front formed by three trees, one additional source tree was placed on each side of the first source tree located at the center of the simulation domain also with a crown overlap of 10% of the tree spacing. Tree sizes were randomly selected from the LiDAR dataset for tree attributes. However, a low CBH (i.e., 0.5 m) was assigned to the source trees to ensure tree crown ignition, while the target tree's CBH was kept relatively high (i.e., 3.0 m) to avoid crown fire initiation from a surface fire. Ten repetitions of each fire simulation were developed, resulting in a total of 240 crown fire propagation simulations under each weather condition.

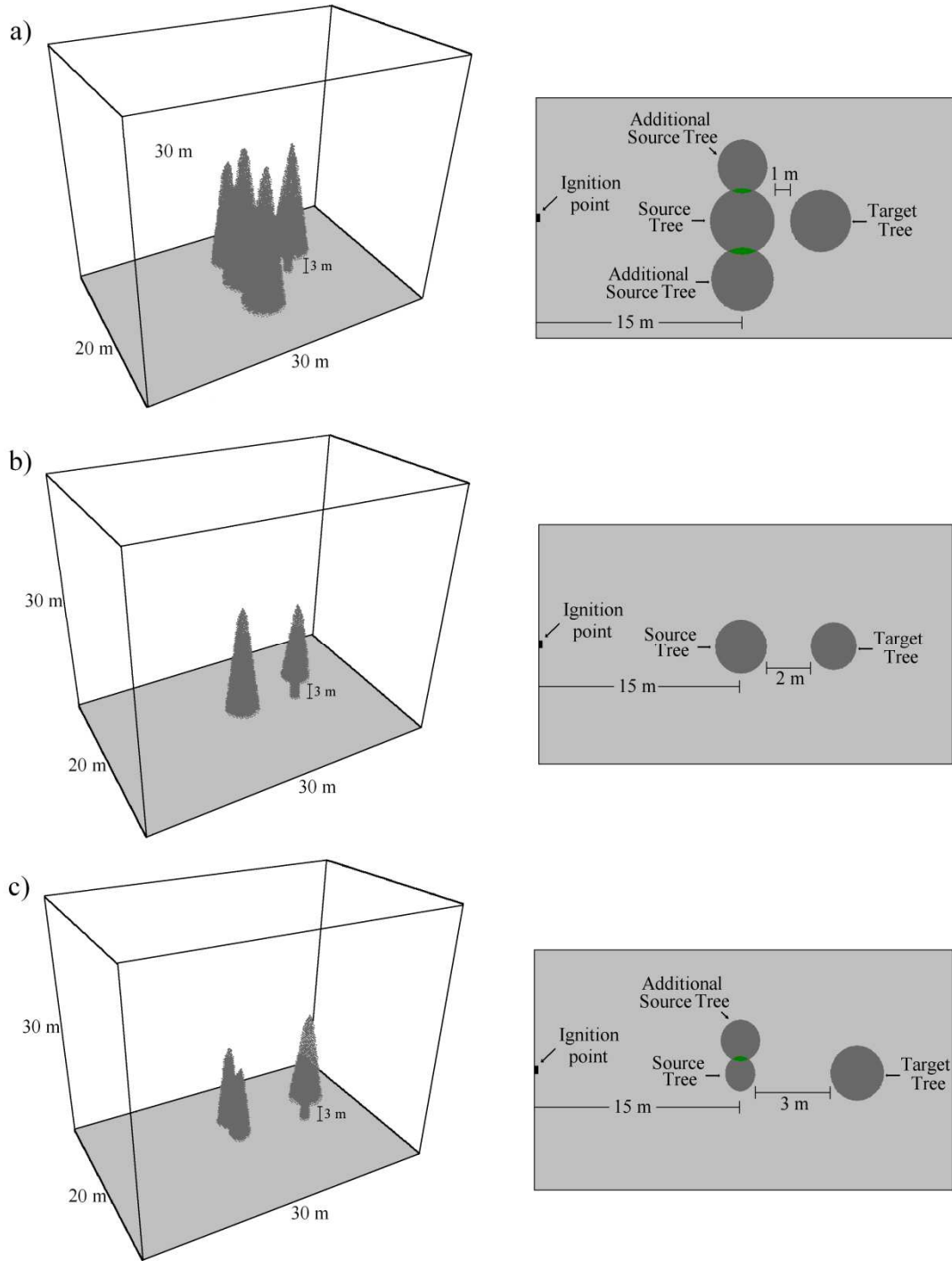


Figure 3.4. WFDS simulation design for crown fire propagation. Examples show three, one, and two trees forming the flaming front (a, b, and c) and increasing spacing between the source and target tree.

3.2.4 Regression Models

We calculated the percentage of dry mass loss (DML) for each tree at the end of all WFDS fire simulations to quantify the extent of tree-level burning (Murray et al. 1971). Percent DML was then converted into a binary variable to represent whether or not tree burning occurred (1 if percent DML > 0.5 and 0 otherwise), and used as a response variable.

Logistic regression analysis was used to model the percent DML because of the nature of our response variable (i.e., the occurrence or not of tree burning). The multiple logistic regression model has the following form:

$$[3.2] \quad P = \frac{e^{g(x)}}{1 + e^{g(x)}}$$

with the logit function given by the equation,

$$[3.3] \quad g(x) = \beta_0 + \beta_1 x_1 + \beta_2 x_2 + \dots + \beta_i x_i$$

where, P is the probability that tree burning will occur, x_i are the independent variables, and β_i are coefficients estimated through the maximum likelihood method, which will select coefficient values that maximize the probability density as a function of the original dataset (Hosmer and Lemeshow 2000).

In the R software platform (The R development team <http://www.R-project.org>), we fit a binomial generalized linear model specified by giving a two-column response using the *glm* function. To predict crown fire initiation, we considered three tree dimensions – DBH, HT and CBH – as potential independent variables. Because CW and crown length can be obtained from HT and CBH, they were not considered as potential

predictors. For crown fire propagation, in addition to the three tree dimensions, we included SP as well as measures of tree density as surrogates of the flaming front size approaching the target tree (see Figure 3.4) and considered them as potential predictors.

For measures of tree density, we used six distance-dependent competition indices to include trees forming the flaming front (i.e., one, two, or three source trees – see Figure 3.4). Table 3.4 shows the distance-dependent competition indices considered in this study. CI_1 (Hegyí 1974) and CI_2 (Baathe 1980, as cited in Pukkala and Kolström 1987) are size-ratio competition indices using DBH and HT as indicators of tree size, respectively. CI_3 through CI_6 are size-ratio indices employing sums of subtended angles (Rouvinen and Kuuluvainen 1997). CI_3 is the sum of horizontal angles originating from the target tree center and spanning the DBH of the each source tree. CI_4 is the sum of the horizontal angles multiplied by the ratio of the DBH of the source trees and the target tree. CI_5 is the sum of vertical angles from the target tree base to the top of the source trees. CI_6 includes the ratio of the HT between the source trees and the target trees. These indices were developed to measure the competition level experienced by a given tree. However, their formulations effectively capture proximity and size of the flaming front by incorporating size and location of trees forming the flaming front which is related to the amount of heat released from the approaching fire and transferred to the target tree.

Table 3.4. Distance-dependent competition indices used to obtain measures of partial tree density.

Index	Source	Equation
CI ₁	Hegyi (1974)	$\sum_{i=1}^n d_i / (d \times dist_i)$
CI ₂	Baathe (1980), cited in Pukkala and Kolström (1987)	$\sum_{i=1}^n h_i / (h \times dist_i)$
CI ₃	Rouvinen and Kuuluvainen (1997)	$\sum_{i=1}^n \arctan(d_i / dist_i)$
CI ₄	Rouvinen and Kuuluvainen (1997)	$\sum_{i=1}^n (d_i / d) \times \arctan(d_i / dist_i)$
CI ₅	Rouvinen and Kuuluvainen (1997)	$\sum_{i=1}^n \arctan(h_i / dist_i)$
CI ₆	Rouvinen and Kuuluvainen (1997)	$\sum_{i=1}^n (h_i / h) \times \arctan(h_i / dist_i)$

n number of source trees forming the flaming front (i.e., one, two, three); d_i DBH of the i^{th} source tree (cm); d DBH of the target tree ahead of the flaming front (cm); $dist_i$ horizontal distance from the i^{th} source tree to the target tree (m); h_i height of the i^{th} source tree (m); h height of the target tree (m).

We calculated three model performance measures: sensitivity (proportion of ignited trees correctly predicted as such), specificity (proportion of not-ignited trees correctly predicted), and overall accuracy. For model selection purposes, we started with all potential predictors, and then removed insignificant variables ($\alpha = 0.05$) to obtain a parsimonious model with high predictive quality in terms of these three performance measures.

3.2.5 Thinning Scenarios

We considered three thinning scenarios to evaluate their effects on reducing crown fire potential. Figure 3.5 shows the location of all LiDAR-derived trees, and the locations of leave-trees considered in each thinning scenario in the study area. Thinning scenario I (Figure 3.5b) represents the case of applying a thinning from below where

primarily small suppressed and intermediate trees are removed to reduce the vertical continuity of fuels and total fuel availability. Under this thinning prescription, all small trees with a DBH less than 12.7 cm (5 inches) were assumed to be cut, piled and burned. Larger trees were considered merchantable and to be extracted for sale. Tree selection (location of cut- and leave-trees) was done manually simulating the marking process carried out by markers on the ground based on spacing between trees and tree sizes. For scenario II, cut-trees were manually selected until a target tree density of 400 leave-trees per hectare was met (Figure 3.5c). For scenario III, additional cut-trees were selected among the leave-trees used in scenario II until a target tree density of 300 leave-trees per hectare was met (Figure 3.5d).

We applied the crown fire initiation models to predict vertical fuel connections for each leave-tree in each thinning scenario based on model selected tree dimensions (i.e., HT, CBH). Horizontal fuel connections among adjacent trees were predicted by applying the crown fire propagation models based on model selected predictors (i.e., tree dimensions, SP and partial tree density). A flaming front area of 1.5 m × 10 m centered at the first source tree location was used to search for additional source trees. Trees inside the flaming front area were then considered as additional source trees. Figure 3.6 shows an example of a flaming front formed by three trees, a source trees and two additional source trees (dashed crown projections), used to predict crown fire propagation between the source tree and the target tree (solid crown projections). We predicted horizontal fuel connections for each pair of leave-trees in each thinning scenario.

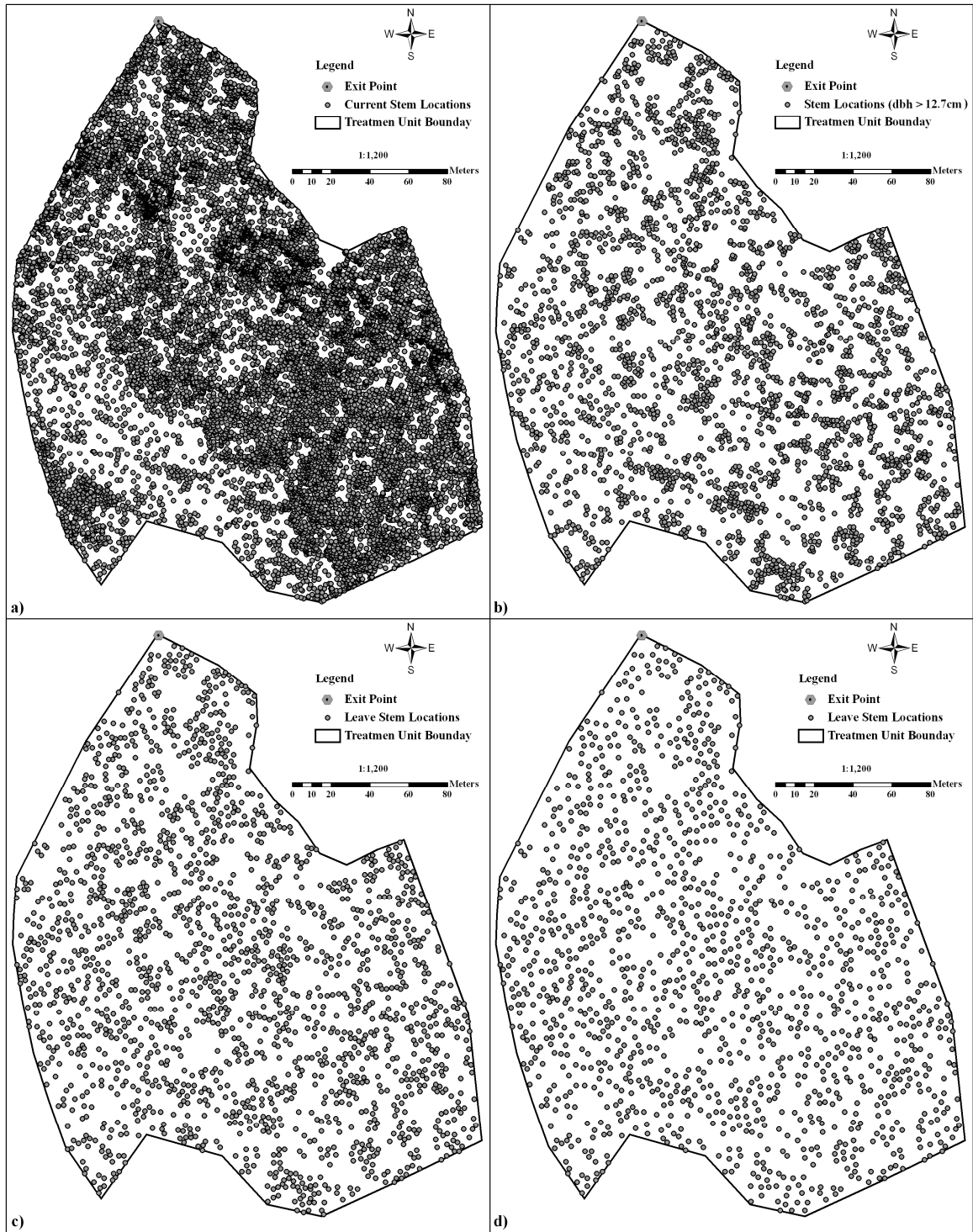


Figure 3.5. LiDAR-derived stem map of trees in the study area (a), and location of leave-tree under thinning scenarios I through III, b) through d) respectively.

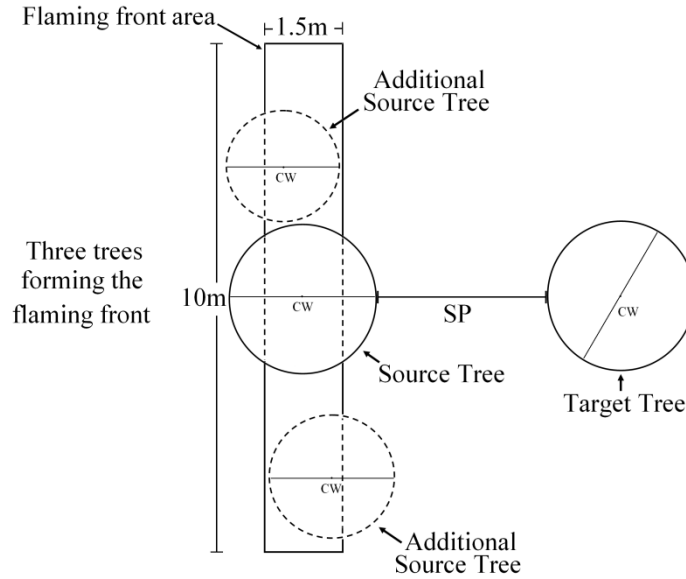


Figure 3.6. Schematic of the flaming front area used to estimate crown fire propagation between a source tree and a target tree.

After predicting tree-level fuel connectivity among leave-trees in the study area, we evaluated the three thinning scenarios in terms of the number of predicted vertical and horizontal fuel connections. The number of vertical connections represents the number of trees that would ignited under a given weather condition. Similarly, for a given weather conditions, the number of horizontal fuel connections represents the amount of trees that would burn after fire reaches crown fuels through vertical fuel connections.

3.3 RESULTS AND DISCUSSION

3.3.1 Regression Models

3.3.1.1 Crown fire initiation – vertical fuel connectivity

WFDS simulation results for predicting crown fire initiation indicate that the range of CBH values that allow crown fire initiation varies with weather conditions. Table 3.5 shows the proportion of trees that ignited at different CBH values analyzed in this study under each weather condition. Based on these results, we limited the range of CBH values considered in the development of regression models to emphasize modeling efforts on effective tree CBH values and avoid over-estimation of models predictive quality. We considered trees with CBH from 1.5 m to 4.5 m and from 3.5 m to 6.5 m for the average and severe weather conditions, respectively.

Table 3.5. Proportion of trees expected to ignite for each target CBH value considered in the crown fire initiation simulations under both weather conditions.

CBH	Average conditions	Severe conditions
0.0	1.00	1.00
0.5	1.00	1.00
1.0	1.00	1.00
1.5	1.00	1.00
2.0	0.93	1.00
2.5	0.89	1.00
3.0	0.33	1.00
3.5	0.15	1.00
4.0	0.11	0.89
4.5	0.00	0.78
5.0	0.00	0.44
5.5	0.00	0.19
6.0	0.00	0.19
6.5	0.00	0.00

The distribution of percent DML for trees considered in the crown fire initiation simulations (Figure 3.7), under both weather scenarios, indicates that most trees either ignited burning crown fuels completely or did not ignite. This also justifies the 0.5 arbitrary threshold selected to determine the binary nature of vertical fuel connections.

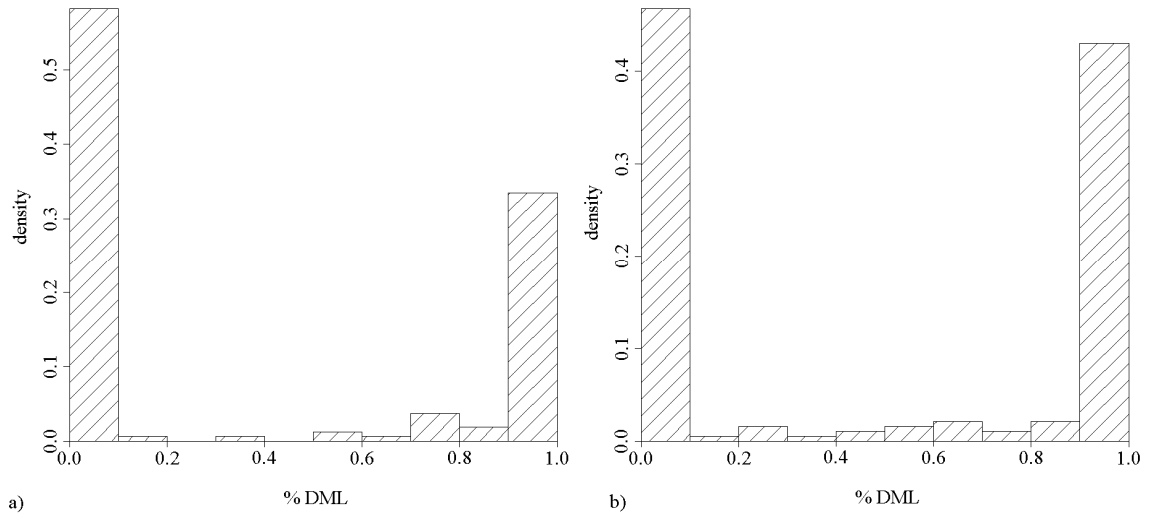


Figure 3.7. Percent dry mass lost distribution from trees in the WFDS crown fire initiation simulations for average (a) and severe conditions (b).

Tree height is the tree attribute directly measured using LiDAR data and because it was used to estimate DBH (Eq. 1), HT and DBH present a strong correlation (Table 3.6). On the other hand, CBH is not well correlated with either DBH or HT. CBH is the tree attribute most strongly correlated with percent DML ($r = -0.723$). This negative correlation indicates that as CBH increases, the probability of crown tree ignition decreases.

Table 3.6. Correlation matrix showing the relationship between the three tree attributes and their relationship with percent DML.

	DBH	HT	CBH	% DML
DBH	–	0.828	0.187	0.054
HT		–	0.195	0.085
CBH			–	-0.727

For both weather conditions, the selected logistic regression model included HT and CBH as independent variables. As CBH directly affects the amount of heat transfer from the surface fire to crown fuels, it is a significant predictor of crown fire initiation. Although, HT is not strongly correlated with percent DML, its inclusion in the logistic model indicates it is a significant variable for predicting the binary response of crown fire initiation. This could be explained because HT is directly proportional to CW, which is related to the crown base area being heated from the surface fire. Thus, trees with larger crown base areas absorb radiative and convective heat from the surface fires for longer periods of time than trees with smaller crown base areas. Interaction between CBH and HT was also tested but it was insignificant for both weather scenarios.

The logit function associated with the final crown fire initiation prediction models for the average and severe weather conditions are presented in Equations 3.4 and 3.5 respectively.

$$[3.4] \quad g(x) = 5.98838 + (0.19224 \times HT) - (2.86137 \times CBH)$$

$$[3.5] \quad g(x) = 10.93897 + (0.24285 \times HT) - (2.84814 \times CBH)$$

The difference in the intercept coefficient value between both models reflects the difference in the surface fire burning conditions, where a tree is less likely to ignite under the average weather conditions than the severe conditions. In concordance with our

assumption of crown fire ignition (percent DML > 0.5), we also assumed ignition will occur when the predicted probability $P > 0.5$. The resulting performance measures for both crown fire initiation models have similar prediction quality with overall accuracy levels of approximately 87% and 86% for the average and severe conditions, respectively (Table 3.7). Sensitivity and specificity indicate similar ability to predict ignited and not-ignited trees in both weather conditions.

Table 3.7. Logistic regression model predictive quality for crown fire initiation under average and severe weather conditions.

Average weather conditions			
	Predicted Not-ignited	Predicted Ignited	
Observed Not-ignited	331	41	Sensitivity = 0.8450
Observed Ignited	40	218	Specificity = 0.8898
Accuracy = 0.8714			
Severe weather conditions			
	Predicted Not-ignited	Predicted Ignited	
Observed Not-ignited	270	47	Sensitivity = 0.8722
Observed Ignited	40	273	Specificity = 0.8517
Accuracy = 0.8619			

3.3.1.2 Horizontal fuel connectivity – crown fire propagation

WFDS simulation results for crown fire propagation show that weather conditions largely affect the ranges of SP values that allow fire propagation between adjacent trees. Under the average weather conditions, fire did not propagate when SP between trees was larger than 1.0 m (Table 3.8). This is mainly because of the relatively low wind speed used in these weather conditions (see Table 3.3). On the other hand, under the severe weather scenario where wind speed is about 60% higher than the average condition, fire propagated in some cases where SP was 3.0 m. These results are in concordance with literature indicating that wind speed is one of the most important drivers of crown fire

propagation (Rothermel 1983, Rothermel 1972). We considered SP from 0.0 m to 1.5 m and from 0.5 m to 3.5 m for average and severe weather conditions, respectively, to emphasize modeling efforts on effective tree spacing in fire propagation and avoid over-estimating the models predictive quality. Although less clear than crown fire initiation, the distribution of percent DML of trees considered in the crown fire propagation simulations (Figure 3.8), under both weather scenarios, also justify the 0.5 arbitrary threshold selected to determine the binary nature of horizontal fuel connections. These results indicate that when fire propagates from an ignited tree(s) to an adjacent tree, most adjacent trees completely burn.

Table 3.8. Proportion of adjacent trees burned through crown fire propagation for each target spacing under both weather conditions.

Spacing	Average conditions	Severe conditions
0.0	0.55	1.00
0.5	0.40	1.00
1.0	0.20	0.89
1.5	0.00	0.67
2.0	0.00	0.56
2.5	0.00	0.22
3.0	0.00	0.33
3.5	0.00	0.00

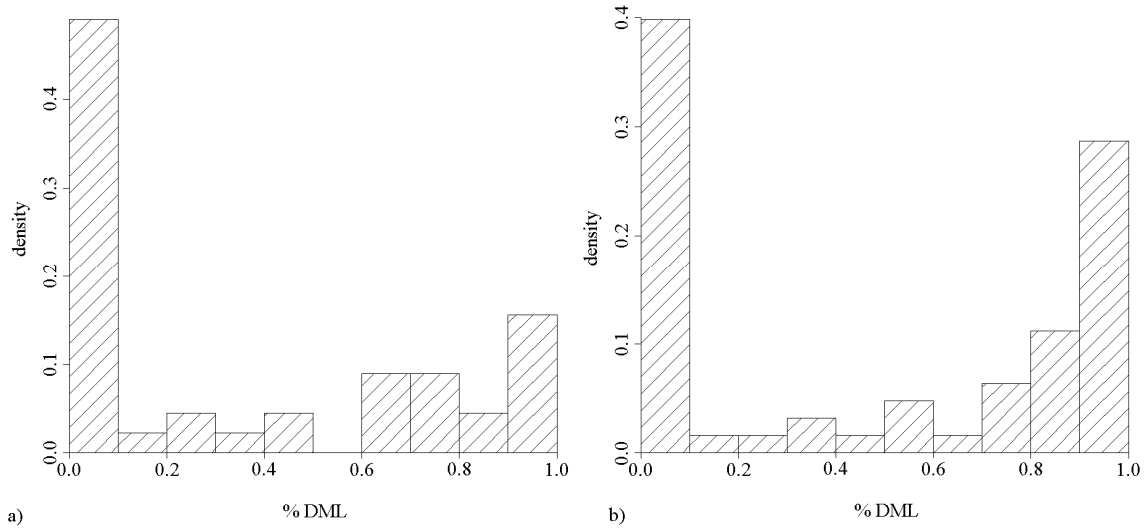


Figure 3.8. Percent dry mass lost distribution from trees in the WFDS crown fire propagation simulations for average (a) and severe conditions (b).

The six measures of partial tree density present strong correlation among each other because of the similarities in their formulation (Table 3.9). These competition indices were evaluated individually along with the other potential predictors to avoid colinearity issues. In general, competition indices are not strongly correlated with percent DML. The indices more correlated with the response variable presented r values of about 0.49.

Table 3.9. Correlation matrix of the six competition indices and their relationship with percent DML.

	CI ₁	CI ₂	CI ₃	CI ₄	CI ₅	CI ₆	% DML
CI ₁	–	0.936	0.828	0.912	0.794	0.896	0.298
CI ₂		–	0.815	0.804	0.836	0.932	0.350
CI ₃			–	0.819	0.969	0.829	0.486
CI ₄				–	0.726	0.902	0.275
CI ₅					–	0.825	0.494
CI ₆						–	0.343

For the average weather conditions, the selected logistic regression model included HT, SP, and CI₁ as independent variables. For the severe conditions, HT and SP were also included; however, CI₃ was the best competition index selected as independent variable. The logit functions associated with the final crown fire propagation prediction models for the average and severe weather conditions are presented in Equations 3.6 and 3.7 respectively.

$$[3.6] \quad g(x) = -5.3475 + (0.2855 \times HT) - (2.1397 \times SP) + (2.2222 \times CI_1)$$

$$[3.7] \quad g(x) = -6.9064 + (0.3194 \times HT) - (3.2356 \times SP) + (69.4118 \times CI_3)$$

Based on the models' coefficients, the probability of crown fire propagating from a source tree to a target tree increases as the target tree's height increases. As expected, the probability of crown fire propagation decreases with increasing spacing between trees. The larger the flaming front, as measured by CI₁ and CI₃, the larger the probability of crown fire propagation. The resulting performance measures for the crown fire propagation model under the average conditions show an overall predictive quality of 80% (Table 3.10). Sensitivity and specificity measures show that the model better predicts cases where fire does not propagate through adjacent trees than when fire propagates (85% vs. 71%). For the severe weather conditions, the model has an overall predictive quality of about 93% and similar sensitivity and specificity levels (Table 3.10). The lower predictive quality of the model for average weather conditions might be explained by the fact that even with zero spacing between trees, fire propagated only to 55% of target trees (see Table 3.8). If trees with overlapping crowns (negative SP values) were included in the analysis to obtain fire propagation to 100% of target trees, predictive quality is likely to increase.

Table 3.10. Logistic regression model predictive quality for crown fire propagation under average and severe weather conditions.

Average weather conditions			
	Predicted Not-ignited	Predicted Ignited	
			Accuracy = 0.8000
Observed Not-ignited	64	11	Sensitivity = 0.7111
Observed Ignited	13	32	Specificity = 0.8533
Severe weather conditions			
	Predicted Not-ignited	Predicted Ignited	
			Accuracy = 0.9381
Observed Not-ignited	93	7	Sensitivity = 0.9369
Observed Ignited	7	104	Specificity = 0.9300

From the results of WFDS fire simulations for both weather conditions, we observed variability in crown fire propagation among trees with similar dimensions as well as trees with an approaching crown fire of similar size (represented by the number and size of trees forming the flaming front). Similarly, fire simulation results present variability in crown fire initiation among trees of similar sizes (i.e., HT and CBH). This variability is likely to be explained by micro fire-fuel, fire-atmosphere interactions considered and modeled in WFDS simulations. Although we could theoretically extract measures of these interactions from the WFDS simulation results (such as resulting flame height, and wind profile) and include them as predictors in our logistical regression models, it would be impractical to obtain this type of information on the ground.

3.3.2 Evaluation of Alternative Thinning Scenarios

The tree-level fuel connectivity results from applying the logistic regression models to each of the three thinning scenarios are presented in Table 3.11. For all thinning scenarios, the number of trees expected to ignite under the average weather

conditions is smaller than under the severe weather conditions because of the less intense surface fire. About five times more trees are expected to ignite under the severe weather conditions than the average conditions. As thinning intensity increases, fewer small trees with low CBH are left in the forest stand, and thus the number of trees expected to ignite decreases under both weather conditions.

Table 3.11. Tree-level fuel connectivity results from the logistic regression models under both weather conditions for each thinning scenario.

Thinning scenario	Weather conditions	Number of trees	Crown fire initiation		Crown fire propagation		
			Number of trees ignited	Percentage of trees ignited	Number of connected clusters	Average connection per tree	Average trees per cluster
I	Average	2645	99	3.75	82	7.28	32.26
	Severe		536	20.26	38	10.49	69.60
II	Average	1840	76	4.13	109	4.29	16.88
	Severe		393	21.36	73	5.27	25.20
III	Average	1380	66	4.78	211	2.63	6.54
	Severe		289	20.94	158	3.09	8.73

Fuel connections between pairs of adjacent trees were also predicted by applying the crown fire propagation prediction models. As crown fire propagates only through nearby adjacent tree crowns (i.e., $SP \leq 1$ m and 3 m under the average and severe weather conditions, respectively), the models predicted clusters of connected trees throughout the forest stand. Figures 3.9 through 3.11 show the spatial distribution and size of clusters formed by tree-level fuel connections among adjacent trees under each weather condition for thinning scenarios I through III, respectively.

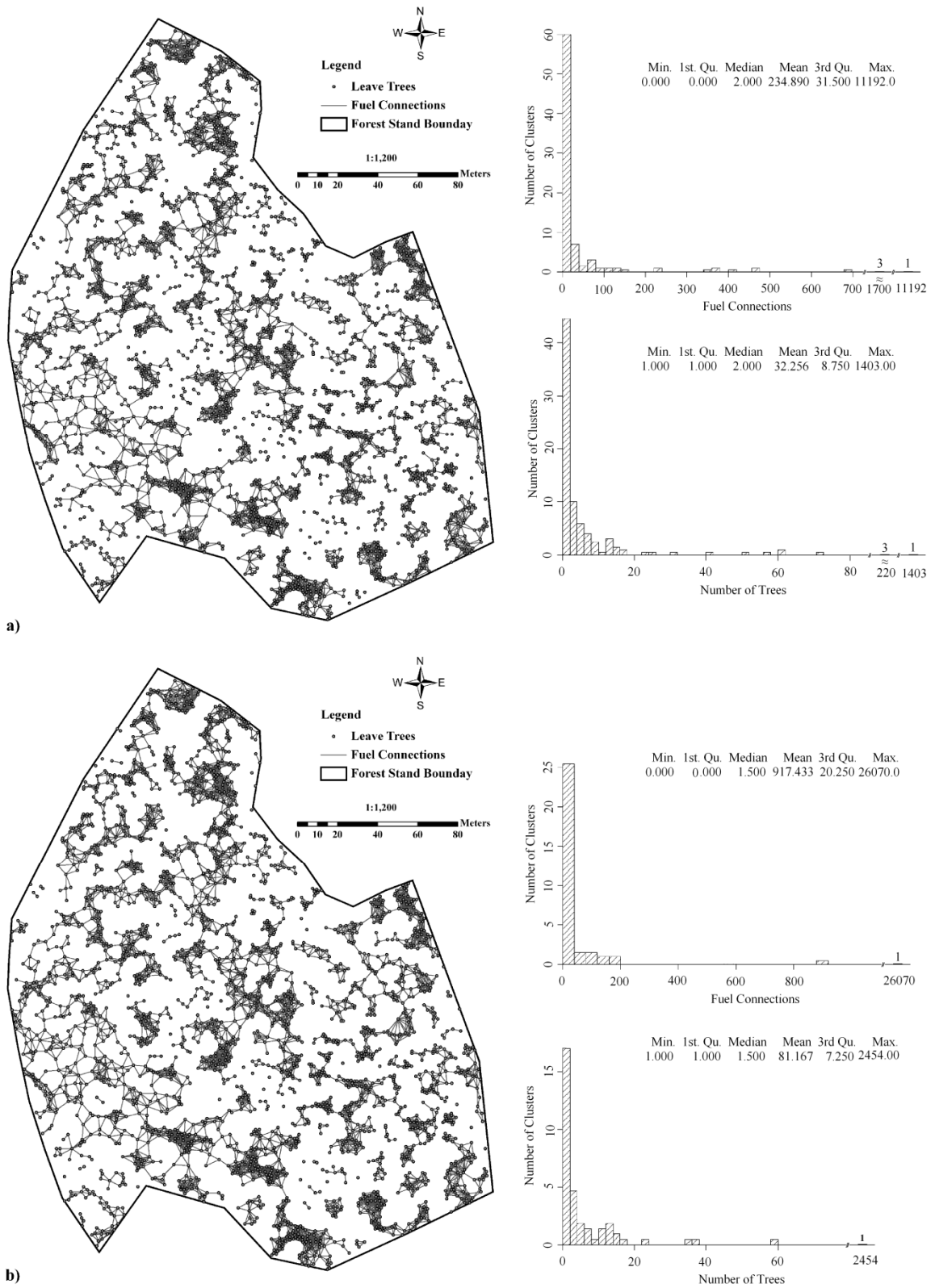


Figure 3.9. Location and size of clusters formed by predicted tree-level fuel connections for thinning scenario I under average (a) and severe (b) weather conditions.

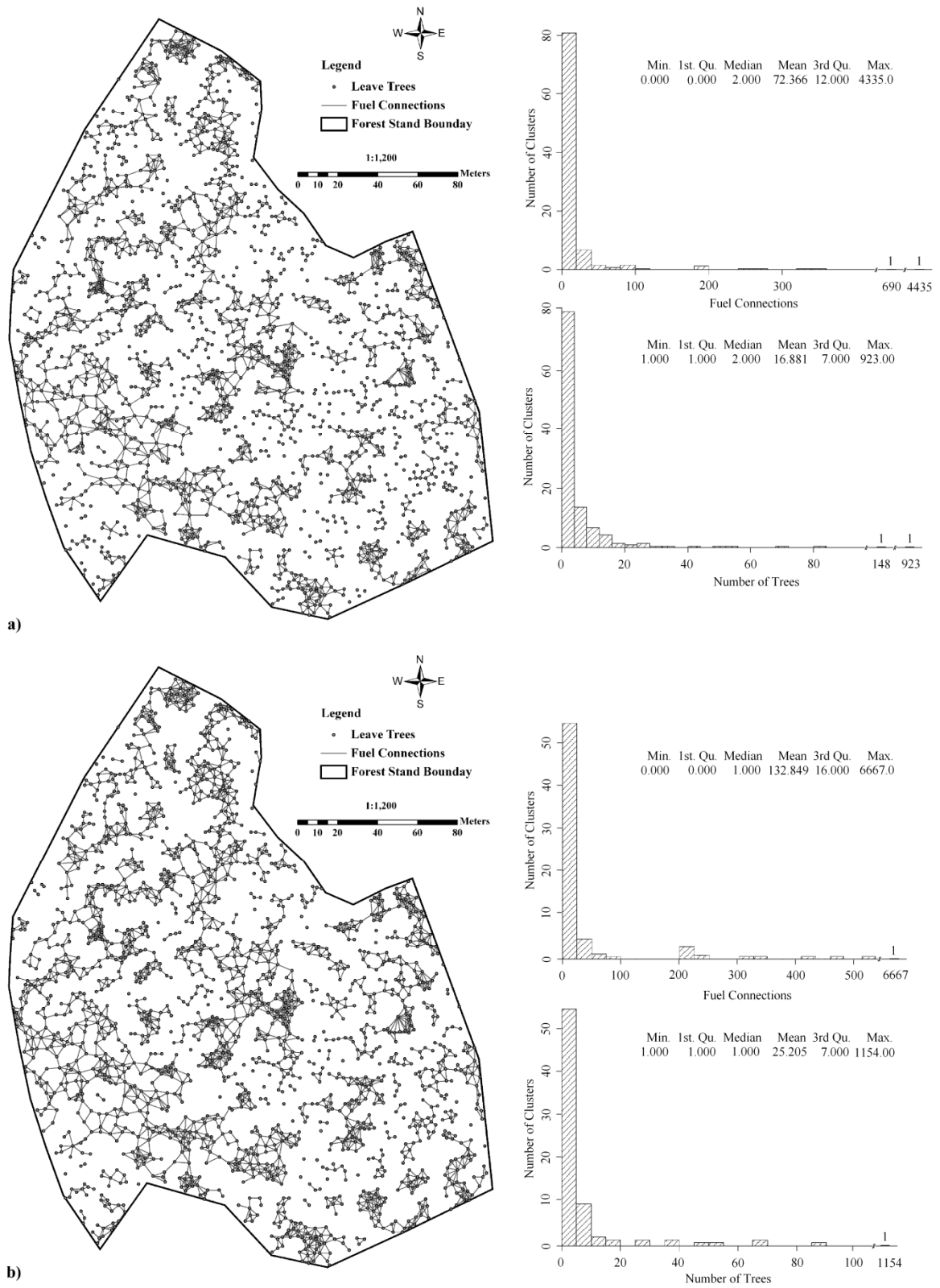


Figure 3.10. Location and size of clusters formed by predicted tree-level fuel connections for thinning scenario II under average (a) and severe (b) weather conditions.

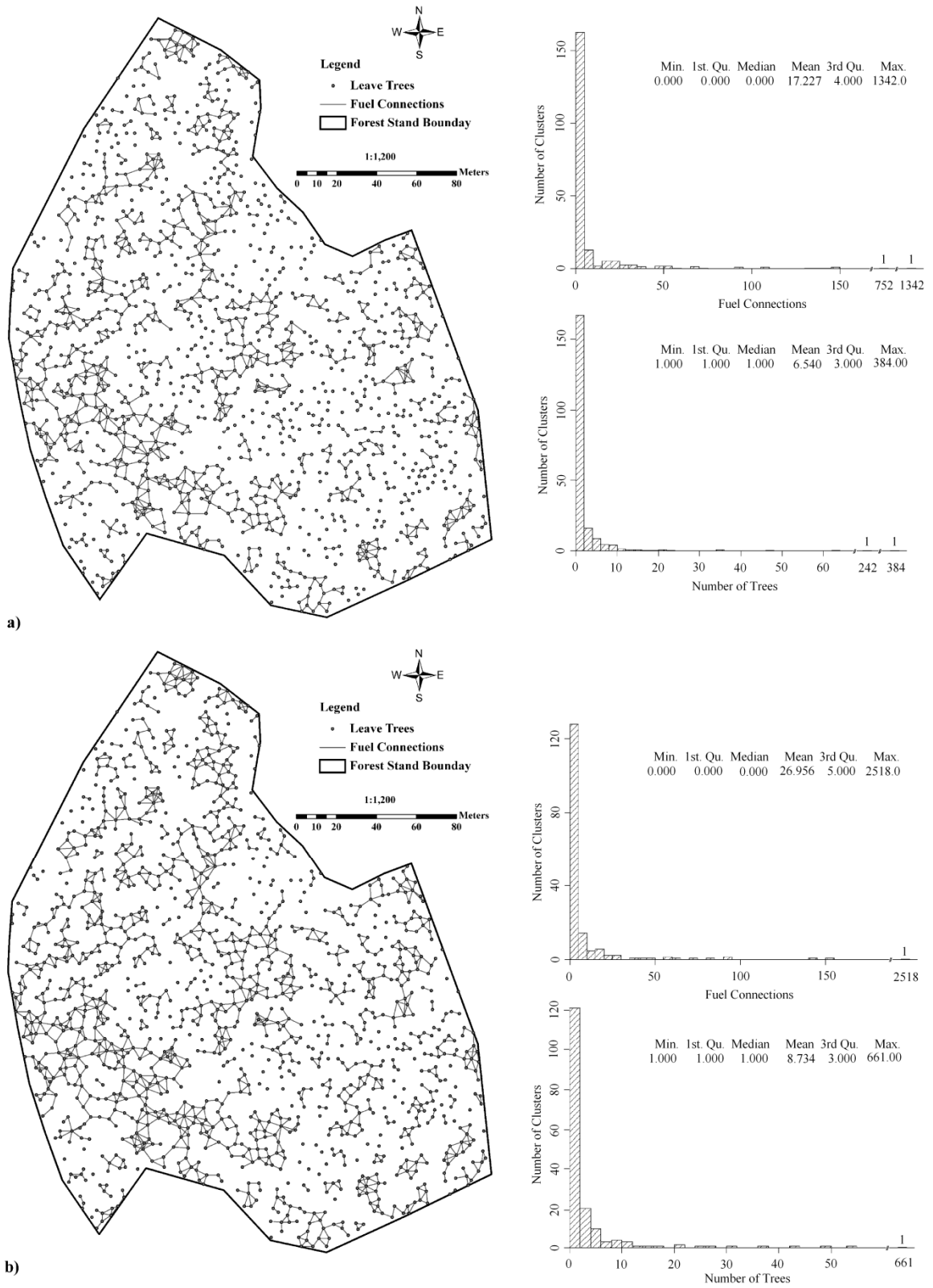


Figure 3.11. Location and size of clusters formed by predicted tree-level fuel connections for thinning scenario III under average (a) and severe (b) weather conditions.

For thinning scenario I, applying the crown fire propagation prediction model for each tree in the stand under the average weather conditions resulted in 82 clusters of connected tree crown fuels (Figure 3.9). Each cluster is formed by an average of 32.26 trees and each tree's crown fuels are connected to an average of about seven adjacent trees. When severe weather conditions are considered, crown fire can propagate over a larger distance between adjacent trees. The model thus predicted fewer clusters of connected trees, and a larger number of average fuel connections per tree compared with the average conditions (Table 3.11). The number of clusters predicted under the severe weather conditions is about 30% of those predicted under the average conditions, and the average cluster is formed by about 2.5 times as many trees, where trees are connected to about 30% more adjacent trees. Under both weather scenarios, most clusters are formed by less than 20 connected trees, but there are a few large clusters connecting a large number of trees. For example, 5% of the clusters connect about 95% of the entire trees in the stand (see Figure 3.9), and the largest cluster connects about 60% and 90% of trees under the average and severe weather conditions, respectively.

For thinning scenario II, the crown fire propagation models predicted a larger number of smaller clusters than those predicted for thinning scenario I because the more intensive thinning intensity left fewer, larger and sparser trees in the stand. Under the average weather conditions there are almost 30% more clusters as those predicted under the severe conditions; however, clusters under severe conditions are much larger and trees are connected to more adjacent trees (Table 3.11). The same pattern of few clusters connecting most trees in the stand observed in thinning scenario I appears in thinning scenario II under both weather conditions (Figure 3.10). The largest cluster connects

approximately 55% and 70% of the trees under the average and severe weather conditions, respectively. For thinning scenario III, the number of clusters under both weather conditions is about twice as many as those predicted for thinning scenario II. However, cluster size is about one third of those in scenario II averaging 6.54 and 8.73 trees under the average and severe weather conditions, respectively (Table 3.11). The largest cluster is also much smaller than those for the previous thinning scenarios connecting about 36% and 59% of the remaining trees under the average and severe weather conditions (Figure 3.11).

3.3.3 Capturing Spatial Variability of Fuels

The results of the tree-level fuel connectivity prediction models from the three thinning scenarios suggest that as thinning intensity increases crown fire potential decreases, as represented by the number of vertical and horizontal fuel connections. Same results can be obtained using the widely-used existing fire behavior model such as FlamMap (Finney 2006) to predict crown fire potential for the study unit. However, as mentioned before, existing models are designed for stand-level predictions and ignore spatial variability of fuels within stands, which can have a significant effect on changing fire behavior. For example, for the same thinning prescription, a given combination of cut-trees might result in minimal crown fire propagation through adjacent tree crowns because of relatively large spacing among leave-trees (i.e., SP larger than 3.5 m), while an alternative combination of cut-trees might lead to fire propagating through most leave-trees because of small trees spacing.

To illustrate the importance of capturing the spatial variability of fuels (i.e., tree locations) within stands, we compared alternative combinations of leave-tree locations under the same thinning intensity. We applied the fuel connectivity predictive models under the severe weather conditions to the manually selected leave-tree locations considered in thinning scenario III, as well as five alternative combinations of randomly selected leave-trees. The results of the predicted fuel connectivity show that the spatial distribution of leave-trees can have a considerable effect on crown fire potential. Tree-level fuel connectivity among the five combinations of random leave-tree locations is relatively similar. However, all these combinations of random leave-trees have a larger number of fuel connections than the combination of manually selected leave-tree locations (Table 3.12). The number of fuel connections in combinations of randomly selected leave-trees is about 50% larger than in combination of manually selected leave-trees. Additionally, all combinations of randomly selected trees have fewer and larger clusters with more fuel connection per tree than in the case of manual leave-tree locations.

Table 3.12. Tree-level fuel connectivity results under the severe weather conditions for six alternative combinations of leave-trees under the same thinning intensity.

Leave-tree selection	Crown fire initiation		Crown fire propagation				
	Number of trees ignited	Percentage of trees ignited	Horizontal fuel connections	Number of connected clusters	Average connections per cluster	Average connection per tree	Average trees per cluster
Manual	289	20.94	4259	158	26.96	3.09	8.73
Random 1	297	21.52	6302	140	45.01	4.56	9.86
Random 2	291	21.09	6326	137	46.18	4.58	10.07
Random 3	292	21.16	6532	145	45.04	4.73	9.52
Random 4	265	19.20	6438	150	42.92	4.67	9.20
Random 5	283	20.51	6214	152	40.88	4.50	9.08

All these alternative combinations of leave-trees have practically the same aggregated stand values (Table 3.13). Consequently, predictions of crown fire potential using existing fire behavior models will also be very similar. Determining crown fire potential by predicting tree-level fuel connectivity can provide more a detailed assessment of fire hazard than existing fire behavior models which can improve the evaluation of alternative fuel treatments effects on changing fire behavior.

Table 3.13. Summary statistics for average stand attributes obtained after six alternative combinations of leave-trees.

Leave-tree selection	Tree attribute	Range of values					
		Min.	1 st Qu.	Median	Mean	3 rd Qu.	Max.
Manual	HT	7.79	12.20	15.02	15.49	17.94	33.05
Random 1		7.93	12.32	14.95	15.50	18.13	32.09
Random 2		7.93	12.33	14.96	15.48	18.09	32.09
Random 3		7.79	12.44	15.04	15.62	18.14	33.05
Random 4		7.79	12.44	15.15	15.56	18.10	33.05
Random 5		7.79	12.45	15.06	15.55	18.11	29.59
Manual	DBH	12.70	15.39	19.35	21.53	25.13	60.85
Random 1		12.70	15.57	19.19	21.54	25.38	60.85
Random 2		12.70	15.57	19.24	21.51	25.36	60.85
Random 3		12.70	15.86	19.43	21.79	25.75	60.85
Random 4		12.70	15.68	19.40	21.67	25.48	60.85
Random 5		12.70	15.63	19.37	21.58	25.46	58.07
Manual	CBH	0.00	5.35	6.96	7.05	9.03	15.08
Random 1		0.00	5.50	7.16	7.11	8.93	15.08
Random 2		0.00	5.54	7.16	7.12	8.93	15.08
Random 3		0.00	5.51	7.23	7.18	9.08	15.08
Random 4		0.00	5.61	7.22	7.23	9.12	14.81
Random 5		0.00	5.61	7.27	7.28	9.11	15.08
Manual	CW	2.34	3.66	4.51	4.65	5.38	9.91
Random 1		2.38	3.70	4.48	4.65	5.44	9.63
Random 2		2.38	3.70	4.49	4.65	5.43	9.63
Random 3		2.34	3.73	4.51	4.69	5.44	9.91
Random 4		2.34	3.73	4.54	4.67	5.43	9.91
Random 5		2.34	3.73	4.52	4.67	5.43	8.78

Although the models for predicting tree-level crown fire initiation and propagation have relatively high predictive quality, their accuracy depends largely on the accuracy of the input tree locations and sizes. There are a number of ways to obtain tree locations varying from traditional field measurements and GPS devices to advanced remote sensing technologies such as high-resolution aerial photos (Hirschmugl et al. 2007), multispectral imaging (Popescu and Wynne 2004), and LiDAR (Maltamo et al. 2004). The algorithms used to develop LiDAR-derived stem maps in our study area have provided stem detection accuracies of approximately 53 % when considering all tree classes (Suratno et al. 2009). However, stem detection accuracy increases significantly on dominant trees. In similar forest conditions to those of our study area, the stem detection algorithm provided an accuracy of about 90% when considering only dominant trees (Rowell et al. 2006). In this study, we considered only dominant trees with DBH larger than 12.7 cm, thus we expect the stem map used for our study has a high stem detection accuracy level.

Additionally, the relatively high predictive quality of the developed regression models is measured based on tree-level fire behavior as modeled by WFDS and not on the observation of real fires. Therefore, the models' ability to predict tree-level fire behavior on real fires is likely to differ. Although it is theoretically possible to measure fire behavior at the tree-level on the ground, the inability to predict the exact location of fire beforehand makes obtaining this type of data practically impossible. As a result, we need to rely on advanced physics-based numerical fire behavior model such as WFDS to simulate tree-level fire initiation and propagation.

3.4 CONCLUSIONS

Advanced physics-based numerical fire behavior models coupled with high precision vegetation mapping technologies have enabled us to consider individual tree-level fuel characteristics in understanding fire behavior and evaluating thinning regimes to maximize fuel treatment effects in reducing crown fire hazards.

To facilitate practical application of the three-dimension, fine-scale fire behavior model, such as WFDS, we demonstrated methods to develop regression models to predict crown fire initiation and propagation using a fire simulation domain with tree arrangements. We also applied the regression models to evaluating various thinning treatments in terms of the number of trees that can ignite and the number of trees through which fire can propagate after reaching canopy fuels under a given weather condition. The developed regression models should be applied to areas with weather parameters similar to the weather conditions considered in this study. Applying these models to drier, hotter and windier areas would likely result in underestimating the number of trees that would ignite and the distance over which fire can propagate through adjacent crowns.

We evaluated the effectiveness of alternative thinning treatments for reducing crown fire potential more precisely than existing fire behavior models by applying tree-level fuel connectivity predictive regression models. These regression models can also be implemented into algorithms to optimize the selection of individual tree removal at the stand level, so the combination of leave-trees with the most efficient reduction of crown fire potential is selected for a given thinning intensity. The number of tree-level fuel connections, or other measures of fuel connectivity such as the average number of fuel

connections per tree or average trees forming a cluster of connected tree fuels, can be used as indices to optimize the allocation of thinning treatments for altering fire behavior and reducing fire spread at the landscape level.

Further research needs to be conducted to expand the applicability of our approach. A more exhaustive set of WFDS fire simulation should be designed to include additional weather factor and vegetation characteristics. Tree-level fire behavior should be simulated for a range of values of FMC, ambient temperature and wind speed to better account for variability existing in the real environment. Regression models including these additional factors as predictors of crown fire initiation and propagation can then be applied to different areas under any weather conditions.

3.5 REFERENCES

- Ager, A, M. Finney, and A. McMahan. 2006. A wildfire risk modeling system for evaluating landscape fuel treatment strategies. In Fuels Management – How to Measure Success Conference Proceedings. 28-30 March 2006, Portland, OR. Edited by Andrews, P.L. and Butler, B.W. Proceedings RMRS-P-41. Fort Collins, CO: USDA, Forest Service, Rocky Mountain Research Station. 809 p.
- Allen, C.D., M. Savage, D.A. Falk, K.F. Suckling, T.W. Swetnam, T. Schulke, P.B. Stacey, P. Morgan, M. Hoffman, and J.T. Klingel. 2002. Ecological restoration of southwestern ponderosa pine ecosystems: a broad perspective. *Ecol. Appl.* 12(5):1418-1433.

- Anderson, H.E. 1969. Heat transfer and fire spread. Res. Pap. INT-69. Ogden, UT.
USDA, Forest Service, Intermountain Forest and Range Experiment Station. 20 p.
- Anderson, H.E. 1982. Aids to determining fuel models for estimating fire behavior. Gen. Tech. Rep. INT-122. Ogden, UT: USDA, Forest Service, Intermountain Forest and Range Experiment Station. 22 p.
- Andrews, P.L., C.D. Bevins, and R.C. Seli. 2005. BehavePlus fire modeling system, version 3: Users Guide. Gen. Tech. Rep. RMRS-GTR-106WWW Revised. Ogden, UT: USDA, Forest Service, Rocky Mountain Research Station. 134 p.
- Arno, S.F., and S. Allison-Bunnell. 2002. *Flames in our Forest: Disaster or Renewal?* Island Press, Washington, DC.
- Arno, S.F., and J.K. Brown. 1991. Overcoming the paradox in managing wildland fire. *Western Wildlands* 171:40-46.
- Chung, W., G. Jones, J. Sullivan, and P. Aracena. 2009. Developing a decision support system to optimize spatial and temporal fuel treatments at a landscape level. Proceeding: "Environmentally Sound Forest Operations". Council of Forest Engineering (COFE). 32th Annual Meeting. Kings Beach (Lake Tahoe), California, USA.
- Cruz, M.G. 2004. Ignition of crown fuels above a spreading surface fire. PhD dissertation, University of Montana, Missoula, MT. 240 p.
- Cruz, M.G., M.E. Alexander, and R.H. Wakimoto. 2004. Modeling the likelihood of crown fire occurrence in conifer forest stands. *For. Sci.* 50(5):976-983

- Cruz, M.G., B. Butler, M. Alexander, J. Forthofer, and R. Wakimoto. 2006a. Predicting the ignition of crown fuel above a spreading surface fire. Part I: model idealization. *Int. J. Wildland Fire* 15(1):47-60.
- Cruz, M.G., B. Butler, M. Alexander, J. Forthofer, and R. Wakimoto. 2006b. Predicting the ignition of crown fuel above a spreading surface fire. Part II: model evaluation. *Int. J. Wildland Fire* 15(1):61-72.
- Daniels, R.C. 2001. Datum conversion issues with LIDAR spot elevation data. *Photogrammetric Engineering & Remote Sensing* 67(6):735-740.
- Finney, M.A. 1998. FARSITE: Fire Area Simulator—model development and evaluation. Res. Pap. RMRS-RP-4. Fort Collins, CO: USDA, Forest Service, Rocky Mountain Research Station. 47 p.
- Finney, M.A. 2006. An overview of FlamMap fire modeling capabilities. In *Fuels Management – How to Measure Success Conference Proceedings*. 28-30 March 2006, Portland, OR. Edited by Andrews, P.L. and B.W. Butler, Proceedings RMRS-P-41. Fort Collins, CO: USDA, Forest Service, Rocky Mountain Research Station. 809 p.
- Finney, M., and J. D. Cohen. 2003. Expectation and evaluation of fuel management objectives. Pages 353-366 in Omi, P.N. (ed.). *Fire, Fuel Treatments and Ecological Restoration*. USDA, Forest Service, Rocky Mountain Research Station. 29p.
- Hegy, F. 1974. A simulation model for managing jackpine stands. P. 74-90 in *Proceedings of conference on: Growth models for tree and stand simulation*. Fries, J. (ed.). IUFRO meeting S4.01.04, Royal College of Forestry, Stockholm.

- Hessl, A.E., D. McKenzie, and R. Schellhaas. 2004. Drought and Pacific Decadal Oscillation linked to fire occurrence in the inland Pacific Northwest. *Ecol. Appl.* 14(2):425-442.
- Hirschmugl, M., M. Ofner, J. Raggam, and M. Schardt. 2007. Single tree detection in very high resolution remote sensing data. *Remote Sens. Environ.* 110(4):533-544.
- Hosmer, D.W., and S. Lemeshow. 2000. *Applied logistic regression*. 2nd Ed. John Wiley & Sons, Inc., New York. 375 p.
- Linn, R., J. Reisner, J.J. Colman, and J. Winterkamp. 2002. Studying wildfire behavior using FIRETEC. *Int. J. Wildland Fire* 11(3-4):233-246.
- Maltamo, M., K. Mustonen, J. Hyypä, J. Pitkänen, and X. Yu. 2004. The accuracy of estimating individual tree variables with airborne laser scanning in a boreal nature reserve. *Can. J. For. Res.* 34(9):1791-1801.
- Maltamo, M., K. Eerikäinen, P. Packalén, and J. Hyypä. 2006. Estimation of stem volume using laser scanning-based canopy height metrics. *Forestry* 79(2):217-229.
- Mell, W., M.A. Jenkins, J. Gould, and P. Cheney. 2007. A physics-based approach to modelling grassland fires. *Int. J. Wildland Fire* 16(1):1-22.
- Mell, W.E., J.J. Charney, M.A. Jenkins, P. Cheney, and J. Gould. 2005. Numerical simulations of grassland fire behavior from the LANL-FIRETEC and NISTWFDS models. East FIRE conference, May 11-13, 2005. George Mason University, Fairfax, VA.
- Murray, J.R., L.I. Northcutt, and C.M. Countryman. 1971. Measuring mass loss rates in free burning fires. *Fire Technology* 7(2):162-169.

- Mutch, R.W. 1994. Fighting fire with prescribed fire: a return to ecosystem health. *J. Forest.* 92(11): 31-33.
- Packalén, P., and M. Maltamo. 2006. Predicting the plot volume by species using airborne laser scanning and aerial photographs. *For. Sci.* 52(6):611-622.
- Parsons, R. 2006. Fuels 3-D: A spatially explicit fractal fuel distribution model. In *Fuels Management – How to Measure Success Conference Proceedings*. 28-30 March 2006, Portland, OR. Edited by Andrews, P.L. and Butler, B.W. Proceedings RMRS-P-41. Fort Collins, CO: USDA, Forest Service, Rocky Mountain Research Station. 809 p.
- Popescu, S.C., and R.H. Wynne. 2004. Seeing the trees in the forest: Using LIDAR and multispectral data fusion with local filtering and variable window size for estimating tree height. *Photogrammetric Engineering & Remote Sensing* 70(5):589-604.
- Potter, B.E. 2002. Dynamics-based view of atmosphere-fire interactions. *Int. J. Wildland Fire* 11:247-255.
- Pukkala, T., and T. Kolström. 1987. Competition indices and the prediction of radial growth in Scots pine. *Silva Fenn.* 21(1):55-67.
- Reinhardt, E.D., and N.L. Crookston (tech. eds.). 2003. *The Fire and Fuels Extension to the Forest Vegetation Simulator*. Gen. Tech. Rep. RMRS-GTR-116. Ogden, UT: USDA, Forest Service, Rocky Mountain Research Station. 209 p.
- Rothermel, R.C. 1972. A mathematical model for predicting fire spread in wildland fuels. Gen. Tech. Rep. INT-11. Ogden, UT: USDA, Forest Service, Intermountain Forest and Range Experiment Station. 40p.

- Rothermel, R.C. 1983. How to predict the spread and intensity of forest and range fires. Gen. Tech. Rep. INT-143. Ogden, UT: USDA, Forest Service, Intermountain Forest and Range Experiment Station. 161 p.
- Rothermel, R.C. 1991. Predicting the behavior and size of crown fires in the northern Rocky Mountains. Res. Pap. INT-RP-438. Ogden, UT: USDA, Forest Service, Intermountain Forest and Range Experiment Station. 46p.
- Rowell, E., C. Seielstad, J. Goodburn, and L. Queen. 2009. Estimating plot-scale biomass in a western North American mixed-conifer forest from lidar-derived tree stems. *Silvilaser 2009. Proceedings of the 9th International Conference on Lidar Applications for Assessing Forest Ecosystems*. Texas A&M University. October 15, 2009.
- Rowell, E., C. Seielstad, L. Vierling, L. Queen, and W. Shepperd. 2006. Using laser altimetry-based segmentation to refine automated tree identification in managed forests of the Black Hills, South Dakota. *Photogrammetric Engineering & Remote Sensing* 72(12):1379-1388.
- Rouvinen, S., and T. Kuuluvainen. 1997. Structure and asymmetry of tree crowns in relation to local competition in a natural mature Scot pine forest. *Can. J. For. Res.* 27(6):890-902.
- Scott, J.H. 2006. Comparison of crown fire modeling systems used in three fire management applications. Res. Pap. RMRS-RP-58. Fort Collins, CO: USDA, Forest Service, Rocky Mountain Research Station. 25 p.
- Scott, J.H. 1999. NEXUS: a system for assessing crown fire hazard. *Fire Management Notes*. 59(2):20-24.

- Scott, J.H., and E.D. Reinhardt. 2001. Assessing crown fire potential by linking models of surface and crown fire behavior. Res. Pap. RMRS-RP-29. Fort Collins, CO: USDA, Forest Service, Rocky Mountain Research Station. 59 p.
- Schmidt, K.M., J.P. Menakis, C.C. Hardy, W.J. Hann, and D.L. Bunnell. 2002. Development of coarse-scale spatial data for wildland fire and fuel management. Gen. Tech. Rep. RMRS-GTR-87. Fort Collins, CO: USDA, Forest Service, Rocky Mountain Research Station. 41 p.
- Suratno, A., C. Seielstad, and L. Queen. 2009. Tree species identification in mixed coniferous forest using laser scanning. *ISPRS Journal of Photogrammetry and Remote Sensing* 64(6):683-693.
- Swetnam, T.W., C.D. Allen, and J.L. Betancourt. 1999. Applied historical ecology: using the past to manage for the future. *Ecol. Appl.* 9(4):1189-1206.
- Terrasolid, 2004. TerraScan user's guide. Helsinki.
- USDA, Forest Service, and USDI, Bureau of Land Management. 2001. The National Fire Plan: Managing the Impacts of Wildfires on the Communities and the Environment. URL: <http://www.forestsandrangelands.gov/>
- Van Wagner, C.E. 1977. Conditions for the start and spread of crown fire. *Can. J. For. Res.* 7(1): 23–34.
- Van Wagendonk, J.W. 1996. Use of a deterministic fire growth model to test fuel treatments. Sierra Nevada Ecosystem Project: Final report to Congress, Vol. II, Assessments and scientific basis for management options. Davis: University of California, Centers for Water and Wildland Resources.

CHAPTER 4:

DEVELOPING A COMPUTERIZED APPROACH FOR OPTIMIZING INDIVIDUAL
TREE REMOVAL TO EFFICIENTLY REDUCE CROWN FIRE POTENTIAL

4.0 ABSTRACT

Thinning is being widely used to restore different types of overstocked forest stands because of its effect on changing fire behavior. Typically, thinning is applied at the stand level using prescriptions derived from sample plots that ignore variability in tree sizes and location within stands. Thinning prescriptions usually specify tree removal in terms of number of trees or basal area, resulting in a large number of cut-tree spatial patterns that meet the same prescription. However, the effect of each pattern on reducing crown fire potential can vary widely depending on the resulting spatial distribution of leave-trees. Additionally, thinning prescriptions ignore cut-tree location, which influence economic efficiency and also affect future competition levels of remaining trees. To address the limitations of current thinning practices, we designed a computerized approach to optimize individual tree removal and produce site specific thinning prescriptions that efficiently reduce crown fire potential. Based on stem map and tree attributes derived from light detection and ranging (LiDAR) technology and an individual tree growth, current and future tree-level fuel connectivity is predicted. The approach makes the spatial selection of cut- and leave-trees that most efficiently reduces crown fire initiation and propagation over time while ensuring cost efficiency of the thinning treatment. Application results on a forest stand in western Montana show that the computerized approach tree selection can reduce crown fire potential more efficiently than current thinning practices represented by the manual selection of tree removal.

Keywords: tree growth model, skidding trail network, fire modeling and simulation

4.1 INTRODUCTION

High intensity wildfires have resulted in large financial, social, and environmental costs in western U.S. This trend is not likely to abate soon; some estimates suggest that more than 27 million ha of forestland in the western U.S. have departed significantly from natural wildland fire conditions and are at medium to high risk of catastrophic wildfires (Schmidt et al. 2002). In response to the continuing threat of severe wildfires, the National Fire Plan (USDA and USDI 2001) and the Healthy Forest Restoration Act (2003) mandated forest managers to restore forest habitats and reduce the risk of wildfire on federal lands.

Thinning has been widely used for restoring different types of overstocked forest stands (O'Hara et al. 1994) because it can change stand structures and alter fire behavior (Graham et al. 1999, Graham et al. 2004, Agee and Skinner 2005). Typically, thinning treatments are applied at the stand-level using prescriptions developed from field sample plots, and cut-trees are subjectively selected by forest practitioners according to given prescriptions. However, the efficiency and effectiveness of these stand-level thinning practices are hardly evaluated when applied for reducing crown fire potential due to the following reasons. First, it is difficult to estimate the effects of thinning on altering fire behavior within a stand using the average stand attributes. Stand-level thinning prescriptions are designed to reduce the likelihood of crown fire initiation by increasing canopy base height, and reduce crown fire propagation by decreasing canopy bulk density (Keyes and O'Hara 2002, Graetz et al. 2007). However, due to variability within stands, canopy base height is difficult to estimate and neither the lowest nor the average

crown base height (measured on an individual tree) is likely to be representative of the stand as a whole (Scott and Reinhardt 2001). Moreover, the calculation of canopy bulk density assumes canopy fuels are distributed uniformly throughout the stand, which is unlikely the case even in stands with simple structures (Scott and Reinhardt 2001). Secondly, current thinning prescriptions usually specify percentages of total tree removal or per size class in terms of number of trees or basal area, resulting in a large number of spatial patterns of cut-trees that meet the same thinning prescription for a stand. Individual foresters who select and mark cut-trees are unable to evaluate the effects of each pattern on reducing crown fire potential, which can vary widely depending on the resulting spatial distribution of remaining trees after treatment. Thirdly, stand-level thinning prescriptions often ignore the location of cut-trees relative to extraction points (i.e., road side or log landings), and thus forest practitioners often pursue “easy” trees to extract as long as it meets the thinning prescription without considering the effects on altering fire behavior. Lastly, decisions on cut-tree selection also affect micro conditions and competition levels of remaining trees, thus influencing tree growth and fire behavior within a stand over time. However, spatial and temporal effects of remaining trees on individual tree growth and crown fire potential over time have not been considered in developing thinning prescriptions.

The limitations described above are mainly due to the lack of individual tree-level information available for development and evaluation of detailed and site-specific thinning prescriptions. However, LiDAR technology, which has been widely used in recent years to obtain individual tree locations and attributes (Maltamo et al. 2006, Packalén and Maltamo 2006, Maltamo et al. 2004), can be used to capture spatial

variability of individual trees within a stand and produce a stem map with tree attributes. To address the limitations of current stand-level thinning practices, we designed a computerized approach to optimize selection of tree removal for an individual stand that can most efficiently reduce the susceptibility to high intensity crown fires over time while ensuring the economic efficiency of thinning operations. Using LiDAR-derived stem map and tree attributes, we characterize fuels by quantifying fuel connections among individual trees and make spatial selection of cut- and leave-trees to reduce the risk of crown fire initiation and propagation to and through the stand canopy. Our approach design includes four functional modules: 1) quantifying vertical and horizontal fuel connectivity of individual trees in a stand, 2) predicting individual tree growth over time using a distance-dependent growth model, 3) estimating location-specific costs of timber harvesting for individual trees, and 4) optimizing selection of cut-trees to maximize and maintain discontinuities in fuel connectivity over time while ensuring cost efficiency. We applied our computerized approach to a 4.6-ha forest stand located in the University of Montana's Lubrecht Experimental Forest (LEF) in western Montana. We considered an initial thinning prescription that removed all trees with diameter at breast height less than 12.5 cm (5 in.). Cut- and leave-tree selection was then optimized for the remaining trees to meet a target tree density of 300 leave-trees per ha after the initial thinning prescription.

4.2 METHODOLOGY

4.2.1 LiDAR Data and Tree Attributes

In this study, we used LiDAR data acquired by the National Center for Landscape Fire Analysis (NCLFA) over the LEF located approximately 48 km northeast of Missoula, Montana in the Blackfoot River drainage (N 46°53'30", W -113°26'3") (Figure 4.1). LiDAR data acquisition parameters used for LEF (Table 4.1) provided an average return density of about 1 return per 2.29 m² on the ground with a vertical and horizontal accuracy of 0.15 m and 0.25 m, respectively (Suratno et al. 2009).

Table 4.1. LiDAR data acquisition parameters used for Lubrecht Experimental Forest¹.

Date of acquisition	June 2005
Elevation	1100 – 1900 m
LiDAR system	Leica geosystems ALS50
Average flight height above surface	1900 m
Average flight speed	70.76 ms ⁻¹
Number of strips	54
Scan frequency	25.5
Laser pulse frequency	36200 Hz
Scan angle	±35°
Sidelap	50%
Average swath width	1150 m
Average return density	0.44 m ²
Average footprint	1 m ²

¹ Taken from Suratno et al. (2009)

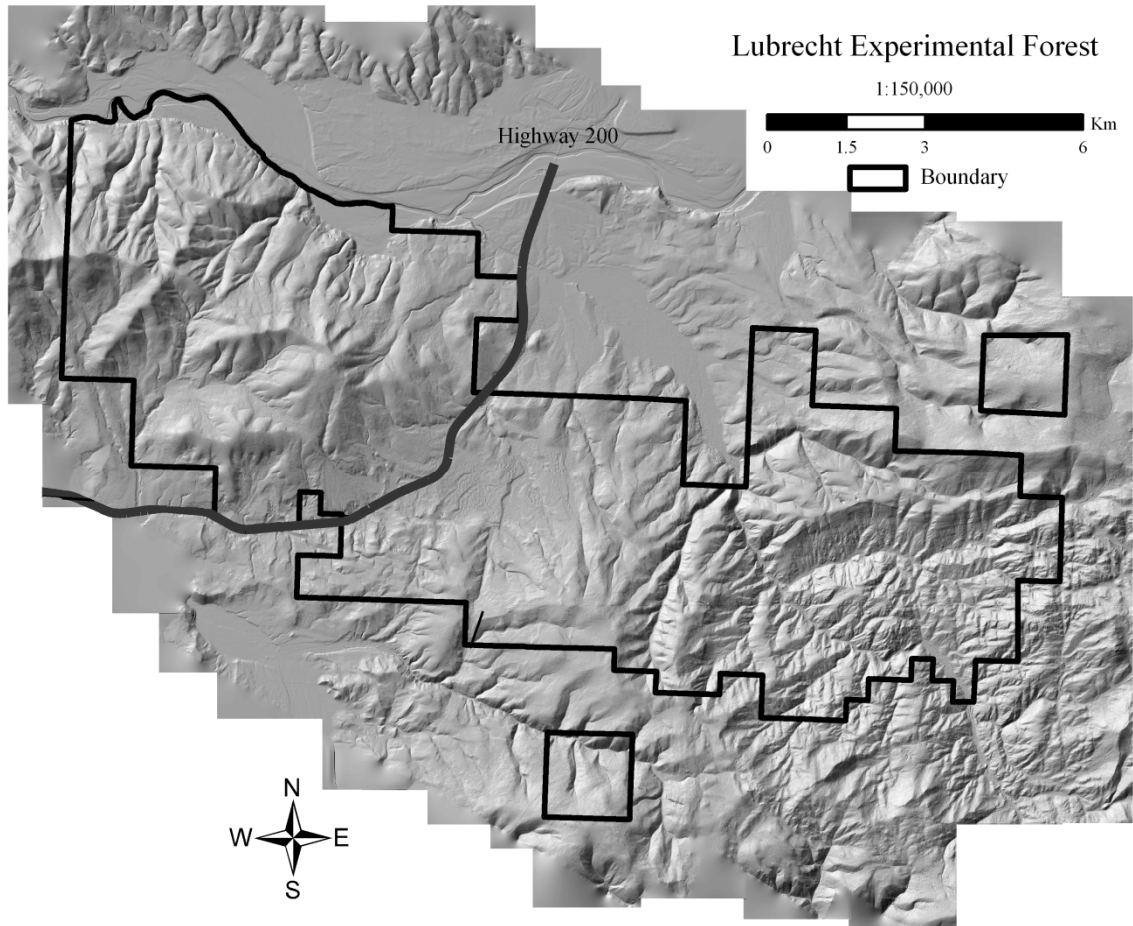


Figure 4.1. University of Montana’s Lubrecht Experimental Forest.

Researchers at the NCLFA separated the raw three-dimensional LiDAR points into vegetation (aboveground) and bare earth points using a triangulated irregular network densification method available in the TerraScan software suite (Terrasolid 2004). Ground points were used to create a digital elevation model (DEM) using inverse distance weighted interpolation at 1 m resolution. The DEM and aboveground points were used to calculate the canopy height model (CHM) using the spot elevation method (Daniels 2001). This approach computed the canopy height (elevation above ground level) at each point by subtracting the DEM height from the CHM (Suratno et al. 2009).

Individual trees were delineated using a stem identification algorithm based on a variable window local maxima filtering and neighborhood canopy height variance (Rowell et al. 2006, Popescu and Wynne 2004). Tree heights (HT) were then obtained from the CHM at each tree location. Crown width (CW) for individual trees was obtained as a function of tree height and stand structure. For trees species at LEF, CW was expected to be 33% of the tree height for trees in stands with canopy cover less than 35%, 16% of tree height for trees in stands with moderately closed canopy cover ranging between 35% and 65%, and 11% of tree height for trees in stands with closed canopy cover greater than 65%. Tree crown base height (CBH) was estimated using a square search window of $2 \times CW$ meters centered at the tree location. CBH was then estimated as the mean height of all CHM points inside the search window divided by the associated standard deviation of the heights. Individual tree diameter at breast height (DBH) were estimated using the following log-linear model ($n=1555$, $R^2= 0.76$, Error = 7.6%) (Rowell et al. 2009).

$$[4.1] \quad \ln \text{DBH} = 1.732 + (0.041 \times \text{HT}) + (0.798 \times \text{RH}) - (0.007 \times \text{SD})$$

where, HT is the height of the tree (m), RH is the relative height calculated as the tree height divided by the mean height of dominant and co-dominant trees in a $20 \text{ m} \times 20 \text{ m}$ neighborhood, and SD is stem density of dominant and co-dominant stems in the neighborhood. Tree volumes were estimated using an equation from the Northern Idaho / Inland Empire of the Forest Vegetation Simulation (Keyser 2008).

$$[4.2] \quad \text{vol} = \left[\left\{ 0.00171 \times (2.54 \times d)^2 \times \text{HT} \right\} + \left\{ 0.00171 \times (2.54 \times d) \times \text{HT} \right\} \right] \times 0.02831$$

where, vol is the tree volume (m^3), and d is the tree DBH (cm).

4.2.2 Individual Tree Fuel Connectivity

To quantify fuel connections among individual trees in a stand, we used logistic regression models developed to predict tree-level crown fire initiation and propagation (for detailed description of the models development, see Chapter 3). These regression models predict tree-level fuel connectivity under severe weather conditions defined by the 90th percentile of historical observation data from the Seeley Lake (N 47°10'58", W - 113°26'50") weather station located approximately 30 km north of LEF. They are based on expected surface fire burning conditions considering fuel moisture values typical of late summer in the Northern Rocky Mountains (Table 4.2) and surface fuels described by the fuel model 10 (Anderson 1982). Table 4.3 shows the weather and surface fire inputs considered for the development of the regression models.

Table 4.2. Typical late summer surface fuel moisture values used in the development of tree-level fire crown initiation and propagation.

Fuel type	Severe conditions (late summer)
1-h	2
10-h	3
100-h	4
Live woody	75

¹ Adapted from Rothermel (1991) standardized fuel moisture values characteristic of late summer in the Northern Rocky Mountains.

Table 4.3. Weather and surface fire input parameters used in the development of tree-level fire crown initiation and propagation.

	Severe conditions (90 th percentile)
Wind speed	3.56 (m/s)
Adjusted wind speed ¹	1.07 (m/s)
Max. ambient temperature	32.1 °C
Ambient relative humidity	14 %
Fuel moisture content	100 %
Rate of spread	0.1 (m/s)
Heat release per unit area	700 (kW/m ²)
Residence time	20 (s)

¹ After applying a wind reduction factor of 0.3, the ratio of midflame to open windspeeds (Rothermel 1983)

Crown fire initiation and propagation are predicted by the following logistic regression models (Eqs. 4.3 and 4.4):

$$[4.3] \quad P_{CFI} = \frac{e^{g(x)}}{1 + e^{g(x)}}, \quad g(x) = 10.93897 + (0.24285 \times HT) - (2.84814 \times CBH)$$

$$[4.4] \quad P_{CFP} = \frac{e^{g(x)}}{1 + e^{g(x)}}, \quad g(x) = -6.9064 + (0.3194 \times HT) - (3.2356 \times SP) + (69.4118 \times CI_1)$$

where, P_{CFI} is the probability that crown fire initiation will occur at a given tree location, P_{CFP} is the probability that fire will propagate crown-to-crown from a source tree representing the flaming front and a target tree ahead of the flaming front. SP is the distance (m) between the horizontal crown projections (edge to edge) of the source and target trees. CI_1 is a modified distance-dependent competition index (Rouvinen and Kuuluvainen 1997) used as a surrogate of size and proximity of the flaming front approaching the target tree. It is calculated as the sum of the horizontal angles originating from the center of the target tree and spanning the DBH of each tree forming the flaming front (Eq. 4.5). The model uses a flaming front area of 1.5 m × 10 m

centered on the source tree to search for additional trees forming the flaming front (Figure 4.2).

$$[4.5] \quad CI_1 = \sum_{i=1}^n \arctan(d_i / \text{dist}_i)$$

where, n is the number of trees forming the approaching flaming front, d_i is the DBH (cm) of the i^{th} tree forming the flaming front, and dist_i is the horizontal distance (m) from the center of the i^{th} source tree to the center of the target.

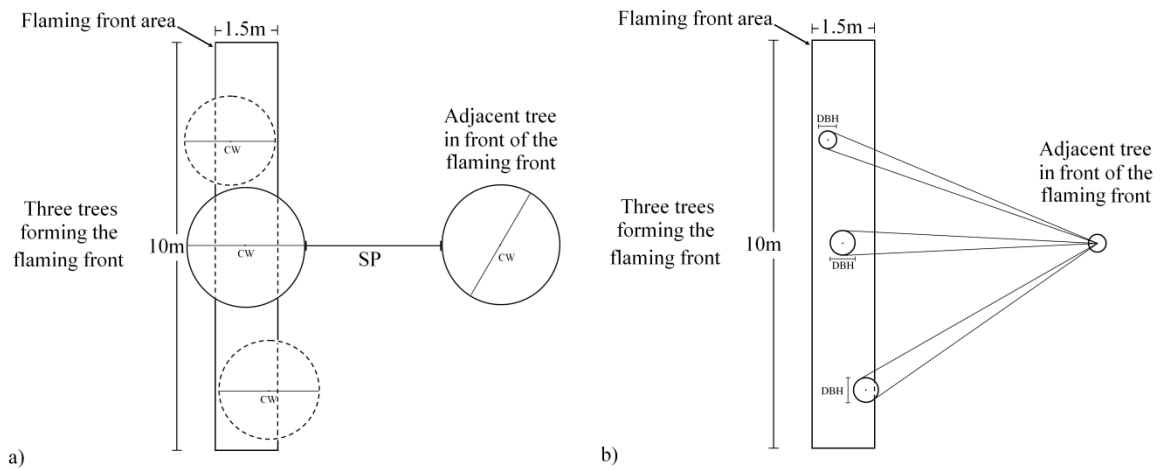


Figure 4.2. Schematic of the flaming front area used to search additional source trees (dashed lines) showing spacing between a source tree and a target tree (solid lines) (a) and the calculation of CI_1 (b) to estimate fuel connectivity.

To use these regression models deterministically, we applied a threshold probability of 0.5. Therefore, when $P_{CFI} > 0.5$, crown fire initiation is expected to occur and the tree's crown fuels are considered vertically connected with surface fuels. Similarly, fire is expected to propagate from the source tree to the target tree when $P_{CFP} > 0.5$, considering both tree crown fuels horizontally connected.

4.2.3 Individual Tree Distance-Dependent Growth Model

We used an individual tree distance-dependent growth model developed to predict average annual basal area increment (BAI) for three common tree species in LEF; Douglas-fir (DF) (*Pseudotsuga menziesii*), ponderosa pine (PP) (*Pinus ponderosa*), and western larch (WL) (*Larix occidentalis*) (see Chapter 1 for more detailed descriptions about the growth model). The model is based on neighboring tree data collected for 285 cored trees (145 of which are DF, 99 are ponderosa pine PP, and 41 are WL) within an 11-meter plot radius. Tree cores were measured and average BAI (cm²/year) was computed for a ten year period from 1998 to 2007.

The individual tree growth model has the expression:

$$[4.6] \quad \text{BAI} = e^{[1.974503 + (0.022768 \times d) - (0.361392 \times \text{CI}_2)]}$$

where, d is the DBH (cm) of the subject tree and CI_2 is a distance-dependent competition index calculated similar to CI_1 . It is calculated as the sum of the horizontal angles originating from the subject tree center and spanning the DBH of each neighbor tree inside the 11-meter plot radius (Eq. 4.7) (Rouvinen and Kuuluvainen 1997).

$$[4.7] \quad \text{CI}_2 = \sum_{j=1}^{\text{ng}} (d_j/d) \times \arctan(d_j/\text{dist}_j)$$

where, d_j is the DBH (cm) of the j^{th} neighbor tree, dist_j is the horizontal distance (m) from the subject tree center to j^{th} neighbor tree center, and ng is the number of neighbor trees inside the 11-meter radius plot.

After the average annual BAI was estimated for a given tree (Eq. 4.6), expected future DBH was calculated. Future HT was then obtained using a logistic height-

diameter equation from the Northern Idaho / Inland Empire of the Forest Vegetation Simulation (Eq. 4.8) (Keyser 2008).

$$[4.8] \quad HT = \left[4.5 \times e^{\{4.81519 - 7.29306 / ((d / 2.54) + 1.0)\}} \right] \times 0.3048$$

Expected future CW was estimated as 16% of tree height assuming a future stand structure would have moderately closed canopy. Future CBH was estimated assuming it increases proportionally to HT. We made these assumptions because of the lack of future vegetation data necessary for projecting CHM over 20 years (Rowell 2010, Personal communication).

4.2.4 Individual Tree Timber Harvesting Cost

We used a computerized model developed to estimate skidding costs of individual trees for ground-based harvesting operations (see Chapter 2). The model considers size and spatial distribution of individual cut-trees and detailed terrain information obtained from a LiDAR-derived stem map and DEM, respectively. First, the model uses a log-bunching algorithm to identify the location and volume of log-piles. A cable skidder operation, which collects nearby cut-trees within a maximum winching radius (MWR) through a cable winch, is simulated to complete a full load close to a target loading capacity (TLC) and skid the load to an extraction point (landing or road side). The log-bunching algorithm begins with sorting all cut-trees based on their slope distance from the extraction point. The algorithm selects the closest cut-tree as the first log-pile location, and all cut-trees within the MWR from the log-pile with a combined volume lower than the TLC are assigned to the first log-pile. Then, the algorithm selects the next

closest non-assigned cut-tree as the second log-pile location, and assigns nearby cut-trees within the MWR to the second log-pile. The process continues until all cut-trees have been assigned to a log-pile. The model then determines least-cost routes connecting each log-pile to the extraction point by developing a skid-trail network formed by vertices and edges. Each vertex, which represents the center of a DEM cell evenly spaced at a five-meter interval is connected to its eight adjacent vertices. Edges represent the connection (skid-trail links) between a vertex and its adjacent neighboring vertices. The model then creates feasible skid-trail links over areas with gentle to moderate slope (i.e., lower than 35%). To avoid damage to remaining tree, no skid-trail links are allowed within 1.5 meters of each leave-tree.

After the skid-trail network has been created, the model determines the skidding cycle time associated with each link based on its distance and slope, using the skidding cycle time models presented in Equations 4.9 and 4.10 (Contreras and Chung 2007).

$$[4.9] \quad CT_{ds} = 3.9537 + (0.0215 \times D)$$

$$[4.10] \quad CT_{us} = 3.9537 + (0.0258 \times D)$$

where, CT_{ds} is the cycle time (min) for downhill skidding, CT_{us} is the cycle time (min) for uphill skidding, and D is the slope distance of the skid-trail link (m).

Skidding cycle time is used as an edge attribute to formulate a network problem. The Dijkstra's shortest path algorithm (Dijkstra 1959) is used to find the set of least-cycle time routes connecting each log-pile to the extraction point. The skidding cost for a given i^{th} log-pile (PSC_i) is estimated using the following equation:

$$[4.11] \quad PSC_i = \left(\frac{CT_i}{60} \right) \times RR$$

where, CT_i is the least skidding cycle time (min) for a round trip between the extraction point and the i^{th} log-pile location and RR is the rental rate of the skidder (\$/hr). Skidding cost of individual trees is estimated by prorating the log-pile's skidding cost based on the volume ratio of the individual tree to the entire log-pile (Eq. 4.12). Thus, bigger cut-trees entail a larger skidding cost than smaller cut-trees in the same pile.

$$[4.12] \quad TSC_j = \left(\frac{\text{vol}_j \times PSC_i}{P\text{vol}_i} \right)$$

where, TSC_j is the skidding cost (\$) of the j^{th} individual cut-tree, vol_j is the volume (m^3) of the j^{th} cut-tree, PSC_i is the skidding cost (\$) of the i^{th} log-pile containing cut-tree j , and $P\text{vol}_i$ is the volume (m^3) of the i^{th} log-pile.

4.2.5 Individual Tree Removal Optimization

To ensure the effectiveness and efficiency of thinning treatment on reducing crown fire potential over time, we considered a period of 20 years and applied the tree-level growth model to estimate future tree sizes as well as future tree-level fuel connections. The approach for optimizing the selection of individual cut-trees considers current fuel connections among all trees, expected future fuel connections after removing the cut-trees and growing the remaining leave-trees for 20 years, and the cost associated with skidding the selected cut-trees.

The tree removal optimization problem is formulated as follows:

$$[4.13] \quad \text{Min. } Z = \left[\sum_{i=1}^{NT} (TSC_i \times \{1 - I_i\}) \right] + \left[\sum_{i=1}^{NT} [(CHFC_i + CVFC_i + FHFC_i + FVFC_i) \times I_i] \right]$$

subject to

$$[4.14] \quad \sum_{i=1}^{NT} \{1 - I_i\} = TCT$$

where, I_i is a binary variable indicating whether the i^{th} tree remains (leave-tree, $I_i = 1$) or is removed from the stand (cut-tree, $I_i = 0$), $CHFC_i$, and $CVFC_i$ are constants representing the number of current horizontal and vertical fuel connections associated with the i^{th} tree, $FHFC_i$ and $FVFC_i$ are constants representing the number of future horizontal and vertical fuel connections associated with the i^{th} tree, TSC_i is the skidding cost (\$) associated with skidding the i^{th} tree, and NT is the total number of trees. The objective function (Eq. 4.13) represent an index set to minimize the skidding cost (first term) and number of fuel connections (second term). Equation 4.14 is a constraint ensuring that the target thinning intensity in terms of the number of trees is met, where TCT is the target number of cut-trees.

We used a network to model fuel connectivity and solve the tree removal optimization problem. A fuel connectivity network consists of a set of vertices V , which represent tree locations, and a set of edges E representing fuel connections between pairs of adjacent trees. Our approach starts with applying the crown fire initiation and propagation regression models to estimate current fuel connections among trees and form the fuel connectivity network. Clusters of connected trees are identified in the fuel connectivity network and characterized in terms of number of trees forming each cluster (ρ). Figure 4.3 shows an example of a fuel connectivity network formed by 43 trees, resulting in nine clusters of connected trees with sizes ranging from 1 to 16. Each cluster represents the extent fire would propagate and the number of trees that would burn after fire reaches crown fuels through vertical fuel connections.

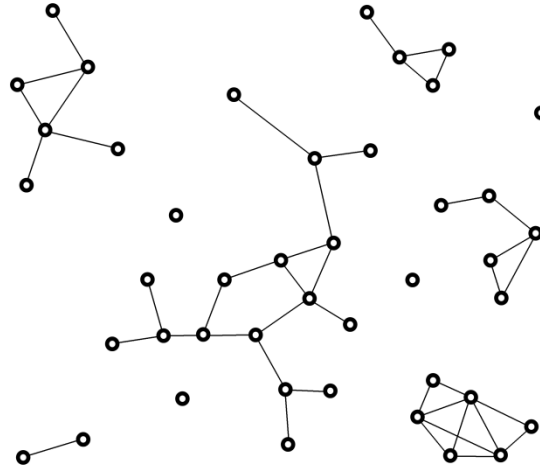


Figure 4.3. Example of fuel connectivity network formed by 43 vertices and 9 clusters of connected trees.

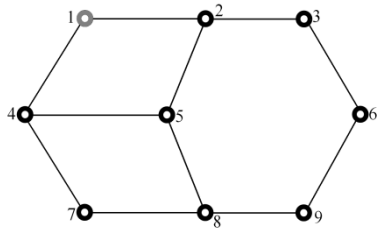
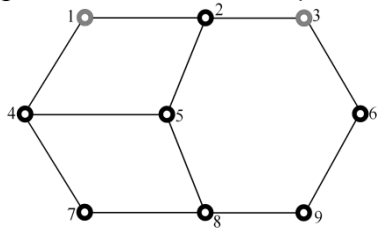
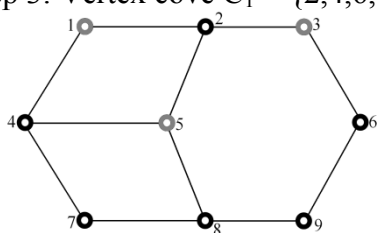
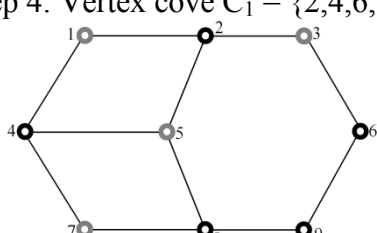
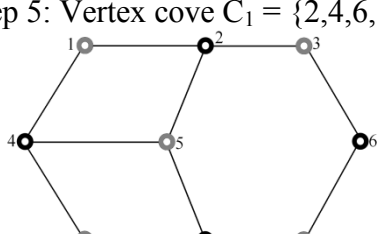
For the purpose of reducing crown fire potential by breaking fuel connectivity throughout a given forest stand, we determine a minimal combination of cut-trees required to remove all horizontal fuel connections within each cluster of connected trees. This is achieved by using an algorithm to identify a minimal vertex cover (MVC) in a graph G . A vertex cover C of G is a set of vertices such that for each edge $\{u,v\}$ in G , at least one of its vertices u or v is in C . Given a vertex cover C of G and a vertex v in G , v is removable if the set $C - \{v\}$ is still a vertex cover of G . A MVC is then a vertex cover with no removable vertices. In our context, a MVC represents a minimal combination of cut-trees required to remove all fuel connections.

4.2.5.1 MVC algorithm

Given a graph G , all vertices are labeled consecutively from $1, 2, \dots, p$. Starting with the first vertex ($i = 1$), the vertex cover is initialized as $C_i = V - \{i\}$. If C_i has no more removable vertices, we stop and store the size $\phi(C_i)$ of the vertex cover C_i . Otherwise for

each removable vertex v of C_i , we find the number $\psi(C_i - \{v\})$ of additional removable vertices of the vertex cover $C_i - \{v\}$. We denote the v_{\max} as the removable vertex such that $\psi(C_i - \{v\})$ is maximum, and then update the vertex cover as $C_i = C_i - \{v_{\max}\}$. When multiple vertices with the same $\psi(C_i - \{v\})$ value exist, we arbitrarily select the first one. Thereafter, vertex v_{\max} is selected and removed from C_i ($C_i = C_i - \{v_{\max}\}$). The process of removing v_{\max} vertices and updating the vertex cover C_i is repeated until no more removable vertices exist. When the process is finished, a MVC initialized with C_i is obtained. Now we move to the next vertex ($i = i+1$) and initialize the vertex cover $C_i = V - \{i\}$ and obtain the associated MVC. We stop when a MVC is obtained for all vertices in G . All resulting MVC are stored and ordered by ascending sizes $\phi(C_i)$. A MVC with minimum size is selected as the final MVC of G . Table 4 shows the steps required to obtain the MVC initialized with the first vertex in a graph with nine vertices.

Table 4.4. Steps required to obtain the MVC initialized with vertex number one.

Step 1: We initialize the vertex cover as $C_1 = V - \{1\} = \{2,3,4,5,6,7,8,9\}$, size $\varphi(C_1) = 8$			
	Removable vertex v of C_1	Removable vertices of $C_1 - \{v\}$	$\psi(C_1 - \{v\})$
	3	5,7,8,9	4
	5	3,6,7,9	4
	6	5,7,8	3
	7	3,5,6,9	4
	8	3,6	2
	9	3,5,7	3
Maximum $\psi(C_1 - \{v\}) = 4$ for $v = 3,5,7$. We arbitrarily remove vertex 3 from C_1			
Step 2: Vertex cover $C_1 = \{2,4,5,6,7,8,9\}$, size $\varphi(C_1) = 7$			
	Removable vertex v of C_1	Removable vertices of $C_1 - \{v\}$	$\psi(C_1 - \{v\})$
	5	7,9	2
	7	5,9	2
	8	none	0
	9	5,7	2
Maximum $\psi(C_1 - \{v\}) = 2$ for $v = 5,7,9$. We arbitrarily remove vertex 5 from C_1			
Step 3: Vertex cover $C_1 = \{2,4,6,7,8,9\}$, size $\varphi(C_1) = 6$			
	Removable vertex v of C_1	Removable vertices of $C_1 - \{v\}$	$\psi(C_1 - \{v\})$
	7	9	1
	9	7	1
Maximum $\psi(C_1 - \{v\}) = 1$ for $v = 7,9$. We arbitrarily remove vertex 7 from C_1			
Step 4: Vertex cover $C_1 = \{2,4,6,8,9\}$, size $\varphi(C_1) = 5$			
	Removable vertex v of C_1	Removable vertices of $C_1 - \{v\}$	$\psi(C_1 - \{v\})$
	9	none	0
Maximum $\psi(C_1 - \{v\}) = 0$ for $v = 9$. We remove vertex 9 from C_1			
Step 5: Vertex cover $C_1 = \{2,4,6,8\}$, size $\varphi(C_1) = 4$			
	Removable vertex v of C_1	Removable vertices of $C_1 - \{v\}$	$\psi(C_1 - \{v\})$
	None	--	--
Step 6: We stop and obtain a MVC C_1 of size $\varphi(C_1) = 4$			

The total number of cut-trees required to remove all fuel connections (RCT) is then determined by summing up the size of the final MVC for each cluster (Eq. 4.15).

$$[4.15] \quad RCT = \sum_{i=1}^{\omega} \phi_i$$

where, ω is total number of clusters in the fuel connectivity network.

Three cases arise when evaluating the thinning intensity constraint (Eq. 4.14). In case I, the target number of cut-trees is equal to the number of trees required to remove all fuel connections ($RCT = TCT$). There are a large number of combinations of cut-trees that remove all fuel connections because most clusters have multiple final MVC of same size. We select final MVC based on their proximity to the extraction point, measured as the average slope distance (AD_MVC) from all forming vertices to the extraction point. The j^{th} final MVC of the k^{th} cluster in the fuel connectivity network is then selected based on a random number and a selection probability calculated by Equation 4.16.

$$[4.16] \quad SP_MVC_{jk} = \frac{AD_MVC_j^{-1}}{\sum_{i=1}^{cn} AD_MVC_i^{-1}}$$

where, SP_MVC_{jk} is the selection probability that the j^{th} final MVC of the k^{th} cluster is selected, and cn is the number of final MVC of the same size associated to the k^{th} cluster in the fuel connectivity network.

Case II represents the case where the target number of cut-trees is smaller than the number of trees required to remove all fuel connections ($TCT < RCT$). In this case, additional leave-trees (ALT) need to remain to meet the thinning intensity constrain. The number of additional leave-trees is calculated ($ALT = RCT - TCT$), and leave-trees are selected based on both their proximity to the extraction point and the number of

remaining fuel connections. After selecting a final MVC for each cluster in the fuel connectivity network (Eq. 4.16), additional leave-trees are selected based on the selection probability calculated as follows:

$$[4.17] \quad SP_LT_j = \frac{(1 - SAD_T_j) + SFC_T_j}{\sum_{i=1}^{ALT} (1 - SAD_T_i) + SFC_T_i} \quad \forall j \in P$$

where, SP_LT_j is the selection probability that the j^{th} tree is selected to remain, SAD_T_j is the standardized slope distance from the j^{th} tree to the extraction point, SFC_T_j is the standardized number of fuel connections between the j^{th} tree and other already selected leave-trees, and P is the set of trees forming the selected final MVC for all clusters.

Standardized values were used to reduce slope distance and the number of fuel connections to the same scale. The equal weight was given to both factors for calculating the tree selection probability.

For case III, the target number of cut-trees is larger than the number of trees required to remove all fuel connections ($RCT < TCT$). Here, additional cut-trees need to be selected for removal. The number of additional cut-trees is calculated ($ACT = TCT - RCT$), and cut-trees are selected based on their proximity to the extraction point (Eq. 4.18).

$$[4.18] \quad SP_CT_j = \frac{AD_T_j^{-1}}{\sum_{i=1}^{ACT} AD_T_i^{-1}} \quad \forall j \in S$$

where, SP_CT_j is the selection probability that the j^{th} tree is selected to be removed, AD_T_j is the slope distance from the j^{th} tree to the extraction point, and S is the set of trees not belonging to the selected MVC for all clusters in the fuel connectivity network (originally selected leave-trees).

As mentioned above, our computerized approach starts with applying the crown fire initiation and propagation regression models to estimating current fuel connections among all trees. Then, the number of fuel connections for each tree and the size of clusters of connected trees are calculated. At iteration one, a randomly selected combination of cut-trees is generated, and then MVC for each cluster and additional cut- or leave-trees are identified based on the number of fuel connections and proximity to the extraction point (Eqs. 4.16 – 4.18). Skidding cost of each cut-tree is estimated and the number of fuel connections among leave-trees is determined. The individual tree growth model is then employed to estimate future tree sizes, and the crown fire initiation and propagation models are applied again to estimate future tree-level fuel connections among the leave-trees. The objective function is then evaluated (Eq. 4.13) and stored. For the next iteration, a different random combination of cut-and leave-trees is generated, and the objective function is evaluated and compared with the previous solution. If the current solution is better than the previous one (lower total skidding cost and lower number of current and future fuel connections), it is stored and save as the best solution found. Otherwise, the current solution is ignored and the next iteration starts. This iterative process to generate and evaluate alternative combinations of cut- and leave-trees continues until a stopping criterion is met. We used a maximum number of iteration, I_{\max} , to stop the process in a reasonable amount of time. When the process stops the best solution found is reported. For the model application presented in this study, we set I_{\max} at 15,000 iterations.

4.2.6 Model Application – A Case Study

The study area for this investigation is a forest stand in the LEF (Figure 4.4). The stand is 4.6 ha in size with elevations ranging from 1,270 to 1,310 m, on a north-facing aspect, and an average slope of 13.5% (0.0 – 36.3% slope range). Douglas-fir is the dominant species with a small amount of ponderosa pine trees. The stand has established under- and middle-story vegetation creating continuous canopy fuels from the ground to the top of the canopy, resulting from logging in the mid-1940s and thinning in the mid-1970s. The LiDAR stem detection algorithm identified over 11,000 trees in the stand, most of which are small, suppressed trees. For the purpose of reducing crown fire potential, we first considered an initial thinning prescription that cuts, piles, and burns small trees with DBH less than 12.5 cm (5 in.). Figure 4.4b presents the LIDAR-derived stem map showing the remaining 2,645 individual trees in the study area after the initial thinning prescription was applied. Cut-tree selection was then optimized for the remaining trees to meet a target tree density of 300 leave-trees per ha or $TCT = 1,265$ trees.

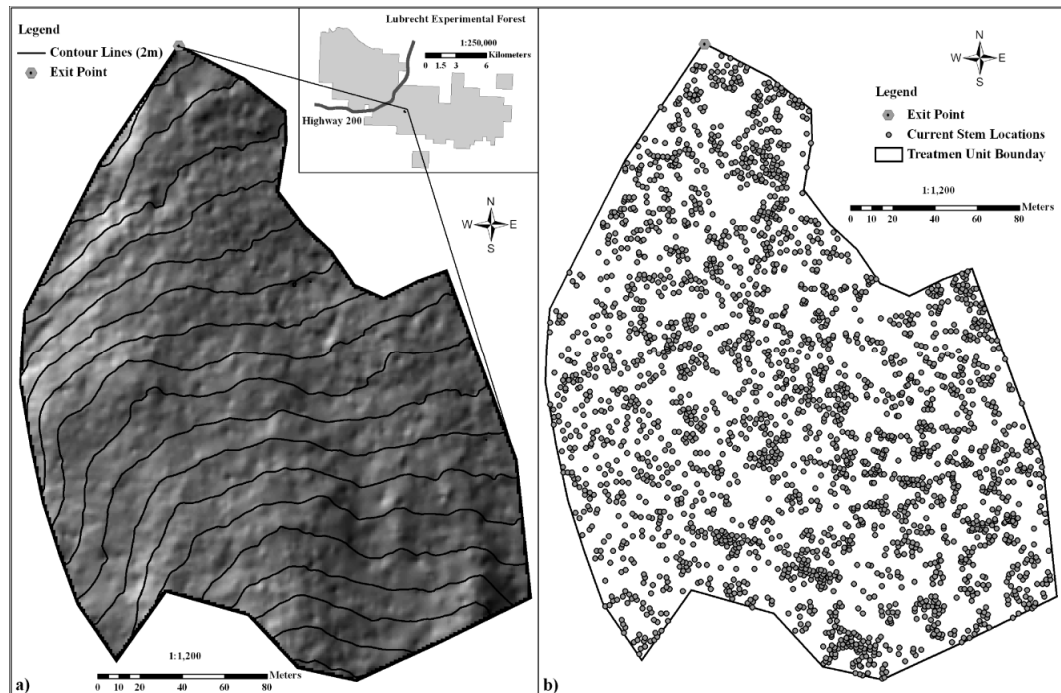


Figure 4.4. LiDAR-derived digital elevation model (a) and stem map (b) for the 4.6-ha study area in LEF.

4.3 RESULTS AND DISCUSSION

Based on the current LiDAR-derived tree locations and attributes, the tree-level fuel connectivity logistic regression models predicted crown fire ignition at 536 tree locations which is over 20% of trees in the study area (Table 4.5). Additionally, due to the relatively large number of trees and dense stand structure under the current conditions, over 27,700 horizontal fuel connections were predicted between adjacent pairs of trees in the study area. These predicted horizontal fuel connections formed a fuel connectivity network consisting of 38 clusters of connected trees. Clusters are formed by an average of 70 trees and crown fuels of each tree are connected to an average of over

ten adjacent trees. Most clusters are formed by less than 15 connected trees, but there are a few large clusters that connect most trees in the study area (Figure 4.5). For example, only two clusters connect almost 95% of trees and the largest cluster connects over 92% of trees. These results suggest that, after reaching crown fuels through vertical fuel connections, fire can propagate throughout the stand burning most trees in the study area. Additionally, the large number of fuel connections, average connections per tree, and average connections per cluster indicate a relatively high crown fire potential under the current stand structure.

Table 4.5. Tree-level fuel connectivity results from the logistic regression models for trees under the current stand condition and the projected future condition after a 20-year growing period.

Stand Condition	Crown fire initiation		Crown fire propagation				
	Number of trees ignited	Percentage of trees ignited	Horizontal fuel connections	Number of connected clusters	Average connections per cluster	Average connection per tree	Average trees per cluster
Current	536	20.26	27755	38	730.39	10.49	69.60
After thinning	315	22.68	4051	173	23.41	2.94	7.98
Future	189	17.68	5648	56	100.86	4.09	24.64

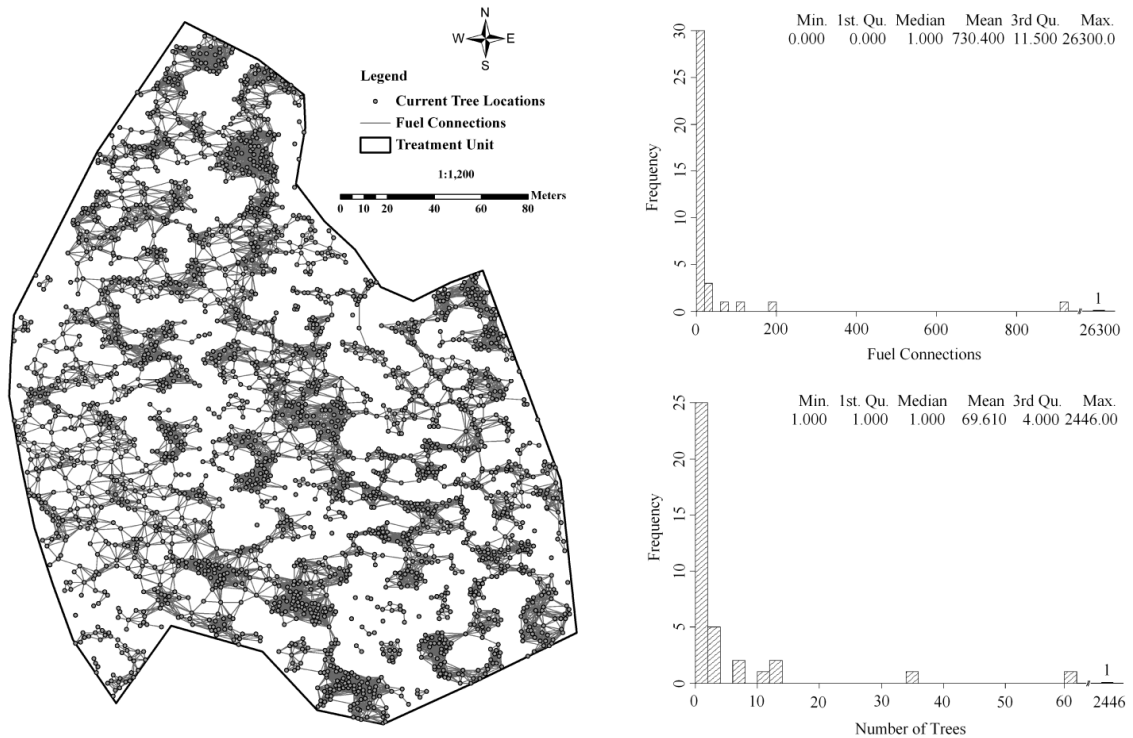


Figure 4.5. Location, size, and summary statistics of clusters formed by predicted tree-level fuel connections under the current conditions in the study area.

The MVC algorithm was applied to the clusters in the fuel connectivity network to identify all possible final MVC associated with each cluster. After adding the size of the final MVC for each cluster, a total of 1,996 cut-trees were required to remove all fuel connections in the study area (over 75% of total trees) resulting in only 649 leave-trees. Consequently, 673 additional leave-trees were required to meet the thinning intensity constraint of 300 leave-trees per ha. The computerized approach generated and evaluated alternative combinations of leave-trees. The best solution, yielding the minimum tree-level fuel connections as well as skidding cost, was found at iteration 12,023, and no better solution was found for next 3,000 iterations (Figure 4.6). The objective function value of the best solution was 13,706, consisting of 4,366 remaining fuel connections

(315 vertical and 4,051 horizontal), 5,837 future fuel connections (189 and 5,648 vertical and horizontal, respectively) among the selected leave-trees, and a skidding cost of \$3,503 associated with the selected cut-trees.

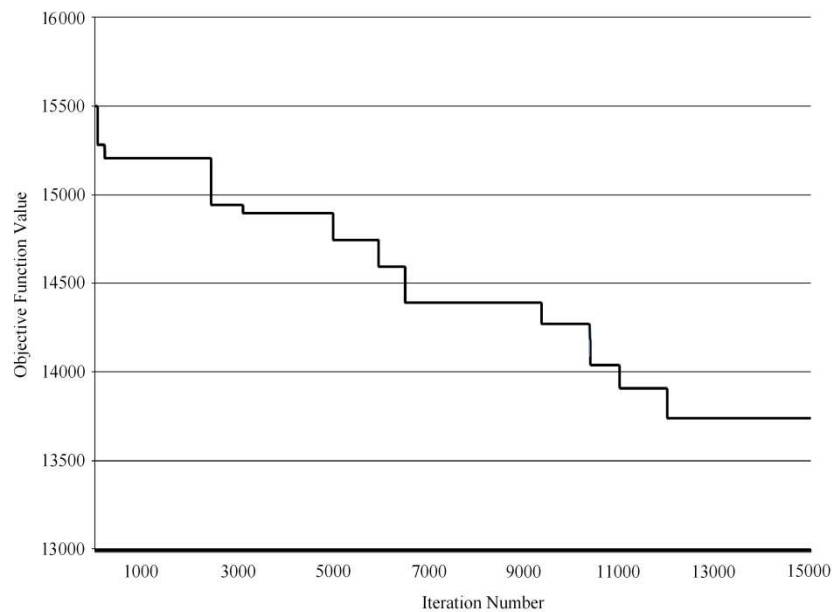


Figure 4.6. Changes in objective function value over 15,000 iterations. The best solution was found at iteration 12,023.

Fuel connectivity throughout the study area was largely reduced by removing about 48% of the total number of trees in the study area (1265 cut-trees). The best solution found by our tree removal optimization approach identified a combination of leave-trees that reduced fuel connectivity by almost 85% from over 28,000 current fuel connections to about 4,365 remaining fuel connections (Figure 4.7). The number of trees expected to ignite decreased by about 41% from 536 to 315 trees. Fuel discontinuity was largely introduced as indicated by the increase in the number of clusters of connected leave-trees from 38 to 173 clusters. The average cluster size dropped from 69.6 trees to 8

trees, the average fuel connections per tree decreased from over 10 to about 4 (Table 4.5). Similarly to the current conditions before treatment, most clusters are formed by less than 15 connected trees. However, 5 % of clusters now connect about 72% of leave-trees after treatment and the largest cluster connects only about 59% of leave-trees.

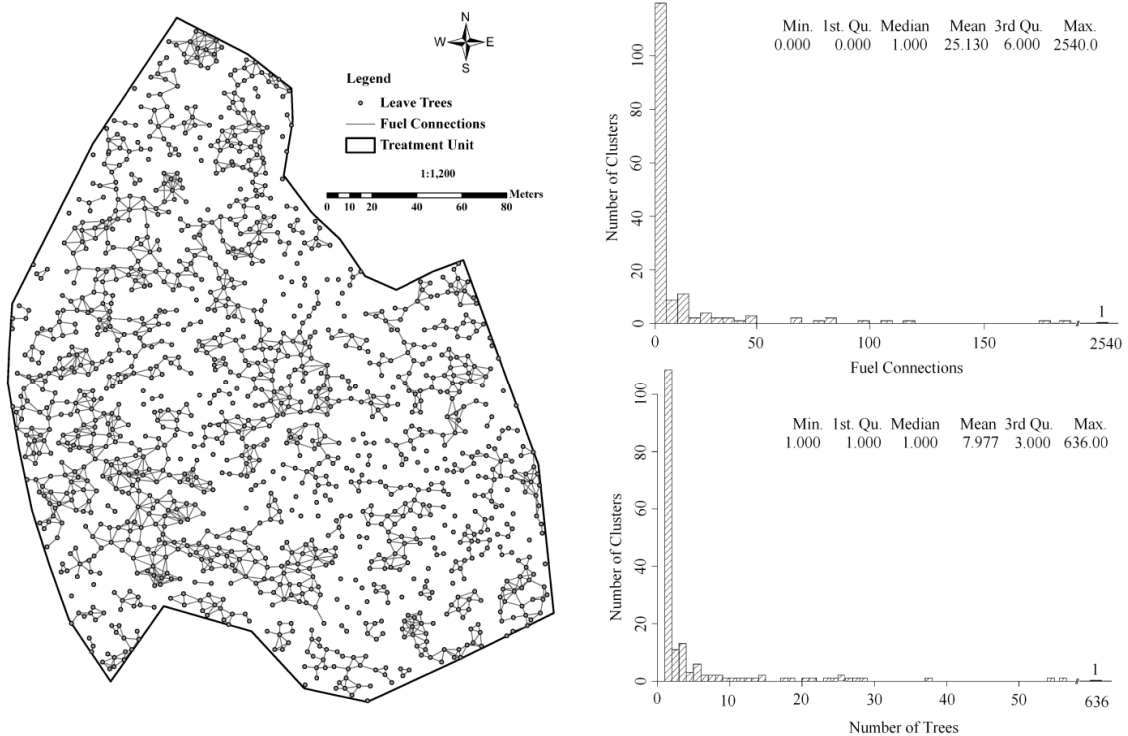


Figure 4.7. Leaf-tree locations and summary statistics of clusters formed by remaining fuel connections found by the best solution.

The individual distance-dependent tree growth model was applied to the selected leave-trees based on their locations and sizes to estimate tree growth under the new stand conditions after the thinning treatment. Average periodic increment in DBH of leave-trees was 5.08 cm for a 20-year period (Table 4.6). Future tree HT estimated by the height-diameter relationship (Eq. 4.8) shows that HT increases by 34%. Future average

tree CBH was estimated to increase by the same proportion as tree HT, and future CW was expected to increase by an average of 0.47 m (Table 4.6).

Table 4.6. Current and future tree attributes predicted using the individual tree growth model over a 20 year period.

Time	Tree attribute	Range of values					Periodic increment over 20 years
		Min.	1 st Qu.	Median	3 rd Qu.	Max.	
Current	HT	8.79	12.23	14.96	17.93	33.05	5.27 m
Future		15.77	18.41	20.31	22.68	35.79	(33.98%)
Current	DBH	12.70	15.46	19.40	25.18	60.85	5.08 cm
Future		16.76	20.86	24.48	30.09	66.00	(23.53%)
Current	CBH	0.00	5.33	6.99	9.03	15.08	2.48 m
Future		0.11	7.47	10.45	11.81	19.00	(34.18%)
Current	CW	2.34	3.67	4.49	5.38	9.91	0.47 m
Future		2.64	4.04	4.94	5.92	10.90	(9.92%)

The total number of tree-level fuel connections among the selected leave-trees was predicted to increase over 20 years because of growth in tree size. The number of trees expected to ignite under the future stand conditions is smaller than the number of ignitable trees under the current conditions (Table 4.5). As future tree size gets larger and tree spacing gets smaller compared with the current conditions, the number of future horizontal fuel connections between adjacent pairs of leave-trees increase by about 39% (Table 4.5). The number of clusters of connected trees decreases by more than 68%. The average cluster size almost triples, and the average fuel connections per tree increase from 2.94 to 4.09 (Table 4.5). Figure 4.8 shows the location and sizes of clusters formed by future fuel connections among leave-trees. Although future fuel connectivity increases throughout the study area compared with the stand conditions right after thinning, crown fire potential remains still low after 20 years. The number of future tree-

level fuel connections is about 20%, the average cluster size is one third, and the average connections per tree is about 40% compared with the stand conditions before thinning.

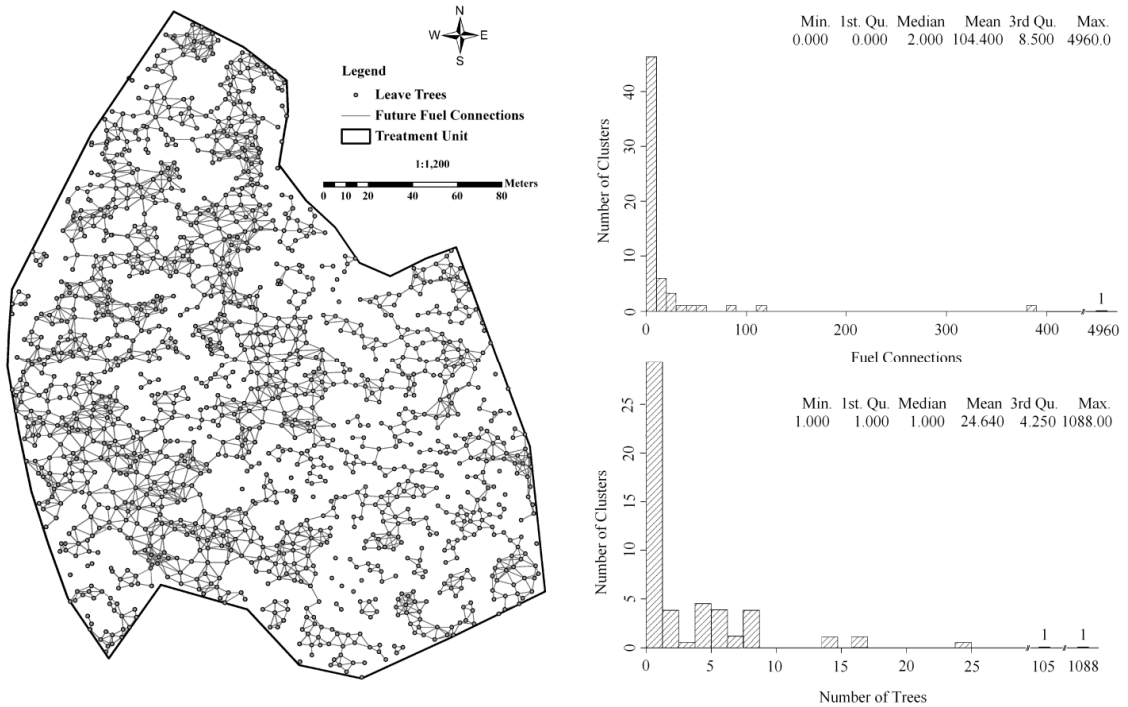


Figure 4.8. Leave-tree locations and summary statistics of clusters formed by future fuel connections after a 20-year growth period.

The individual tree skidding cost model identified log-pile locations and the optimal skid-trail network connecting each log-pile to the extraction point that ensures the cost efficiency of thinning treatment (Figure 4.9). Based on the location and sizes of the 1,245 cut-trees (Figure 4.9a), the log-bunching algorithm identified 275 log-piles (Figure 4.9b). A skid-trail network composed of almost 3,450 feasible skid-trail links was created over the study area based on the location of the 275 log-piles and the remaining 1,380 leave-trees (Figure 4.9c). The optimal skid-trail network that minimizes the skidding cost from each log-pile to the extraction point was developed. The optimal

network is formed by about 1,080 ski-trail links. Figure 4.9d shows the optimal skid-trail network with traffic level on each skid-trail link in terms of the number of passes (turns). The average skidding cost per log-pile is about \$12.5 and the average skidding distance from a log-pile to the exit point is about 224 m (Table 4.7). Figure 4.10a shows the range of skidding costs per log-pile. Log-piles located farther away from the exit point have larger skidding costs. Skidding costs of individual cut-trees ranged from \$0.19 to about \$17 with an average of \$2.8 (Table 4.7). Cut-trees with large skidding costs can be found throughout the study area because cost is a function of both tree size and distance from the extraction point (Figure 4.10b).

Table 4.7. Statistics on individual tree skidding costs estimated for the selected cut-trees in the study area.

Total		Log-piles	
Total Skidding Cost (\$)	3,503	Min. Number of Trees per Pile	1.00
Number of Log-piles	275	Aver. Number of Trees per Pile	4.52
Number of Cut-trees	1,265	Max. Number of Trees per Pile	16.00
Harvestable Volume (m ³)	36.6	Min. Pile Volume (m ³)	0.05
		Aver. Pile Volume (m ³)	1.31
		Max. Pile Volume (m ³)	2.79
Cut-trees			
Minimum Tree Volume (m ³)	0.05	Min. Pile Distance (m)	14.21
Average Tree Volume (m ³)	0.29	Aver. Pile Distance (m)	224.37
Maximum Tree Volume (m ³)	3.02	Max. Pile Distance (m)	391.38
Minimum Tree Cost (\$)	0.19	Min. Pile Cost (\$)	6.05
Average Tree Cost (\$)	2.77	Aver. Pile Cost (\$)	12.52
Maximum Tree Cost (\$)	17.27	Max. Pile Cost (\$)	17.27

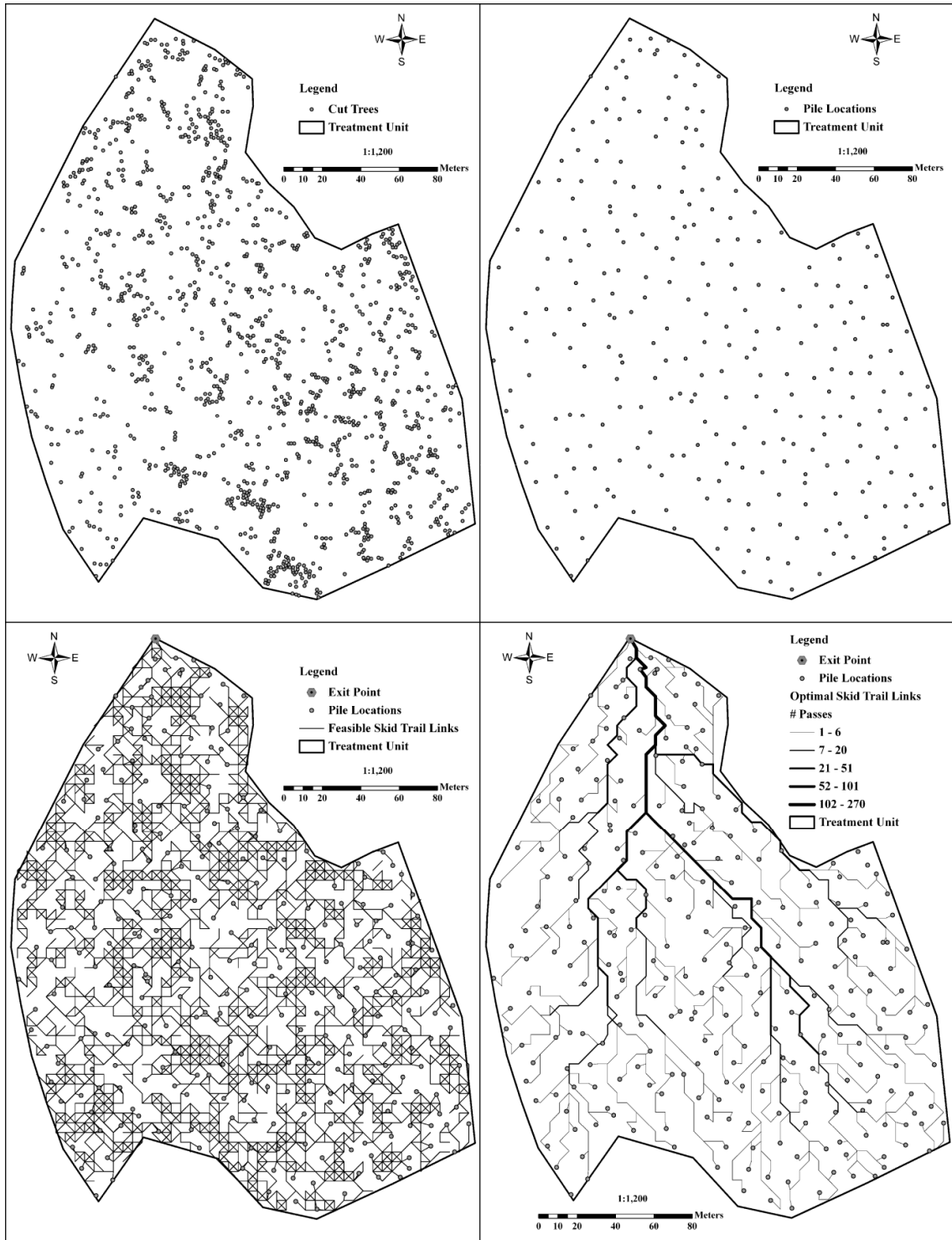


Figure 4.9. Cut-tree locations (a) and log-piles (b), feasible skid-trail links (c), and optimal skid-trail network (d) for the selected cut-trees in the best solution found.

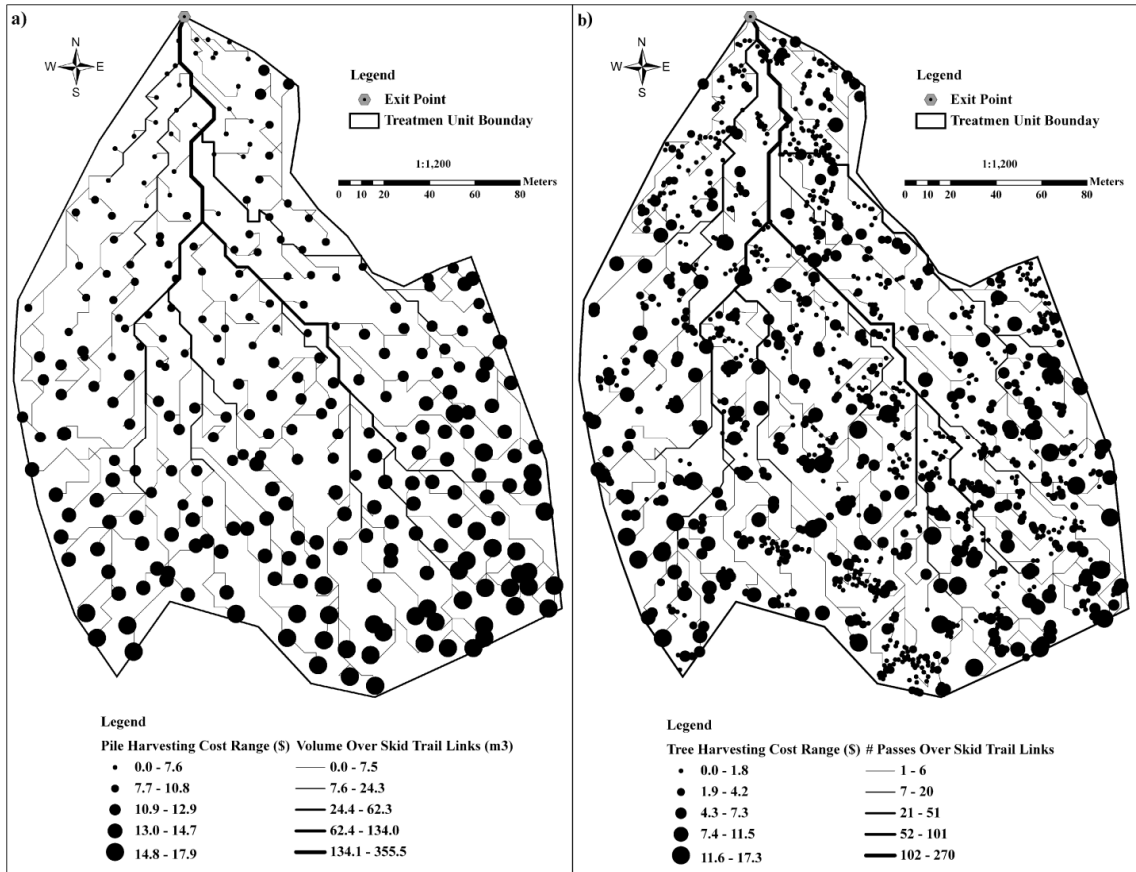


Figure 4.10. Distribution of skidding costs over the study area showing cost per log-pile (a) and cost per individual cut-tree (b).

As mentioned above, the best tree removal selection found by the computerized approach appears to largely reduce crown fire potential as measured by the tree-level fuel connectivity. However, it is difficult to prove solution quality due to the lack of efficient optimization algorithms (i.e., mixed-integer programming) capable of solving the tree removal problem to optimality within a reasonable amount of computing time. Therefore, we compared the best solution found with two alternative combinations of cut- and leave-trees under the same thinning intensity (a total of 1,380 leave-trees). One combination consists of cut-trees selected manually simulating the marking process carried out by markers on the ground based on spacing between trees and tree sizes, while

the other combination selects cut-trees randomly. Then, we obtained the number of remaining and expected future fuel connection among the selected leave-trees, and determined the skidding costs associated with the selected cut-trees for both alternative tree selections. The manual and random cut- and leave-tree selection resulted in objective function values about 5% and 34% higher, respectively, than the objective function value of the best solution found by the computerized approach (Table 4.8). The number of remaining and future tree-level fuel connections among the selected leave-trees as well as the skidding cost of the selected cut-trees from our computerized model solution is lower than those from the manual and random solutions. The number of remaining tree-level fuel connections from the manual selection is about 4.2% higher than the number of remaining fuel connections from the model solution, whereas the random cut-tree selection resulted in 51% more remaining fuel connections than those from the best solution (Table 4.8). This indicates that there is large variability in tree-level fuel connectivity among alternative combinations of trees. Our approach, besides optimizing the cut- and leave-tree selection, provides a more consistent and objective method to evaluate alternative cut-tree patterns and improve the efficiency of thinning treatments for reducing crown fire potential.

Table 4.8. Comparisons on solution quality between the best tree selection found by the computerized approach and two alternative selections of cut- and leave-trees.

Tree selection method	Objective function value	Skidding cost (\$)	Remaining tree-level fuel connections	Future tree-level fuel connections
Computerized model	13,706	3,503	4,366	5,837
Manual	14,327	3,483	4,548	6,296
Random	18,379	3,654	6,599	8,126

Our computerized approach to optimize the selection of tree removal can efficiently break fuel connectivity throughout a forest stand to reduce crown fire potential. However, the results of the computerized approach depend heavily on the accuracy of input data such as tree locations, and current and projected future tree attributes. There are several forms to acquire tree locations varying from traditional field measurements and GPS devices to advanced remote sensing and GIS technologies such as high-resolution aerial photos (Hirschmugl et al. 2007), multispectral imaging (Popescu and Wynne 2004), and LIDAR (Maltamo et al. 2004). The algorithm used to obtain LiDAR-derived stem maps by NCLFA researchers provided stem detection accuracies of approximately 53% when considering all tree classes at LEF (Suratno et al. 2009). However, stem detection accuracy increases significantly on dominant trees. In similar forest conditions to those of our study area, the stem detection algorithm provided an accuracy of about 90% when considering only dominant trees (Rowell et al. 2006). In this study, we considered only dominant trees with DBH > 12.7 cm, thus we expect the stem map used for our study has a high stem detection accuracy level.

Appropriate tree-level growth models are also required to accurately predict future tree dimensions and consequently tree-level fuel connectivity. We predicted future tree diameters using a basal area increment model parameterized for species commonly found at LEF. However, for CBH and CW, we assumed that CBH and CW increments are proportional to HT which was derived from DBH. These assumptions may introduce uncertainty to the accuracy of projected tree sizes and future tree-level fuel connections. Underestimation of future CBH could result in overestimating the number of ignitable

trees. Similarly, underestimating future CW could result in underestimation of the number of fuel connections among adjacent pairs of trees.

4.4 CONCLUSIONS

Our computerized approach for optimizing individual tree removal provides an analytical method to evaluate spatial and temporal effects of thinning on reducing crown fire potential within a stand, and thus can help forest managers develop more effective and efficient thinning prescriptions that are site-specific to given stands. Our approach considers spatial variability of fuels within a stand, the effects of cut-tree selection on future tree growth and stand conditions, and skidding costs of individual trees into the development of thinning prescriptions.

The application results show that crown fire potential can be effectively reduced over time while ensuring the cost efficiency of thinning treatments. Fuel connectivity throughout forest stands can be largely reduced in terms of the number of tree-level fuel connections as well as number of clusters of connected trees, average number of trees forming a cluster, and average fuel connections per tree. By selecting the combination of cut-trees that removes the most tree-level fuel connections, our approach can reduce fuel connectivity over time more effectively than existing thinning practices. In addition to reducing crown fire potential, our approach can potentially be modified and used for other forest management objectives. Tree growth can be included in the objective function to increase timber production as well as reducing crown fire potential. Our

approach can also be applied with a modification to develop tree-level thinning prescriptions for the purpose of efficiently increasing carbon sequestration or improving wildlife habitat for given species upon availability of tree level measures of carbon sequestration and wildlife habitat quality.

Further research needs to be conducted to enhance the performance of the computerized approach and evaluate the feasibility of implementing the results on the ground. Widely used heuristic optimization techniques such as simulated annealing (Kirkpatrick et al. 1983), tabu search (Glover 1989, 1990), and ant colony (Dorigo et al. 1996) can be applied to solve the optimal tree removal selection problem and compared with the current random search techniques. Time required to locate and mark selected cut-trees should also be measured and compared with conventional tree marking practices to evaluate the cost efficiency of implementing the model results.

Despite the imitations, our approach has the potential to enable forest managers to customize site-specific thinning guidelines for individual stands and to implement cost-efficient fuel treatments to reduce the risk of high-intensity wildfires. Given that high resolution vegetation mapping technology such as LiDAR is becoming more widely available, our approach can be a useful tool when thinning is applied to restore overstocked forested lands in need of fuel treatments.

4.5 REFERENCES

- Agee, J.K., and C.N. Skinner. 2005. Basic principles of forest fuel reduction treatments. *For. Ecol. Manage.* 211(1-2):83-96.
- Anderson, H.E. 1982. Aids to determining fuel models for estimating fire behavior. Gen. Tech. Rep. INT-122. Ogden, UT: USDA, Forest Service, Intermountain Forest and Range Experiment Station. 22 p.
- Contreras, M. and W. Chung. 2007. A computer approach to finding an optimal log landing location and analyzing influencing factors for ground-based timber harvesting. *Can. J. For. Res.* 37(2):276-292.
- Daniels, R.C. 2001. Datum conversion issues with LIDAR spot elevation data. *Photogrammetric Engineering & Remote Sensing* 67(6):735-740.
- Dijkstra, E. 1959. A note on two problems in connexion with graphs. *Numerische Math.* 1:269-271.
- Dorigo, M., Maniezzo, V., and Colomi, A. 1996. The ant system: optimization by a colony of cooperating agents. *IEEE Trans. Syst. Cybernet. B*, 26: 29–41. doi:10.1109/3477.484436.
- Glover, F. 1989. Tabu Search – Part I. *ORSA Journal on Computing*, 1(3):190–206.
- Glover, F. 1990. Tabu Search – Part II," *ORSA Journal on Computing*, 2(1):4–32.
- Graetz, D., J. Sessions, and S. Garman. 2007. Using stand-level optimization to reduce crown fire hazard. *Landscape and Urban Planning* 80(3):312-319.
- Graham, R.T., A.E. Harvey, T.B. Jain, and J.R. Tonn. 1999. The effects of thinning and similar stand treatments on fire behavior in Western forest. Gen. Tech. Rep. PNW-

- GTR-463. Portland, OR: USDA, Forest Service, Pacific Northwest Research Station.
27 p.
- Graham, R.T., S. McCaffrey, and T.B. Jain (tech. eds.) 2004. Science basis for changing forest structure to modify wildfire behavior and severity. Gen. Tech. Rep. RMRS-GTR-120. Fort Collins, CO: USDA, Forest Service, Rocky Mountain Research Station. 43 p.
- Hirschmugl, M., M. Ofner, J. Raggam, and M. Schardt. 2007. Single tree detection in very high resolution remote sensing data. *Remote Sens. Environ.* 110(4):533-544.
- Keyes, C.R. and K.L. O'Hara. 2002. Quantifying stand targets for silvicultural prevention of crown fires. *West. J. Appl. For.* 17(2): 101-109.
- Keyser, C.E., comp. 2008. Northern Idaho / Inland Empire (NI/IE) Variants Overview – Forest Vegetation Simulator. Internal Rep. Fort Collins, CO: USDA, Forest Service, Forest Management Service Center. 49p. (revised February 3, 2010).
- Kirkpatrick, S., C.D. Gelatt, and M.P. Vecchi, Optimization by simulated annealing. *Science* 220:671–680.
- O'Hara, K.L., R.S. Seymour, S.D. Tesch, and J.M. Guldin. 1994. Silviculture and our changing profession. *J. For.* 92(1):8-13.
- Maltamo, M., K. Mustonen, J. Hyypä, J. Pitkänen, and X. Yu. 2004. The accuracy of estimating individual tree variables with airborne laser scanning in a boreal nature reserve. *Can. J. For. Res.* 34(9):1791-1801.
- Maltamo, M., K. Eerikäinen, P. Packalén, and J. Hyypä. 2006. Estimation of stem volume using laser scanning-based canopy height metrics. *Forestry* 79(2):217-229.
- Packalén, P., and M. Maltamo. 2006. Predicting the plot volume by species using airborne laser scanning and aerial photographs. *For. Sci.* 52(6):611-622.

- Popescu, S.C., and R.H. Wynne. 2004. Seeing the trees in the forest: Using LIDAR and multispectral data fusion with local filtering and variable window size for estimating tree height. *Photogrammetric Engineering & Remote Sensing* 70(5):589-604.
- Rouvinen, S., and T. Kuuluvainen. 1997. Structure and asymmetry of tree crowns in relation to local competition in a natural mature Scot pine forest. *Can. J. For. Res.* 27(6):890-902.
- Rowell, E. 2010. Personal communication. Remote Sensing Analyst. National Center for Landscape Fire Analysis. College of Forestry and Conservation, University of Montana, Missoula, MT.
- Rowell, E., C. Seielstad, L. Vierling, L. Queen, and W. Shepperd. 2006. Using laser altimetry-based segmentation to refine automated tree identification in managed forests of the Black Hills, South Dakota. *Photogrammetric Engineering & Remote Sensing* 72(12):1379-1388.
- Rowell, E., C. Seielstad, J. Goodburn, and L. Queen. 2009. Estimating plot-scale biomass in a western North American mixed-conifer forest from lidar-derived tree stems. *Silvilaser 2009. Proceedings of the 9th International Conference on Lidar Applications for Assessing Forest Ecosystems*. Texas A&M University. October 15, 2009.
- Schmidt, K.M., J.P. Menakis, C.C. Hardy, W.J. Hann, and D.L. Bunnell. 2002. Development of coarse-scale spatial data for wildland fire and fuel management. *Gen. Tech. Rep. RMRS-GTR-87*. Fort Collins, CO: USDA, Forest Service, Rocky Mountain Research Station. 41 p.

Scott, J.H., and E.D. Reinhardt. 2001. Assessing crown fire potential by linking models of surface and crown fire behavior. Res. Pap. RMRS-RP-29. Fort Collins, CO: USDA, Forest Service, Rocky Mountain Research Station. 59 p.

Suratno, A., C. Seielstad, and L. Queen. 2009. Tree species identification in mixed coniferous forest using laser scanning. ISPRS Journal of Photogrammetry and Remote Sensing 64(6):683-693.

Terrasolid, 2004. TerraScan user's guide. Helsinki.

USDA, Forest Service, and USDI, Bureau of Land Management. 2001. The National Fire Plan: Managing the Impacts of Wildfires on the Communities and the Environment.
URL: <http://www.forestsandrangelands.gov/>